Investigations of marine microplastic pollution, effects of weathering on microplastic chemical identification, and development of computer vision tools to facilitate microplastic studies

Samantha Phan

A dissertation

submitted in partial fulfillment of the

requirements for the degree of

Doctor of Philosophy

University of Washington

2021

Reading Committee:

Christine K. Luscombe, Chair

Alshakim Nelson

Cody W. Schlenker

Jacqueline L. Padilla-Gamiño

Program Authorized to Offer Degree:

Chemistry

University of Washington

Abstract

Investigations of marine microplastic pollution, effects of weathering on microplastic chemical identification, and development of machine learning tools to facilitate microplastic studies

Samantha Phan

Chair of the Supervisory Committee:
Professor Christine K. Luscombe
Materials Science and Engineering and Chemistry

Plastic-waste leakage is a major unintended consequence of plastic usage and consumption. Plastic waste is a long-term environmental challenge and global concern that inspires increasing efforts to prevent further pollution and understand the impact of plastic pollution on the environment. Microplastic identification is a necessary first step in investigating the harmful effects in the environment and efforts have been made to characterize the types of microplastics in marine organisms inhabiting the Salish Sea and Gulf of Alaska. Unfortunately, no single analytical approach is flawless in determining the identity of microparticles and studies on the chemical transformation of microplastics is a must. Environmentally weathered microplastics can differ significantly from their un-weathered counterparts which the identification of microplastics. It was found that weathering conducted with Puget Sound seawater show different weathering byproducts compared to other simulated environments. This implies that studies with environmental water is needed to further understand degradation mechanisms and microplastic pollution effects. Despite this, Raman spectroscopy retains great fidelity of weathered polymer spectra and show little variation with increasing exposure to sunlight and may serve as a more accurate and versatile tool for microplastic identification compared to IR spectroscopy. While these tools are helpful, computer vision and machine learning have significant potential to recognize morphological features to classify the shape of microplastics <100 μm, further advancing the microplastic field.

Table of Contents

List of Figures

List of Tables

ACKNOWLEDGEMENTS

This scientific journey has been challenging and I am very thankful for being able to meet so many incredibly talented, kind, and passionate individuals during my PhD.

I first want to acknowledge the support from the Luscombe group and especially my PI, Prof. Christine Luscombe for her tremendous support, guidance, and understanding. I am incredibly thankful for her giving me a chance to work in her lab and develop a new branch of studies in her lab. Prof. Luscombe is a brilliant mentor who let me know many opportunities I wasn't aware of before. She's helped me grow into the scientist I am today. Additionally, I want to thank Dr. Jeffrey Buenaflor for the tremendous support given to me during a crucial time and the cherished advice he's bestowed upon me.

I want to thank the Clean Energy Institute, Center for C-H functionalization, Inclusion in Chemical Sciences, Theater for Change at UW for contributing to an amazingly emotionally rich graduate experience.

I also want to share special thanks to my undergraduate mentor Prof. Kirk S. Schanze for taking me on as a student when I was a freshman. Prof. Schanze supported me as an undergraduate in ways that not many advisers would do for their undergraduates. I did not have to concentrate so hard to make a living during college and was therefore able to focus on research more than I would have been able to at the time. He inspired me and allowed me to grow as a scientist. A main reason why I have been so motivated with this journey is because of the Schanze group's encouragement and mentorship early in my career. For giving me that first research experience and making it a positive one, I am forever grateful.

I would also like to thank the many peers, colleagues, and friends that I've made over these past years. Thank you for being there for me and making sure we're all okay together. I wouldn't have made it without your constant and daily support. Thank you all so much.

DEDICATION

To R.D.W., Ebi, and my family.

Chapter 1. Introduction to microplastics

1.1 Global plastic generation and consumption

Plastics are widely used as materials for their interesting properties and low costs. Since the 1950s, the global plastic production has increased exponentially and accelerated more so recently due to consumer behavior shifting from reusable plastics to single-use products.[1, 2] In the beginning, a major focus in synthetic plastics was to maintain their performance and resist damage when exposed to the natural environment. While beneficial for active use, plastic durability also allows them to exist in the environment for hundreds or thousands of years. Plastic-waste leakage is a considerable and an enormous unintended consequence of plastic usage and consumption. In 2010, it was estimated that 5 to 13 million tons of plastic enter the environment each year.**Error! Reference source not found.** Plastic waste is a long-term environmental challenge and is a major global concern that inspires increasing efforts to prevent further pollution and understand the impact of plastic pollution on the environment. Figure 1.1 shows a visualization of the general pathway by which plastics reach the ocean. Plastics are made with thousands of different types of polymers and different properties for human consumption. Additionally, the coronavirus pandemic has brought an unprecedented and significant increase in the demand and use of plastics that further adds to the plastic pollution that threatens ocean and marine life. Disposable face masks, gloves, and other personal protective equipment being used to prevent the transmission of COVID-19 are produced using polymer materials (such as polyethylene, polypropylene, or polystyrene) and are often carelessly thrown away into the environment.[4] In the context of PPE for the coronavirus pandemic, China increased daily production of medical mask production to 14.8 million as of February 2020 and the Japanese Ministry of economy, trade, and industry ordered over 600 million face masks per month as of April 2020.[4] When these plastics and polymers enter the environment, they are

further modified through fragmentation, photodegradation, biofouling, or coagulation, ultimately forming microplastics.[5, 6]

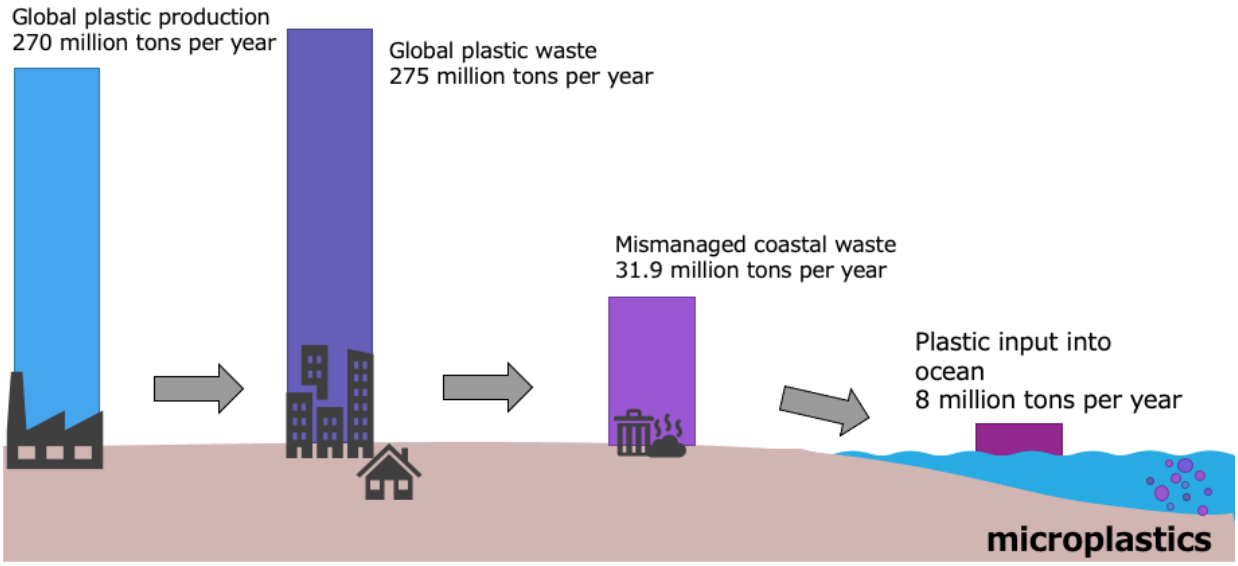

Figure 1. 1 The pathway by which plastics enter the ocean. Adapted from Reference 1.

1.2 What are microplastics?

Microplastics, plastic particles < 5 mm in size, exist in different forms composed of the different types of plastics leaked into the environment.[7] Unlike other kinds of waste, plastics do not decompose, but rather fragment and degrade into smaller sized pieces called microplastics (< 5 mm) and nanoplastics (< 1 um).[8, 9] Microplastic pollution is an emerging global concern and there is an urgent need to understand the accumulation and transport of microplastics smaller than 1 mm near coastal regions. The various types of microplastics found in the environment change depending on the types of plastics leaked into the environment and degraded after time. Microplastics are categorized as primary or secondary microplastics depending on their origin. Primary microplastics are particles that are designed and manufactured to be small, such as microbeads used in cosmetics, whereas secondary microplastics are the result from breakdown of larger plastic items (also called macroplastics). Thousands of plastics have been synthesized with

different densities and textures and when those polymers enter the environment, they are further modified through environmental processes (e.g., fragmentation, photodegradation, or biofouling).[5, 6] Such processes are complex and are constantly occurring in the environment which result in the various physical characteristic (such as size, density, and shape) of microplastics. Each different physical characteristic determines microplastic trajectory, sources, sinks, residence times, and travel distances, but more studies are needed to understand the dynamic distribution of microplastics in coastal landscapes.[10, 11] Global shifts in consumer behavior towards single-use plastic products has dramatically accelerated microplastic pollution all around the world in the water, marine organisms, air, and arctic regions.[12, 13, 14] Despite the prevalence of microplastics in the world, little is known about their patterns of occurrence in different areas and transport mechanisms.

1.3 What happens when microplastics enter the environment?

When microplastics enter the environment, they are subjected to weathering, fragmentation and ingestion by marine organisms which can change microplastic physical and chemical properties. Because of their small size, microplastics can be easily ingested by marine organisms, particularly by species that have limited ability to select particles during feeding.[15, 16] The accumulation of microplastics in organisms may have detrimental effects on feeding rates, energy storage, reproduction and overall fitness.[17–20] Furthermore, microplastics do not degrade quickly and may be transferred through trophic interactions, creating a pathway to ingestion of microplastics by animals at higher trophic levels, including fish, predatory.[21, 22] Microplastics are usually transported in the water, either by marine currents or in freshwater systems by rivers.[23–25] In regions with high population density, it is likely that more microplastics will be released to the

waterways.[26] Similarly, waters that are stagnant, or have longer residence times (e.g., in a bay, inlet, or fjord), may accumulate more microparticles at depth and in sediments.[27] Therefore, marine organisms living under different oceanographic conditions could be differentially exposed to microplastic contaminants. Different plastic types also sorb various types of persistent organic pollutants and knowing the types of polymers present in marine environments allow researchers to investigate toxicological effects.[28–30] Therefore, to fully understand the effects of microplastic pollution, identification of the chemical identity of microplastics is crucial.

Chapter 2. Characterization techniques for microplastics

2.1 Physical and chemical characterization

No single analytical approach is flawless in determining the identity of microparticles but analysis typically involves physical characterization (e.g. microscopy) followed by chemical confirmation (e.g. spectroscopy).[31–33] Early studies on microplastics relied primarily on visual recognition and discernment of particles as microplastic or non-microplastic; however, this inaccurately estimates the actual amount of microplastics found in the environment as visual inspection leads to both false positives and false negatives.[32, 33] Chemical analysis increases the accuracy of microplastic identification, but each technique has advantages and disadvantages.[31, 8] Thermal analysis, such as differential scanning calorimetry and pyro-GC-MS, results in destruction of microplastics preventing additional subsequent analysis.[31, 34, 35] Some microscopy techniques such as scanning electron microscopy plus energy-dispersive X-ray spectroscopy can provide high-resolution and high-magnification images, but is more expensive and time consuming for extensive microplastic analysis.[31, 33] Two common and non-destructive methods are Fourier transform infrared microspectroscopy (μ-FTIR) and Raman microspectroscopy (RMS).[8, 3, 31–36] These microscopy combined with vibrational spectroscopy techniques provide two distinct complementary techniques to collect unique vibrational fingerprints and identify specific microplastic types. Recently, FTIR has been more frequently used for marine microplastic identification than RMS.[31–33, 37] However, RMS can provide advantages over μ-FTIR such as lower minimum particle size identification, analysis on thicker or strongly absorbing microparticles, and weaker bands from oxidative products.[37, 38]

2.2 Microplastic identification challenges

Identification of microplastics is challenging because of the variety of polymers and chemicals used to produce plastics and the numerous weathering processes that chemically change them. Considering the thousands of polymers, additives, copolymers used in plastics, identification requires the usage of an extensive polymer library for spectral matching.[31, 8, 39, 40] Unfortunately, environmentally weathered microplastics can differ significantly from their un-weathered counterparts, thus complicating the identification of microplastics.[5, 37, 39, 41]

Although there are the advantages using RMS for microplastic analysis, there are major challenges that impede efficient and accurate identification of microplastics: resource-intensive imaging procedures, fluorescence interference, and limited Raman spectral libraries. Especially considering the breadth of commercial plastics produce and structural alterations caused by the environment, standard spectral libraries have limited utility. Currently, imaging and analysis is time-intensive, and completed by human experts with ample experience in microplastic analysis; though some efforts have been made to automate the imaging process.[3, 36, 42] About 0.5 to 2 hours was required to image particles on each filter paper sample with RMS and then many hours afterwards for spectral background correction, spectral matching, and analysis for each particle imaged.

Raman scattering and fluorescence emission are competing photophysical processes. Unfortunately, despite tedious optimizations, strong fluorescence background can mask weak Raman signals which renders Raman spectral acquisition difficult which requires longer acquisition times. Many materials (including the sample itself, the substrate, and the microscope objective) produce a background signal which may mask any weak Raman signals present.[43] Some substrates (especially glass) emit a large fluorescent background signal as the laser moves towards

longer wavelengths, making lasers with shorter wavelengths more ideal.[43, 44] The intensity of Raman is indirectly proportional to the fourth power of the laser wavelength, so shorter wavelengths will be able to produce more intense Raman signals for the same power level.[44] However, many molecules and materials emit fluorescence when excited at shorter wavelengths, which then overpowers the Raman signal.[43] A simple common method to avoid fluorescence is therefore careful selection of the laser excitation wavelength, with lasers with longer wavelengths providing the best results in reducing fluorescence (especially for biological samples).[43–45] For this reason, most of the microparticles in the following chapters were analyzed with the 785 nm laser.[40] Additionally, Raman spectroscopy is sensitive to additive and chemical pigments in microplastics, which interfere with polymer identification.[31] Some fluorescence sources in microparticles can originate from coloring agents, biological material (bacteria, biofilm, algal phaeopigments), or environmental degradation products on the plastic surface.[8, 45–47] In attempts to reduce fluorescence interference in some samples, it was necessary to photobleach or illuminate them with the laser before spectral acquisition. This treatment, however, often caused microparticles degradation and prevented analysis of the polymer.

Commercially manufactured plastics are produced with different additives that can also alter Raman signals.[3] Additives (such as plasticizers, antioxidants, and lubricants) are chemical compounds added to plastics to increase their performance, functionality, and aging properties of the polymers.[48] Similarly, plastic microparticles obtained from the marine environment can have altered Raman signals as a result of weathering, aging, and degradation which can lead to misidentification. In FTIR unique fingerprints were observed when PE pellets exposed to artificial seawater demonstrated the formation of oxidized groups, such as hydroxyls (with peaks around 3300 – 3370 cm^{-1}), carbonyls (1600 – 1630 cm^{-1}), and ethers (1050 cm^{-1}), and higher content of

organic matter.[2] FTIR is the main technique to quantify oxidation, since the oxidation products show extremely weak bands in the Raman spectrum but recently a preliminary database of weathered microplastics revealing that most identifiable peaks can weaken and disappear completely.[49]

A main disadvantage of matching spectra to a library is because standard reference libraries cannot cover the whole variety of particles present in marine samples, both in terms of additives and/or degradation.[3, 49] A recommendation to circumvent this challenge is to further develop polymer libraries and include spectra from degraded polymers in order to increase the possibility of identification of environmentally-exposed microplastics.[37, 50] Additionally, different plastics undergo different degradation pathways making individual studies of plastic types necessary.[36] Challenges in microplastic identification have pushed researchers to call for weathered polymer spectra to be included in polymer libraries.[31, 37, 39–41] Most weathered spectra are included in in-house polymer libraries, but few if any have been included in commercial libraries for widespread use.[51] Considering the many variations of polymer type and weathering environment, it may even be impractical to include all possible weathered spectra for a comprehensive library.

With the increase of environmental pollutions from microplastics it is imperative that scientists have the appropriate tools are equipped with appropriate tools to categorize the pollutants in a timely manner. While some microplastics seem easily identifiable by their colors or obvious resemblance to plastic, many smaller microplastics (that represent much of the microplastic pollution) are indistinguishable to natural particles. As the world continues to use and produce plastic, there is no doubt that microplastic pollution will increase and understanding the fate of microplastics will help the world devise the proper plans for clean-up and prevention.

Chapter 3. Investigations of microplastics in marine organisms

3.1 Microplastics in Pacific oysters

*The work in sections 3.1 has been previously published as an article: *Sci Total Environ.* 715 (2020) 136826; DOI: 10.1016/j.scitotenv.2020.136826

3.1.1 Introduction

Microplastics have been found in ecologically and commercially important bivalves from Europe, Asia, Brazil, Canada, and the United States,[52–55] however, there is a lack of research in the eastern North Pacific, one of the most productive regions in the world and with high potential for marine aquaculture.[56, 57] On the west coast of the United States, two studies have assessed and quantified the presence of microplastics in commercially important bivalves.[54, 56] One study found that 33% of the Pacific oysters sampled in California markets (n = 12) contained 0–2 microparticles per individual.[54] These particles were identified as microfibers using visual sorting but no further analyses were performed to assess their chemical identity. The other study carried out in the Oregon coast found that microplastics were present in Pacific oysters and razor clams, but only 26 of the 2428 microfibers were analyzed with FTIR. In Canada, visual sorting also revealed the presence of microparticles in wild and cultured Manila clams (8–11 particles/clam[58, 59]), oysters, and mussels (5.6–6.57 per gram[53, 59]). Murphy (2018) was the only other study in addition to Baechler *et al.* (2019) that examined the chemical identity of microparticles.[59, 56] Using FTIR analysis, this study showed that only half of the microparticles extracted were synthetic polymers (including plastic). In this context, it is fundamental that microplastic determinations are based on chemically identified polymers, otherwise overestimation of microplastics and misinterpretation of results may occur.[60]

In this study, we examine the presence and distribution of microplastic pollution in the Pacific oyster, *Crassostrea gigas*, an ecologically and economically important shellfish species in Washington State, USA (Figure 3.1.1). As ecosystem engineers, their presence creates a hard-bottom substrate that provides habitat and protection for other organisms. Furthermore, oysters are important food sources for aquatic animals and can filter high volumes of water removing organic and inorganic particles from the water column, resulting in cleaner water.[61] In the Salish Sea and Puget Sound in particular, there are multiple self-sustaining *C. gigas* populations in bays and inlets where the oysters grow either individually or in dense mats on rocks and soft-bottom substrates. Economically, the hardiness and rapid growth (10–15 cm in 2 years) of *C. gigas* are major advantages for the aquaculture industry. Pacific oysters currently lead the production output of the aquaculture industry in Washington State, the top producer of shellfish in the US with around 200 million dollars in sales in 2014.[62] Understanding the abundance and diversity of microplastics in *C. gigas* will help determine if the species is vulnerable to these contaminants and to what degree. Specifically, our goals are to: (i) determine the abundance and type of microplastics in naturally occurring populations of C. gigas in Washington State, (ii) identify the material of these microplastics, and (iii) identify potential areas that are 'hotspots' for microplastic accumulation in Washington State. We hypothesize that microfibers will be the dominant type of microplastics in oysters, and that regions with longer water residence times will have oysters with higher concentration of microplastics due to longer exposure to these contaminants over time. Considering that marine plastic waste is expected to increase,[63–65] this study will contribute to establishing a baseline for the eastern North Pacific, and provide evidence to inform and direct mitigation strategies aimed at aiding in the detection of microplastic sources and the production of healthy shellfish.

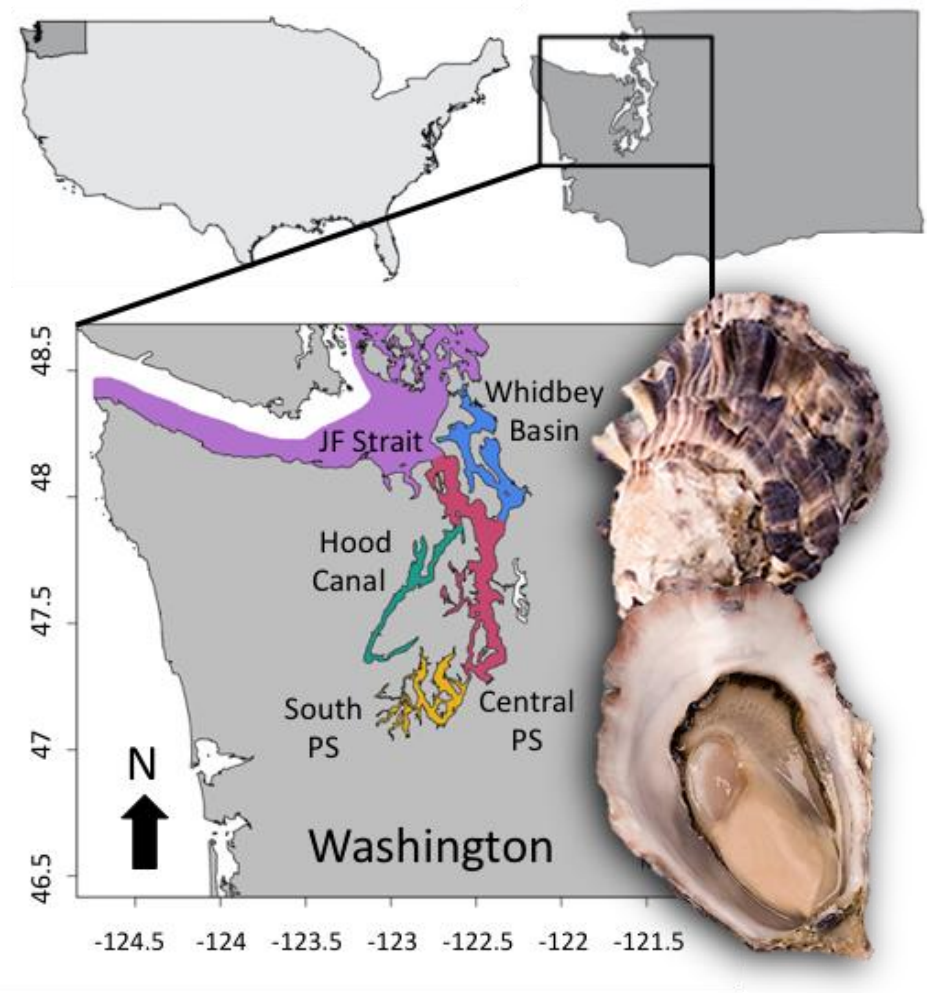

Figure 3.1. 1 Location of Puget Sound and its basins in Washington State, USA. The four basins indicated are Hood Canal in green, South Puget Sound (PS) in yellow, Central Puget Sound in red, Whidbey Basin in blue and the Juan de Fuca Strait (JF) in purple. The image on the right shows the study species, the Pacific oyster, Crassostrea gigas.

3.1.2 Methods

Location and species

The study was performed in Puget Sound in Washington State, the leading producer of farmed bivalves in the United States (Figure 3.1.1). Puget Sound is located in the southern end of the Salish Sea, is the second largest estuary in the country, and is a complex glacial system with four basins that have distinct characteristics due to the degree of water mixing, freshwater influence,

and wind fetch. The sampling sites are located throughout Puget Sound and in the Juan de Fuca Strait to capture the variability in environmental conditions between basins along the estuary (Figure 3.1.1, Table 3.1.1). Sites in Northern Puget Sound often experience shorter water residence times (2 months) than the average for Puget Sound due to their proximity to the Pacific Ocean.[66] In contrast, South Puget Sound has longer water residence times (2–4 months) due to limited water circulation and mixing.[67] Puget Sound estuary is within close proximity to some of the largest cities in Washington State (Seattle, Tacoma and Olympia, Figure 3.1.1) with a population of approximately 3,867,000 people, making it the 14th largest metropolitan area in the United States.[68] Previous studies in the Puget Sound region have found that microplastics are present in sediment and water samples.[69, 70] However, there are no published studies examining accumulation of microplastics in shellfish that naturally grow in the area.

Sample collection and processing

We collected 30 C. gigas individuals during the low tide at ten sites in Puget Sound estuary between January and April 2018 (Table 1, Figure 3.1.1). All collection sites are State Parks or public access beaches with self-sustaining Pacific oyster populations. Within 48 h of collection, we dissected oysters and measured the right and left valves to the nearest mm with a digital caliper. We then removed the soft tissue from the shells, weighed it to the nearest mg with an XS304 Mettler Toledo digital scale, and stored it at -20 °C until the microplastic extraction protocol was performed.

Table 3.1. 1 Sampling sites organized N-S according to the Puget Sound basin where they are located and the Juan de Fuca Strait (see Figure 1). Site coordinates and characteristics of the basins are also included. 'SP' indicates State Park and 'CP' indicates County Park.

Basin	Site	Coordinates	Characteristics
Juan de Fuca Strait	Sequim Bay	48° 2' 26" N, 123° 2' 6" W	Open basin connected to the Pacific Ocean shorter water residence times than average for Puget Sound (approximately 1 month). Sequim Bay is however narrow and north-facing, factors that increase water residence times relative to the rest of the basin.
Whidbey Basin	Samish Bay	48° 35' 23" N, 122° 30' 7" W	Close to Juan de Fuca Strait, shorter water residence times than average for Puget Sound (approximately 1 month)
Central Puget Sound	Heritage CP	47° 50' 24" N, 122° 35' 16" W	This basin includes areas draining into small creeks that flow directly into Puget Sound from Seattle and off Vashon Island. Water residence time approximately 2 months.
	Illahee SP	47° 35' 48" N, 122° 35' 57" W	
	Jacoby SP	47° 52' 7" N, 122° 38' 12" W	
	Mystery Bay SP	48° 3' 34" N, 122° 41' 50'' W	
South Puget Sound	Kopachuck SP	47° 18' 31" N, 122° 41' 16" W	Long, narrow bays, islands and small inlets. Water residence time approximately 2 months.
	North Bay	47° 23' 25" N, 122° 48' 51" W	
	Oakland Bay	47° 13' 29" N, 123° 4' 8" W	
	Penrose Point	47° 15' 32'' N, 122° 44' 54" W	

Tissue digestion and microplastic extraction

We used a standardized extraction protocol developed by Li *et al.* (2015) to extract potential microplastics from oysters.[71] We placed each oyster tissue in a 1 l glass beaker and digested it with 250 ml of 30% hydrogen peroxide in an oscillator (3500VWRAdvanced) at 65 °C for 24 h. In some cases, larger oysters took up to 48 h to be fully digested. During digestion we covered the beakers with aluminum foil to prevent dehydration and airborne contamination of the samples. Each digestion cycle, we processed three samples and a blank extraction control. This number was determined by the maximum number of beakers that fit into the oscillator in the incubator (4 beakers total). We then added 750 ml of 25% saline solution to the digested solution. The water for the saline solution was filtered with a 1.0 μm pore size nuclepore hydrophilic membrane (VWR Whatman). In the saline solution, positively buoyant microparticles floated to the surface while heavier, biotic (undigested tissue), and abiotic (sediment) sank to the bottom. After 24 h, we filtered the solution with 5 μm pore size Whatman nitrate cellulose membrane using a vacuum pump system under a fume hood. Finally, we placed each filter membrane in a labeled and sealed Petri dish and left it to dry for 48 h.

Given that airborne microplastic contamination is very common,[72, 73, 57] we adopted a series of measures to prevent it. In addition to the control blanks throughout the protocol, we rinsed the glass beakers and other lab material with deionized filtered water three times prior to use.[71] To prevent contamination from our own clothing we used a 100% cotton laboratory coat during all experimental procedures and analyses of the filters.[52]

Observation and quantification of microplastics and microparticles

Determination of microplastics was performed using the definition proposed by Frias and Nash (2019).[74] Only synthetic polymers identified by RMS, ATR-FTIR, or μ-FTIR were considered microplastics. Other particles similar in size and visual characteristics to microplastics but with unknown composition are referred as microparticles throughout the manuscript. Once the filters were dry, we visually sorted and enumerated microparticles under a dissecting microscope. Visual sorting is one of the most common ways to quantify and identify potential microplastics, and differentiate morphotypes such as fibers (slender and elongated), spheres (round, similar to a ball in shape), flakes (small and very thin layer of larger plastic debris), and fragments (isolated or incomplete part of larger plastic debris that did not fit any of the previous categories.[75, 55] The dimensions and coloration of the microparticles on the filters were obtained by taking pictures (Nikon Eclipse Ni camera with a 4× objective attached to a dissecting scope) and estimating their length using the open software ImageJ.

D'Agostino test for normality revealed our data was not normally distributed (skew = 2.38, z = 9.21, $p < 2.2e\text{-}16$) Thus, a Kruskal-Wallis rank sum test was used to determine if there were significant differences in oyster weight per site and microparticle abundance between sites. A Spearman correlation test was also used to determine if there was a significant positive association between number of microparticles and oyster weight per site. All analyses were carried out in R Statistical Computing software, version 3.5.3.[76] To account for potential sources of contamination we visually inspected the filters of blank extraction controls, and compared the microparticles found in them with those retrieved in the filters with sample after digestion. If there was an agreement between the type or color of microparticle in the samples, with the ones found in the

controls, these microparticles were not considered towards the total count as they were considered to come from contamination.

Validation of microplastic identity through polymer chemical analysis

After categorizing and measuring microparticles retained in filters we employed RMS and ATR-FTIR to determine the identity of the polymers that make up those microparticles. These non-destructive techniques record the signals absorbed or produced from individual microparticles, and are commonly used for microplastic identification due to their high accuracy in polymer recognition.[77–80] RMS provides information about the structure of a molecule depending on its polarizability, while FTIR identifies the presence of certain functional groups in an organic molecule depending on the molecules' change in dipole moment.[81]

In recent studies, FTIR has been more frequently used for marine microplastic identification than RMS.[37] However, RMS can provide advantages over FTIR such as lower minimum microparticle size identification.[37, 82] In addition, RMS measurements can be done on thicker or strongly absorbing microparticles because measurements do not depend on the transmission of excited light through the sample material.[37] Both RMS and FTIR have limitations in the identification of molecules because of the different approaches used to determine the polymer identity. However, when used in combination they become a powerful tool for polymer characterization.

Across ten locations, we randomly selected 69 oyster samples and 23 controls to analyze by RMS. For each oyster (filter sample) we selected representative microparticles (n =3–10 depending on microparticle density on the filter) of various sizes and shapes and analyzed them using a Renishaw in Via Raman microspectrometer with 785 nm and 514 nm lasers. Two different

objectives (5× and 10×) were used to optimize the analytical laser spot for spectral analysis, and the laser power and acquisition times were varied depending on each microparticle's sensitivity to thermal damage. Then, we individually and manually matched each microparticle's Raman spectrum to a known plastic Raman spectrum in the Renishaw Raman Database of Polymers library, containing 267 polymer entries (Renishaw). Each spectrum was subjected to data processing depending on the signal-to-noise ratio and fluorescent interference (which produces a curved, sloped baseline). Baseline correction allows for the removal of a distorted spectrum before comparing to a known reference spectrum. While some spectra received baseline correction (linear or polynomial baseline correction available in the Renishaw Windows-based Raman environment soft- ware) not every spectrum required baseline correction before library searching. The reference spectrum from the library database matched when all the reference peaks (in wavenumbers) appeared in the sample spectrum. Additional peaks appear in the sample spectrum because of proteinaceous or biological contaminants or effects from environmental degradation. It is important to note that all the spectra present in the polymer library correspond to virgin polymers which have not been subject to any environmental degradation. Comparing spectra between virgin polymers and non-virgin polymers exposed the marine environment can hinder the ability to detect and identify microplastics.

In our samples, physical degradation (such as cracks, color change, or embrittlement) of the microplastics was not observed or quantified visually. However, it is possible that fragmentation, due to physical degradation, occurred as the microplastics identified were all <50 μm in size. For the positively identified microplastics in our samples, the Raman spectrum and all of the major peaks matched the reference spectrum exactly indicating that degradation did not hinder our identification analysis via RMS.[37]

We also used a Bruker Vertex 70 ATR-FTIR to determine polymer identification of 70 filters with samples and 24 filters used as controls. Since the diamond ATR crystal has an area of 4 mm2 and the filters have an area of ~1662 mm^2, each filter was analyzed in two different random areas to confirm that the microparticles were distributed homogeneously in the filter. We first analyzed the control filters to obtain a background spectrum and capture background sources such as light or other residual signals from the atmosphere. Next, we obtained the samples' spectrum and subtracted the background spectrum from the sample's spectrum to obtain the FTIR spectrum which we then matched to an FTIR spectral library. Similar to RMS, the FTIR library contained only virgin polymer spectra.

μ-FTIR was performed on selected individual microparticles from three filters that had confirmed microplastics from RMS to determine if both techniques detected the same contaminants. μ-FTIR was per- formed on 5 μm – 50 μm microparticles with a Thermo Scientific Nicolet iNTM10 FT-IR microscope with a fixed focal length 15× objective. The microparticles were isolated from the filters and, depending on the sample, were analyzed with either micro-ATR or micro-reflection techniques.

3.1.3 Results

Observation and measurement of microparticles

Using a dissecting scope, we counted and measured microparticles from 213 of the 300 oysters collected throughout ten sites in Puget Sound (Table 3.1.2). This difference is due to the fact that several filter had plenty of digested organic matter and we could not process them. Of the 213 filters we were able to process (one filter per oyster), 63% (n = 134) had at least one microparticle visible under the dissecting scope, and in 96% of the cases (n = 129) these microparticles were

microfibers. The rest of the microparticles (4% of the total) were classified as flakes or fragments. For 37% of the filters (n=79) we did not observe microparticles resembling plastic under the dissecting scope. Across all sites, mean microfiber length was 621.93 μm (n = 276), median fiber length was 485.14 μm (n = 276), with minimum and maxi- mum values ranging between 102.45 μm and 2885.49 μm respectively (n = 276).

When grouped per site, the mean number of microparticles per oyster ranged between 0.69 and 3 (Table 3.1.2, Figure 3.1.2A) and there were significant differences between sites (Kruskal-Wallis rank sum test, $\chi 2$ = 32.84, p = 0.0001), where Oakland Bay and Samish Bay had significantly more microparticles than the other sites (Wilcoxon rank sum test, W = 322, p = 0.0099, Figure 3.1.2A). Mean oyster weight per site ranged between 12.23 g to 59.85 g (Table 3.1.2, Figure 3.1.2B). There were significant differences in oyster weights between sites (Kruskal-Wallis rank sum test, $\chi 2$ = 103.07, $p < 2.2^{-16}$), where Oakland Bay oysters were significantly smaller (Wilcoxon rank sum test, W= 101.5, p = 0.0006, Figure 3.1.2B) and Samish Bay oysters were significantly larger than the other sites (Wilcoxon rank sum test, W = 415, $p = 1.41^{-10}$, Figure 3.1.2B). However, overall, the number of microparticles was not associated with the biomass (size) of the oyster (Spearman's correlation, S = 15.983, p = 0.912, Figure 3.1.2C).

In terms of coloration, the majority of the microparticles identified under the dissecting scope were dark (either blue or black), light (yellow, white, silver), clear, red, purple and green (Figure 3.1.3A).

Table 3.1. 2 Number of oysters processed under the dissecting scope and RMS per site. For microparticles identified under dissecting scope we present the mean value of the ones that were visually sorted as microplastics, and the mean value per gram of oyster. For microparticles identified under RMS we present the number of particles analyzed per site and the percentage of those that were confirmed as plastic.

Site	Number of oysters processed	Mean oyster weight	Mean number of particles per oyster (using a dissecting scope)	Mean number of particles per gram (using a dissecting scope)	Particles examined using RMS	Percentage of RMS plastic particles (%)
Heritage CP	20	22.41	2.05	0.09	35	0
Illahee SP	21	28.98	1.71	0.07	28	0
Jacoby SP	23	25.17	0.69	0.03	19	5.3
Kopachuck SP	22	26.66	1.36	0.05	38	0
Mystery Bay SP	21	29.48	0.76	0.02	21	0
North Bay	21	23.48	1.62	0.11	167	2.4
Oakland Bay	21	12.23	3	0.3	42	2.4
Penrose Point SP	24	18.18	2	0.11	40	0
Samish Bay	20	59.85	2.8	0.05	37	2.7
Sequim Bay	20	16.23	1.7	0.14	22	4.5

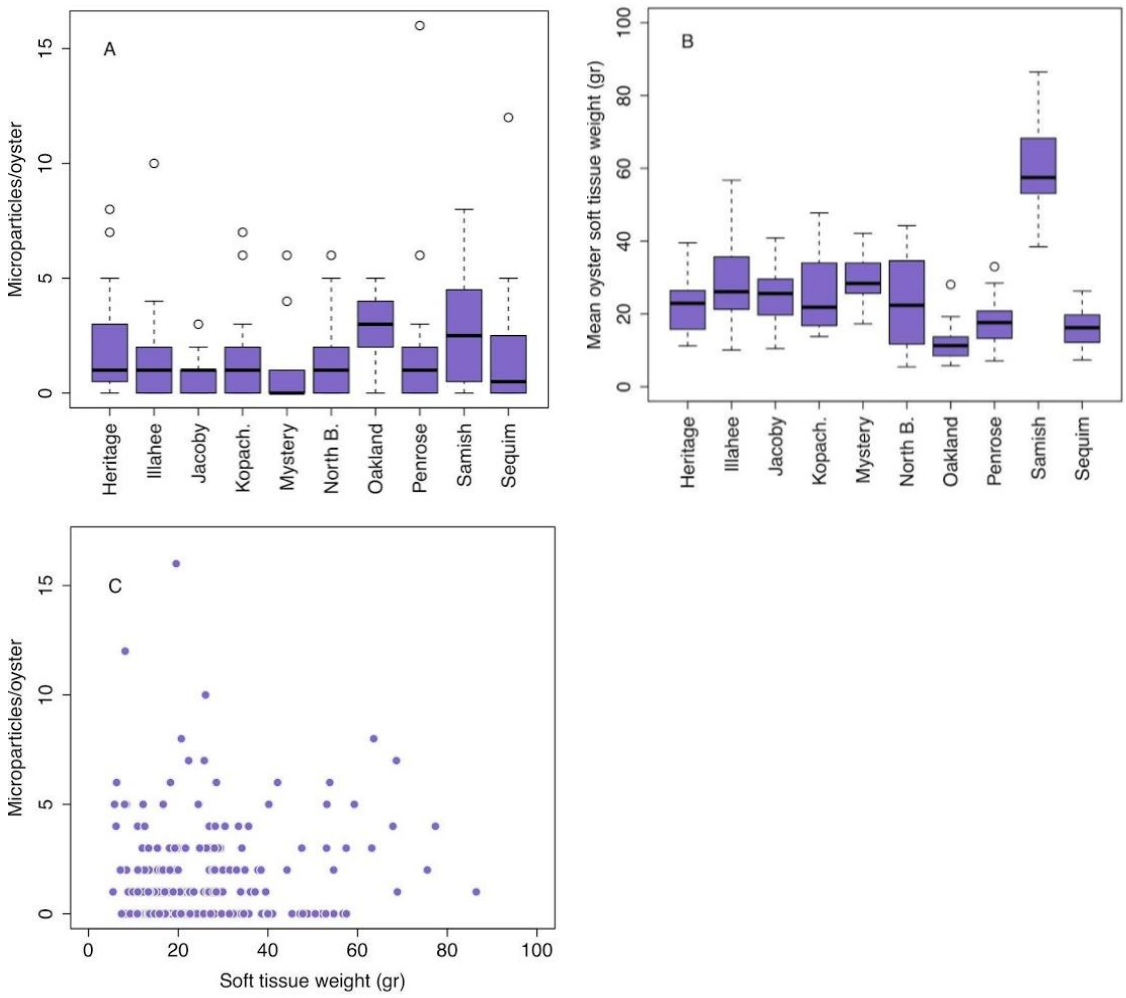

Figure 3.1. 2 Panel showing (A) boxplots with the number of microparticles per oyster that were identified using visual sorting under the dissecting microscope. Site names are organized alphabetically. Thick horizontal lines represent median values per site, boxes enclose the 25th–75th percentiles and whiskers indicate the minimum and maximum values, (B) boxplots showing mean oyster weight per site, (C) scatterplot of the relationship between mean oyster weight and number of microparticles per oyster for all pooled sites. R-squared value for regression: 0.003.

Validation of microparticles through polymer identification analysis

We analyzed a total of 447 microparticles from oyster and control filters using RMS (Appendix A: Supplementary Table 3.1.1). The number of microparticles analyzed per site differed as it depended on the density of microparticles found on each filter. The shapes of the microparticles varied from fiber, shard, irregular, and spheroid with microparticles sizes ranging from 20 µm to

13,000 μm. Out of the 447 microparticles examined, only eight (~2% of the total number of microparticles analyzed) were identified as microplastics (Figures 3.1.4 – 3.1.6, Table 3.1.2, Table 3.1.3). Seven of those microplastics were found in filters with oyster samples and only one microplastic (polystyrene (PS)) was found in one control filter. In the oyster samples, two microparticles were identified as PS, three particles as polypropylene (PP), and two as polyethylene (PE). All of these microplastic samples ranged in size from 50 to 150 μm and the shapes were irregular, spheroid, or shard. In terms of coloration, the majority of the microparticles identified using RMS were clear, light (mostly opaque white), dark (either blue or black), and pink or purple (Figure 3.1.3B).

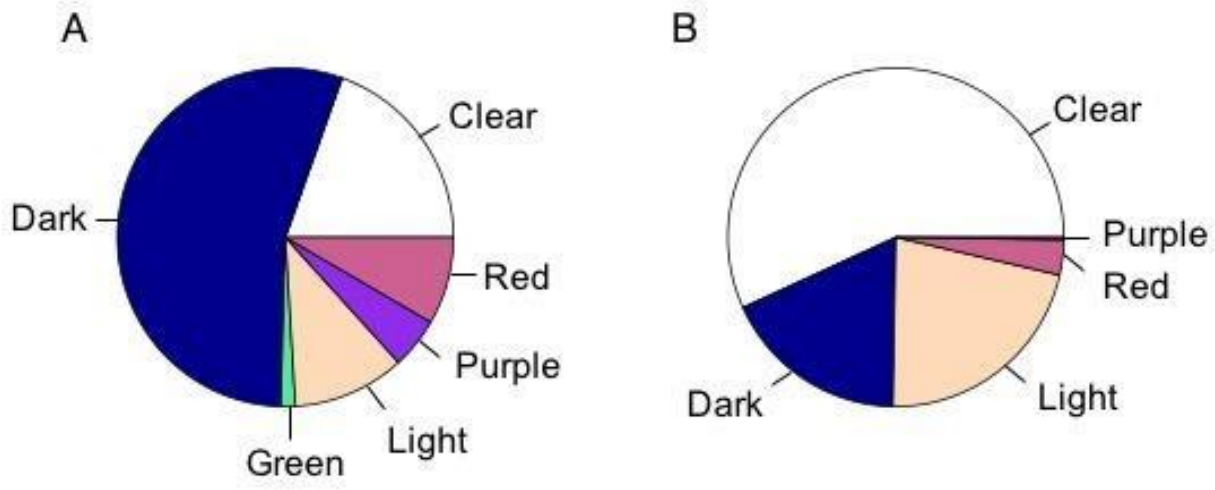

Figure 3.1. 3 Pie charts showing (A) the percentage of different colors observed in microparticles identified as microfibers under the dissecting scope (size ranges: 102 to 2885 μm) and (B) the percentage of different colors observed in microparticles under RMS (size ranges between 20 and 50 μm). In a clockwise direction, 'clear' indicates transparent particles, 'red' indicated red and pink particles, 'purple' indicates violet and purple particles, light indicates white, yellow, silver and amber particles, 'green' indicates greenish particles and 'dark' indicates all particles that were blue, black or dark in coloration.

RMS results showed that 10% (n = 46) of the microparticles that were colorless or opaque, with an irregular or fiber-like shape, were identified as "cellulose", or a mixture of cellulose-derived polymers (Figure 3.1.4). These cellulose-derived microfibers were found on both control

samples and oyster samples, but more predominantly on the control samples and had the same composition of the filter papers used. RMS also identified 18% (n = 81) of microparticles as either poly(ethylene glycol) monooleate or polyamide resin (Table 3.1.3, Figure 3.1.4). Differentiation of these particles were not possible because of a combination of high fluorescence interference and because the spectra for the two polymers are similar.

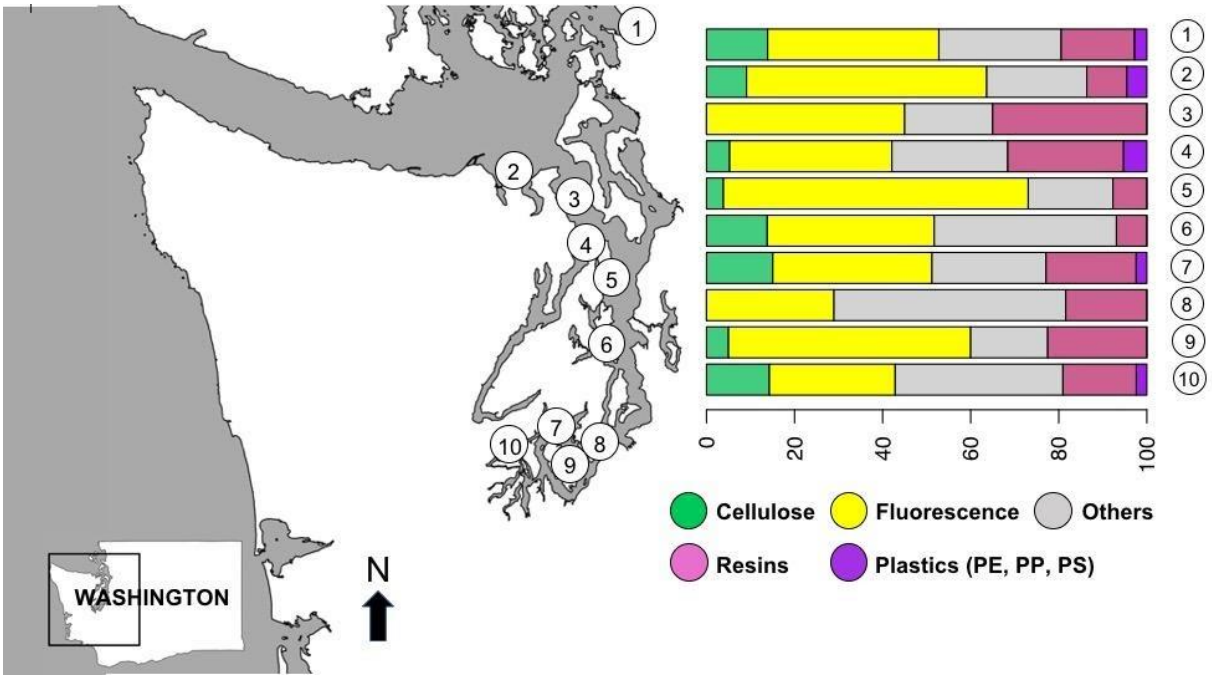

Figure 3.1. 4 Map showing the location of sampling sites (1−10) in the Salish Sea, Washington. Site names are organized N-S as follows: (1) Samish Bay, (2) Sequim Bay, (3) Mystery Bay, (4) Jacoby State Park, (5) Heritage County Park, (6) Illahee State Park, (7) North Bay, (8) Kopachuck State Park, (9) Penrose Point, (10) Oakland Bay. The barplot to the right shows the proportion of different microparticles identified by RMS per site. It is important to note that we did not process 100% of the particles per filter therefore the graph does not represent all the particles that were present, only the ones that were randomly sampled. The number of particles sampled varied per site as it depended on the density of particles per filter (number of microparticles analyzed per site is shown in Table 2). 'Cellulose' are mainly cellulose fibers, 'fluorescence' are unidentified particles due to high fluorescence interference, 'others' are shell particles, grains of sand, and gypsum, 'resins' are polymers such as sorbitan monopalmitate, and 'plastics' are particles that were identified as polyethylene (PE), polypropylene (PP) and polystyrene (PS).

Table 3.1. 3 Number and type of pollutants found per site. The main source of each pollutant is indicated, as well as the method of detection in oyster tissue samples from Washington State.

Pollutant	Possible Sources	No. particles found	Sites	Method used
Polyethylene (PE)	Milk and juice jugs, plastic bags, six pack rings, drinking straws	2	Jacoby SP, Oakland Bay	RMS
Polystyrene (PS)	Plastic utensils, food containers	3	Samish Bay, North Bay	RMS
Polypropylene (PP)	Rope, bottle caps, nettings	3	Sequim Bay, North Bay	RMS
Polyester	Fabrics, fibers and outerwear	1	Oakland Bay	μ-FTIR
Rayon	Semi-synthetic fiber derived from wood pulp	1	Oakland Bay	μ-FTIR
Poly (t-butyl acrylate)	Paints, coatings, adhesives, textiles	1	Oakland Bay	μ-FTIR
Poly (bisphenol A carbonate)	Automotive and transportation, building and construction, packaging, medical, storage devices, interactive software media	1	Jacoby SP	μ-FTIR
Poly(ethylene glycol) monooleate or polyamide resins	Emulsifiers, surfactants, printing inks	81	All sites	RMS
Sorbitan derivatives	Emulsifiers, surfactants	Non-solid polymers (uncountable)	All sites	ATR-FTIR

RMS results showed that 29% (n = 127) of the microparticles surfaces were biological, salt, or mineral in nature. These microparticles were predominantly <75 μm and of various shapes and are labeled as 'others' (Figure 3.1.4). The remaining proportion of the microparticles analyzed, 41% (n=185), contained high fluorescence interference, possibly from a layer of biofilm, and weak Raman signals which prohibited our ability to identify them despite organic matter removal efforts. Based on their RMS spectra, we suspect that some of these microparticles are biological materials (such as protein and carbohydrates), silicates, minerals, or shell fragments, similar to those found by Wagner *et al.* (2017).[33]

Examinations using ATR-FTIR revealed that 100% of the filters examined with oyster samples from all sites (n=71) contained a mixture of sorbitan derivatives such as sorbitan monopalmitate, sorbitan trioleate, sorbitan monolaurate, sorbitan monooleate, or polysorbate (a representative FTIR spectrum of sorbitan monopalmitate is shown in Figure 3.1.7). Sorbitan derivatives were found consistently across the entire filter for all samples. μ-FTIR was performed on selected particles in a small subset of our samples that had microplastics present. μ-FTIR confirmed our RMS results such that the majority of the microparticles were identified as proteinaceous, fatty acid esters, and additionally identified the presence of polyester, rayon, poly(t-butyl acrylate), and poly(bisphenol A carbonate) (Figure 3.1.8, Table 3.1.3).

Due to the small number of microplastics found in this study we were not able to establish any comparisons between sites with different oceanographic conditions. Similarly, the small number of microplastics per site (Table 3.1.2) also limited our ability to determine any hotspots for microplastic contamination in the different basins of Puget Sound estuary.

3.1.4 Discussion

The global demand for plastics has consistently increased over recent years,[63, 83] leading to alarming rates of pollution worldwide.[84] Marine plastics have been estimated to exceed 5 trillion pieces,[85] posing challenges for the health of marine ecosystems and the industries that depend on them. This first baseline of microplastic presence in Pacific oysters from Puget Sound revealed five major findings: (1) ~2% of the microparticles were identified as microplastics using RMS or μ-FTIR, (2) microplastics in oysters were present in five out of ten sites examined, (3) sorbitan derivatives were present in all oyster samples, (4) 41% of microparticles showed fluorescence interference and could not be identified with RMS, and (5) when observed under a dissecting scope, fibers were the most common type of microparticle found, but most of these fibers did not have a plastic composition as indicated by RMS and μ-FTIR.

Particles identified under the dissecting microscope

Oysters from all ten sites had microparticles that were identified mostly as microfibers (96% of microparticles) under a dissecting microscope. Relative abundances of these microparticles varied between sites but mean values ranged between 1 and 4 microparticles per oyster per site (Figure 3.1.2). These findings agree with what has been reported for bivalves from Europe,[52, 86, 87] China,[71, 55, 88] Brazil,[89] Canada,[58] and the United States,[54] among many others. Because visual sorting has limitations for accurate polymer identification, we complemented our observations with three different techniques that allow for polymer identification: RMS, ATR-FTIR, and μ-FTIR.

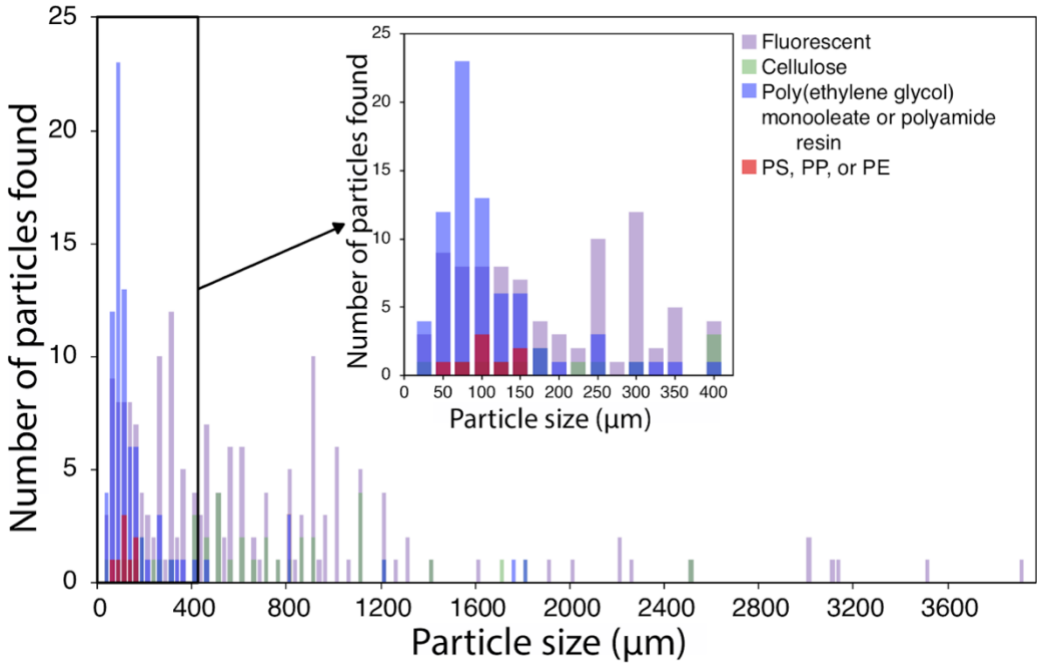

Figure 3.1. 5 Size distribution and identification of microparticles from oyster samples using RMS. Most microparticles ranged between 20 and 50 µm in size. The identity of the particle is color coded according to the key in the top right-hand corner of the image. The darker blue color is an overlap between the blue and pink colors. Polystyrene (PS), polypropylene (PP), and polyethylene (PE) microparticles (in red) were all <150 µm. One 13,000-µm microfiber particle and particles categorized as others (such as gypsum, salt, minerals, or shells) were omitted from the histogram for clarity.

Plastic particles identified using RMS, ATR-FTIR, and µ-FTIR

The majority of microparticles in our study were analyzed using RMS, and this technique was complemented with ATR-FTIR and µ-FTIR for a smaller set of samples. Out of 447 microparticles examined, only eight particles were identified as microplastics by RMS and their spectra matched with PP, PE or PS (Figure 3.1.5 and 3.1.6). These three polymers have been identified in surface waters and sediments in the Atlantic[77,90–92] and North Pacific Oceans,[93] and also in bivalves from China and Europe.[55, 86, 87] PE along with PP are the most commonly used hydrocarbon polymers,[5] and there are many different sources and a wide range of domestic and industrial applications for them.[63, 94] PP for example, is used for rope, bottle caps and nettings.**Error! Reference source not found.** High

and low density PE are used for milk and juice jugs, plastic bags, six pack rings, netting and drinking straws, and PS is used for plastic utensils and food containers.**Error! Reference source not found.**

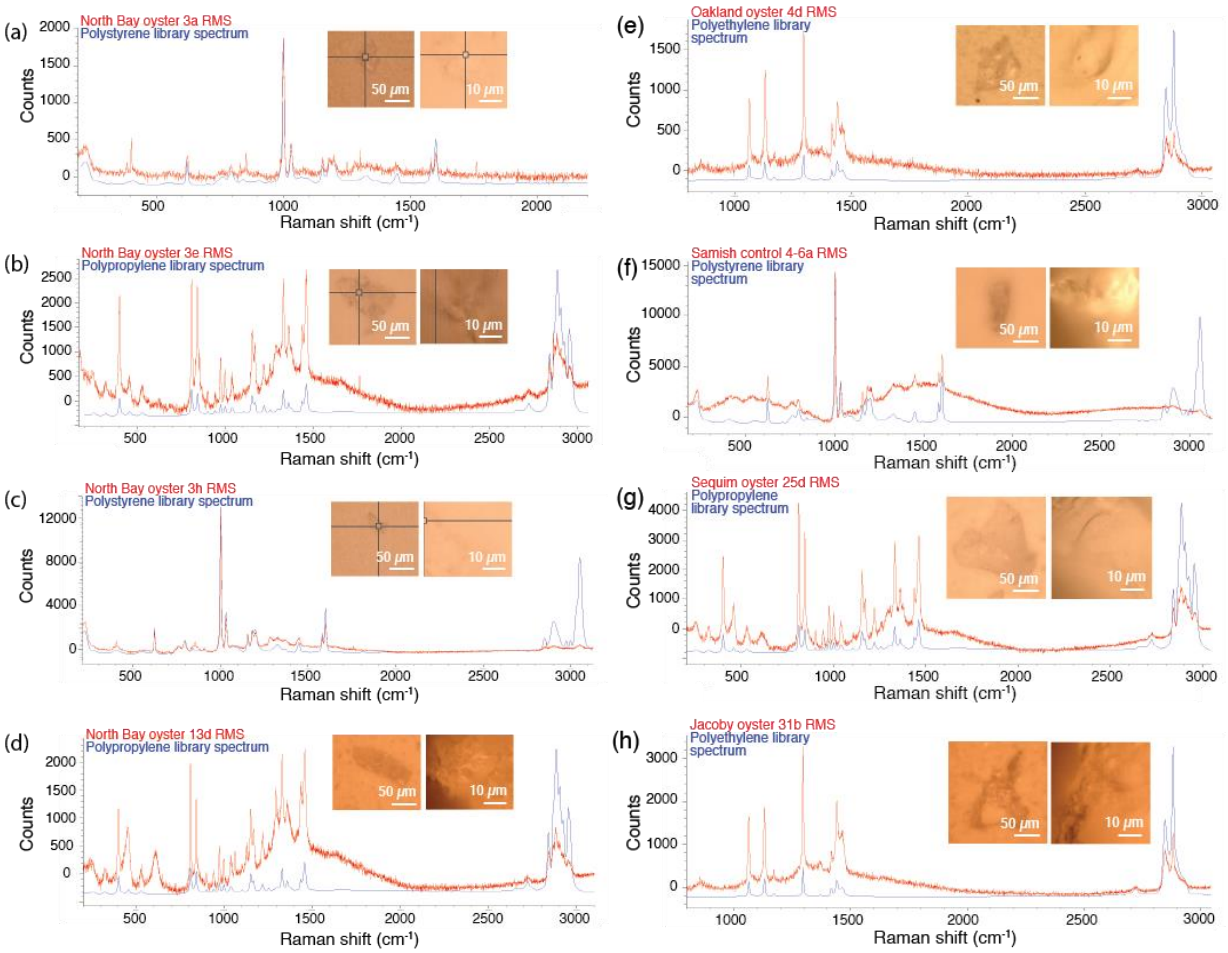

Figure 3.1. 6 Spectra of microplastic particles identified using RMS. Red spectra are the individual plastic RMS spectra and the blue spectra are the reference library spectra. (a) North Bay Oyster 3a is a 75-µm polystyrene shard, (b) North Bay Oyster 3e is a 100-µm polypropylene irregular-shaped particle, (c) North Bay Oyster 3h is 50-µm polystyrene shard, (d) North Bay Oyster 13d is a 150-µm polypropylene spheroid, (e) Oakland Oyster 4d is a 100-µm polyethylene shard, (f) Samish Control 4-6a is a 100-µm polystyrene irregular-shaped particle, (g) Sequim Oyster 25d is a 150-µm polypropylene shard, (h) Jacoby Oyster 31b is a 125-µm polyethylene irregular-shaped particle.

RMS showed that 81 microparticles were either poly(ethylene glycol) monooleate and/or polyamide resin. The similar Raman spectra of these two compounds made differentiation of the exact chemical identification challenging even with samples that have not been exposed to

environmental factors. This challenge coupled with high fluorescence interference and weak Raman signal rendered differentiation impossible for the microparticles analyzed. However, poly(ethylene glycol) monooleate is water soluble and it is likely that this compound was washed away during the sample processing. If this was the case, then the compound in the oyster samples is most likely a polyamide resin. Given that polyamide resins are not ubiquitous or widely used, it is surprising they are found in high abundance in the oyster. If these resins are synthetic in origin they should be considered microplastics,[74] but the resins could also have a natural origin if they are the result of the oxidation of oyster protein by hydrogen peroxide. To test these hypotheses we ran a simple test to determine if the poly- amide resins could be natural in origin by doing the same digestion protocol we used for the oyster samples on an egg. Eggs are also high in protein and are a closed system that should be naturally free of microplastics. The filter resulting from the egg processing was scanned with RMS and the Raman spectra matched the one observed for all the polyamide resin particles found in our samples (Appendix A, Supplementary Figure 3.1.1). While this test is not conclusive, it provides strong support to the idea that these polyamide resins present in every filter can come from oysters instead of synthetic sources. Further, investigations using ATR- FTIR revealed that 100% of the filters with oyster samples from all sites contained sorbitan derivatives. While ATR-FTIR has a penetration depth of ~2 μm, RMS has a penetration depth of 12 μm at 785 nm. Thus, it is possible the microparticles are poly(ethylene glycol) monooleate or polyamide resins coated with sorbitan derivatives.

Both sorbitan derivatives and poly(ethylene glycol) monooleate are most often used as emulsifiers and surfactants.[95] Sorbitan derivatives are not always polymeric (polysorbate being a polymeric sorbitan derivative) and are considered synthetic waxes derived from the dehydration of sorbitol. Sorbitan derivatives such as sorbitan monolaureate, monooleate, and monostearate

are FDA- approved for oral administration up to 25 mg per kg body weight as food additives.[97] In 2018, the European Food Safety Authority re-evaluated the use of sorbitan derivatives as food additives and found that the acute toxicity of these compounds is low, however, more data is needed to decrease uncertainty in exposure assessment.[98]

Other ubiquitous polymers present in the samples were cellulose-derived. It is likely that these polymers originated during the extraction protocol. We used filters that are made up of nitrate-cellulose and it is possible that some degradation occurred during the peroxide treatment that led to cellulose particles in the filters. Future studies could benefit from using other types of filters such as glass filters to solve this. Other cellulose-derived polymers that were identified by RMS included cellulose acetate which are used in cigarette filters, hygiene products, and clothing.[91, 99] This contaminant is usually introduced in marine environments via sewage discharge.[83]

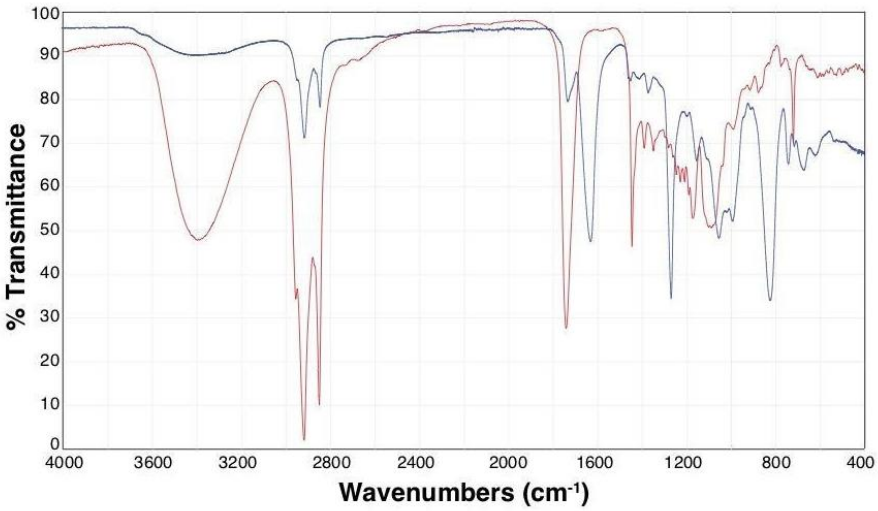

Figure 3.1. 7 FTIR spectrum of North Bay oyster 1 (in red) and FTIR reference spectrum of sorbitan monopalmitate (in blue). This spectrum is representative of the large majority of the spectra observed with FTIR.

Lastly, four additional microparticles were identified as plastics/synthetic polymers with μ-FTIR (Figure 3.1.8). These microparticles came from three of the same filters also used for RMS and were identified as polyester, rayon, poly(t-butyl acrylate), and poly(bisphenol A carbonate). Polyester is a synthetic polymer that is petroleum based and mostly used as fibers used to manufacture fabrics that make up blankets, fleece and other clothing items. Rayon in contrast is considered a semi- synthetic fiber derived from wood pulp. Rayon is mostly used for clothing, and when it is bleached with dioxins to make white clothes it can become toxic. Poly(t-butyl acrylate) is a polymer mostly used in paints, coatings, adhesives, fuel and textiles but there is not enough information available about its toxicity to marine animals. Poly(bisphenol A carbonate) or polycarbonate (PC) is a polymer formed by monomers of bisphenol A carbonate (BPA) and is one of the most widely used thermoplastics.[100] PC is used in a wide range of industrial applications, such as automotive and transportation, building and construction, packaging, medical, data storage, and interactive software media.[101101] Traditional methods of PC disposal (such as landfilling and incineration) are related to the leaching of BPA and PBA products. [101] Previous research has also shown that BPA can be released when polycarbonates are biodegraded by marine microorganisms.[102] PC found in one of the oyster filters warrants some concern as degradation of this polymer to BPA may induce differential effects in the gonads of male and female oysters.[103] BPA has received attention because it is mildly estrogenic[104] and can be an endocrine disruptor toxic to marine organisms.[102]

Methods to identify plastic polymers and associated caveats

Microplastics research is a field that is growing at an exponential pace but there are still several challenges associated with the chemical identification of microparticles. The identification of

polymers is challenging in part due to the large number of mixtures of polymers that are produced by manufacturers today. Therefore, no single analytical approach is perfect to determine the composition of microparticles,[32] and studies aiming to chemically identify microparticles can benefit from using different methods to analyze microplastic composition. This is hard to achieve however, as techniques such as RMS, FTIR, and μ-FTIR require training and expertise to use the equipment appropriately.[57] These methods are also costly and time consuming, particularly in the case of RMS.

Of the three, ATR-FTIR is the least costly and is most suitable to analyze particles that are larger than 100 μm. The caveat of ATR-FTIR is that it can detect materials that are coated on the surface of a sample, but may not identify the underlying material as it only has a penetration depth of ~2 μm. Another disadvantage with ATR-FTIR is that brittle samples can fracture upon contact with the diamond ATR.[33] ATR-FTIR and μ-FTIR use mid-IR light while RMS uses submicron light (usually a laser source) to probe microparticle identities. Therefore, while IR can only identify particles larger than 10–20 μm, RMS has the ability to resolve samples larger than 1 μm.[105] Both μ-FTIR and RMS require low amounts of sample, can identify particles with minimal sample preparation, and distinguish be- tween plastics and natural particles from marine organisms or soil. [105] Compared to Raman, FTIR has been around longer and the technology has evolved with the polymer industry. Thus, there is a greater abundance of historical IR spectroscopic data for polymer analysis and thus more available reference spectra for microplastic identification.[8]

There are also different caveats that need to be taken into account for each technique, such as the issue of fluorescence interference with RMS.[8] In our study, almost 41% of the microparticles analyzed showed high fluorescence and this limited our ability to detect the RMS signal and identify the composition of the particles. Thus, it is likely we may have underestimated the amount

of microplastics present in the samples. The sources of fluorescence in microparticles can be many. Coloring agents, biological material, or degradation products

From from the environment can attach/adsorb to the plastic particles and influence their spectra. Many colorants such as pigments and dyes strongly fluoresce in visible light and can also hinder the acquisition of spectra, while inorganic pigments are more likely to change the pattern of peaks that are displayed.[106] Bacteria present in biofilm[45, 107] and algal phaeopigments[46, 47] can also be major contributors to fluorescence. To reduce fluorescence interference in some of our samples, it was necessary to bleach or illuminate them with the laser before spectral acquisition. This treatment, however, occasionally led to microparticles degradation.

Another caveat is additive compounds included to the basic polymer matrix when commercial plastics are manufactured.[37] These added compounds can alter the reading of the plastic polymers by RMS. Similarly, plastic microparticles obtained from the marine environment can have altered chemical fingerprints as a result of weathering. [37] These alterations can sometimes lead to a falsified polymer type signal and misidentification.[37] This issue has been mentioned as one of the main drawbacks of matching spectra to a library because reference libraries cannot cover the whole variety of particles present in marine samples, both in terms of additives and/or degradation.[37] As this challenge begins to be recognized, several authors have recommended that spectra from degraded polymers are also included in polymer libraries in order to increase the possibilities of identification of microparticles that have been exposed to environmental conditions. Lenz *et al.* (2015) showed for example, that PVC can be degraded to a point where successful identification is not possible if using a virgin PVC reference. Similarly, when exposed to artificial seawater, PE pellets undergo considerable structural modifications as a result of the formation of new functional groups in the polymer that ultimately yield polymers with a distinct composition.[5]

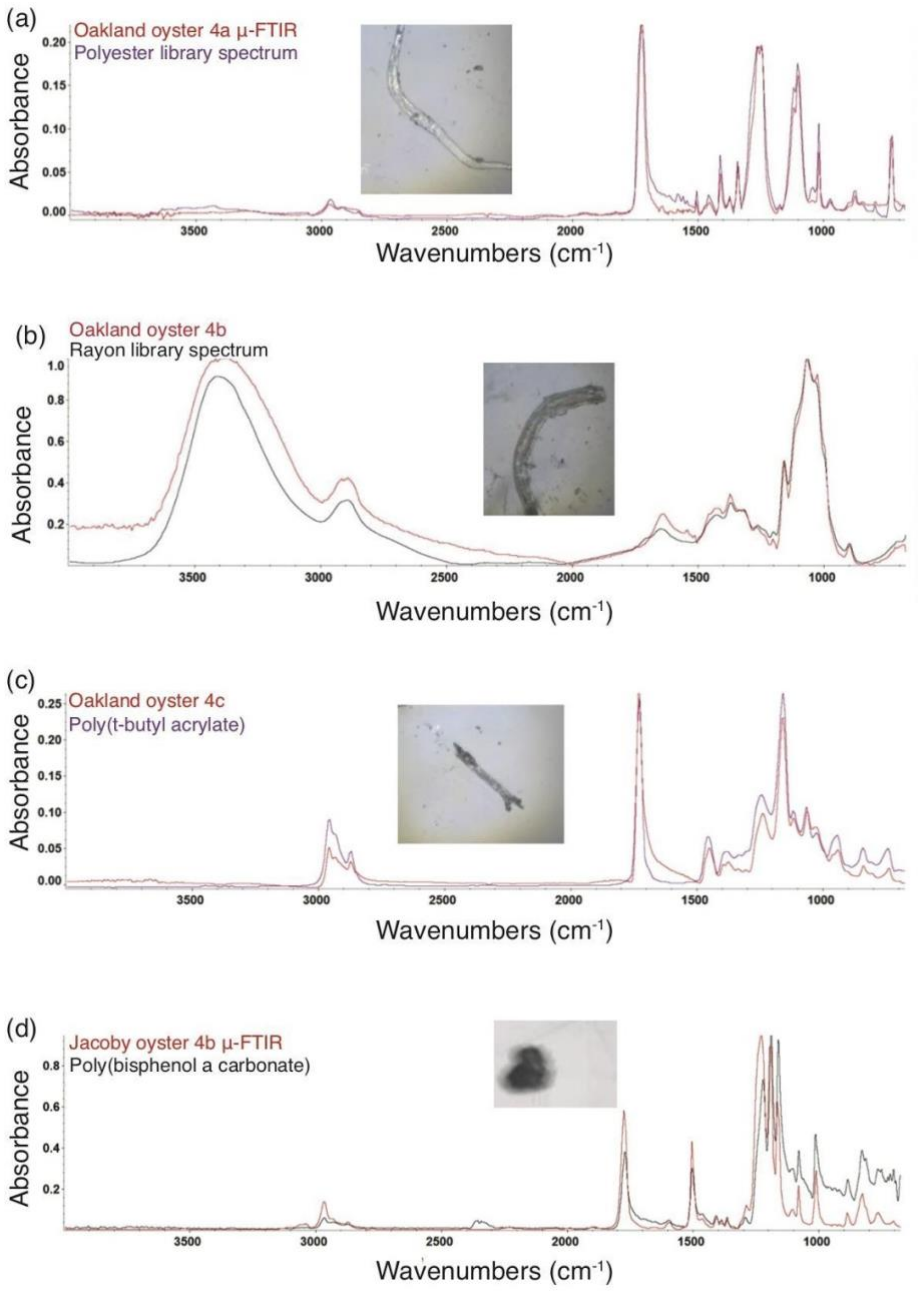

Figure 3.1. 8 Microplastic particles identified from three filter samples using µ-FTIR. Red spectra are the individual microplastic µ-FTIR spectra and the purple or black spectra are the library reference spectra. (a) Oakland Oyster 4a is a polyester fiber, (b) Oakland Oyster 4b is a rayon fiber, (c) Oakland Oyster 4c is a poly(t-butyl acrylate) irregular-fragment, (d) Jacoby Oyster 31a is a poly(bisphenol A carbonate) particle.

3.1.5 Conclusions

The findings presented here indicate that visual sorting should not be assumed to be a reliable method for microplastic identification. Over 60% of the oysters analyzed had microparticles that looked like microplastics however only 2% of the microparticles observed were confirmed to have a plastic composition. Our research further shows that Pacific oysters from Puget Sound in Washington State, USA, are not accumulating large amounts of microplastics, on the contrary, we have no evidence to support the idea that there is more than one microplastic per oyster. As pointed out previously, 41% of the samples were covered with fluorescent material and the methods have caveats to consider, but based on the 60% of the samples that were identifiable, the presence of microplastics is very low. This does not undermine in anyway the seriousness and emergency of plastic contamination in marine environments and its effects on marine biota. This research instead provides the first baseline value for microplastics in Pacific oysters from Washington State based on three different techniques - in addition to visual sorting. Information from this first baseline study will give ecosystem managers, the aquaculture industry, and the general public an important indicator of bivalve health. This pioneer contribution can be considerably improved by analyzing more of the oyster samples with μ-FTIR, by managing fluorescence interference under RMS, and using additional chemical identification techniques. Having a more comprehensive dataset of results as well polymer libraries with spectra of polymers that were exposed to the environmental degradation, will allow scientists to identify with more accuracy the types of microplastics, resins, additives, and other contaminants present in marine organisms.

Supplementary data to this article can be found in Appendix A.

3.2 Microplastics in Mussels

*The work in sections 3.2 will be submitted as an article in September 2021.

3.2.1 Introduction

Due to their small size and ubiquity, organisms from multiple functional groups including suspension feeders, planktivores, detritivores, and carnivores, ingest MP in laboratory experiments and in natural habitats.[108–112, 20, 52] Of these, suspension feeding bivalves are documented to ingest the highest amount of MP.[113] Microparticles can negatively impact physiology (e.g. immune response, reproduction, feeding rate) in marine organisms and can subsequently have ecosystem-level impacts.[114–118]

In coastal environments, suspension-feeding bivalves, such as mussels, have historically served as bioindicators to detect pollution[119–122] and can be used as a biological metric of stressful environmental conditions.[123] Mussels are known to sequester pollution and toxics from surrounding water, making it relatively easy to analyze water contamination levels through mussel tissue samples.[122] Further, mussels act as benthic-pelagic couplers for MP particles, concentrating planktonic particles into biodeposits that are dense and nutrient rich, linking bottom substrate (benthic) to the water column (pelagic; Harris *et al.*).[124]

High concentrations of MP are likely released to the waterways in densely populated urban centers than less populated regions (e.g. Miller *et al.*). [26] However, it is not only population density that contributes to high MP concentrations. Microparticles may accumulate in basins with long residence times (or water that tends to be stagnant) and disperse in fast moving water.[27] Further, marine environments are dynamic and fluctuate spatially and temporally, as waters are continually changing with the tides, currents, and fluvial inputs.[125] Understanding biologically available MP

concentrations in respect to population densities and water residence times may provide insight to current pollution status and how ecologically and economically important species may be affected in the future.

Microparticle concentrations vary broadly in the northeast Pacific Ocean between Washington State and British Columbia, ranging from 0.26 – 9,200 particles m^{-3}.[126, 127] The Salish Sea, located in Western Washington State and Southwestern British Columbia, is a large estuary, receiving freshwater inputs from large rivers (e.g. Duwamish and Frasier Rivers), seawater from the Pacific Ocean, and includes multiple water basins with varying water residence times. The Salish Sea contains the Port of Seattle (one of the largest container terminals of the West Coast of the US; Port of Seattle) and is adjacent to several large cities including Tacoma and Seattle, Washington and Victoria and Vancouver, British Columbia. These hubs of human activity threaten its position as a crucial biodiversity hotspot and "hope spot" (area of ecological importance flagged for protection under a global conservation campaign by Mission Blue).

To understand MP concentrations in marine environments, the majority of MP studies focus on water and sediment, which are thought to reflect transient (in the habitat for a short amount of time) and terminal (in the habitat for a long amount of time) concentrations, respectively. To accurately measure MP contamination in water, large volumes must be sampled, which can be resource prohibitive (e.g. access to boat or large volume seawater pump, funding, etc.), adding a level of inaccessibility for many researchers. Sediment on the other hand, is thought to be the eventual resting place for the majority of MP due to vertical transport and biofouling,[91, 10, 128] containing relatively high concentrations of MP. Small volumes of sediment can be analyzed to accurately measure MP concentration, however, many benthic habitats are difficult to sample and are inaccessible to researchers as well. Water and sediment sampling present two approaches to

measure MP concentrations at transient and terminal time points, however, can be resource restrictive and do not address medium-term, or biologically available, concentrations.

Mussels present a way to measure medium-term and biologically available MP concentrations in the water column, where particles that are filtered and ingested by mussels are processed over an average of 18 – 84 h period.[129] The quantity of water filtered and duration of MP processing in mussels allows for the collection of samples representing vast areas affected by MP pollution, potentially eliminating the need to sample impractically large volumes or difficult to collect environmental material. Taken together, mussels' ability to sequester particles and toxics relative to their environmental contamination, role as bioindicator, and wide-spread availability suggest mussels are an advantageous organism to measure MP concentration at both regional and local scales, and further understand MP contamination levels biotically available to organisms.

Quantifying spatial patterns of MP contamination is pertinent to both current and future water conditions in an economically and ecologically important region. As of 2021, there is a limited number of published studies examining spatial MP concentrations in water (3), sediment (1), and organisms (5) in the Salish Sea.[130–133, 127, 126, 40, 134] In the Salish Sea it is important to understand spatial MP concentrations to inform management plans, aquaculture, and remediation efforts. Further, the Salish Sea presents an opportunity to study MP concentrations near and far to urban centers like Seattle, WA and Tatoosh Island, respectively, as well as across multiple basins with differing water residence times in the same region.

In this study, we compare mussel MP concentrations across 10 regional and 5 localized sites in the Salish Sea, ranging from highly urbanized areas (Tacoma and Seattle) to rural areas (Tatoosh Island). Our research goals were two-fold: 1) Determine if mussel MP concentration and

type differs at regional and local scales and 2) Assess if mussel MP contamination is dependent on factors such as population size or basin residency time.

3.2.2 Methods

Field Collection

Pacific blue mussels, *Mytilus trossulus* (shell length of 45 ± 5 mm), were collected from 10 locations with 15 total sites across the Salish Sea, Washington State, USA (Table 1). Mussels from Tatoosh Island sites (Main Beach, Strawberry Draw, Simon's Landing, Glacier, and North Island) were collected May 2019 and mussels from all other sites were collected July – September, 2018. Mussels were collected from marinas when possible, from either the public boat launch or furthest pier from shore. Mussels from Tatoosh Island were collected from the intertidal during low tide as there is not a marina or boat launch. Moving from the South through the Salish Sea and out to the Pacific Ocean, sites were: Tacoma, Seattle, Kingston, Mukilteo, Coupeville, Anacortes, Friday Harbor, Port Townsend, Port Angeles, Neah Bay, and Tatoosh Island, containing Main Beach, Strawberry Draw, Simon's Landing, Glacier, and North Island (Figure 3.2.1; Table 3.2.1). Mussels were transported from the field to a laboratory at University of Washington, Seattle campus, in acid-washed glass jars.

Table 3.2. 1 Sampling site locations and metadata organized from South Salish Sea towards the Pacific Ocean. Site coordinates (decimal), basin residence time, nearby urban population and size, and number of slips are included. Basin and basin residence times were collected from Sutherland et al. 2011, Martinelli et al. 2020, and Macready et al. 2021.

Basin/Strait/ Watershed	Site	Location	Coordinates	Basin residency time	Nearby urban population	Urban population size	Number of slips
South Puget Sound	Tacoma	Marina at Browns Point	47.295640, -122.416494	1-4 months	Tacoma	209,100	140
Central Puget Sound	Seattle	Shilshole Bay Marina	47.686899, -122.403906	2-5 months	Seattle	730,400	1432
Central Puget Sound	Kingston	Port of Kingston	47.796011, -122.499626	2-5 month	Kingston	2472	312
Whidbey Basin	Mukilteo	NOAA pier	47.949829, -122.302254	1-2 months	Mukilteo	21,320	0
Whidbey Basin	Coupeville	Coupeville Warf	48.222695, -122.687921	1-2 months	Coupeville	1,905	10
San Juan Islands	Anacortes	Cap Sante Marina	48.511972, -122.609556	2-5 months	Anacortes	16,990	466
San Juan Islands	Friday Harbor	Argyle Lagoon boat launch	48.519474, -123.013520	2-5 months	Friday Harbor	2,345	0
Juan de Fuca Strait	Port Townsend	Port Townsend Boat Haven	48.106768, -122.773836	2 months	Port Townsend	9,545	413
Juan de Fuca Strait	Port Angeles	Port Angeles Yacht Club	48.128097, -123.456853	2 months	Port Angeles	19,370	500
Juan de Fuca Strait	Neah Bay	Makah Tribal Marina	48.366488, -124.610993	2 months	Neah Bay	912	200
Pacific	Strawberry Draw	Tatoosh Island	48.392095, -124.738101	2 months	Neah Bay	912	0
Pacific	Glacier	Tatoosh Island	48.391912, -124.740982	2 months	Neah Bay	912	0
Pacific	North Island	Tatoosh Island	48.394774, -124.734938	2 months	Neah Bay	912	0
Pacific	Main Beach	Tatoosh Island	48.391184, -124.732663	2 months	Neah Bay	912	0
Pacific	Simons Landing	Tatoosh Island	48.393349, -124.735385	2 months	Neah Bay	912	0

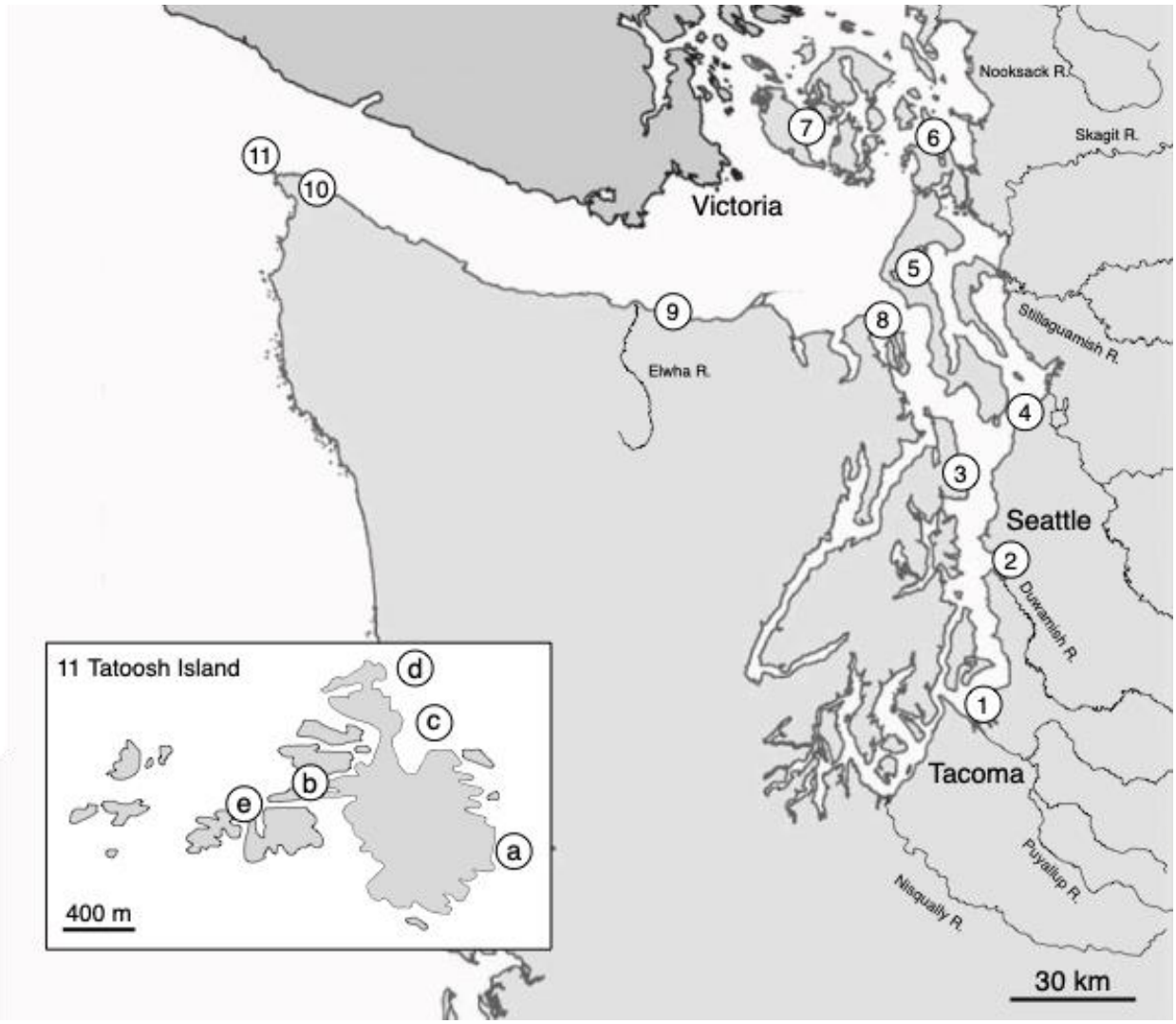

Figure 3.2. 1 Map of the Salish Sea, Washington, showing sampling sites (1 – 11). The site names from the South towards the Salish Sea are as follows: (1) Tacoma, (2) Seattle, (3) Kingston, (4) Mukilteo, (5) Coupeville, (6) Anacortes, (7) Friday Harbor, (8) Port Townsend, (9) Port Angeles, (10) Neah Bay, and (11) Tatoosh Island containing five sites: (a) Main Beach, (b) Strawberry Draw, (c) Simon's Landing, (d) North Island, and (e) Glacier.

Tissue Digestion

Ten mussels from each site were chemically digested and analyzed for microparticle (MP) contamination. Mussel shell lengths were measured, byssal threads were removed, and body tissue was extracted from the shell and placed in aluminum weigh boats and immediately covered with

aluminum foil to reduce contamination. Mussel tissues were weighed for wet weight (g) prior and subsequently transferred to 1 L glass flasks for chemical digestion.

To digest mussel tissue, a standardized wet oxidation extraction protocol[71] adjusted to the wet weight of mussel tissue was used. Each flask contained one mussel and 100 ml 30% H2O2 and was covered with aluminum foil to prevent contamination. Flasks were placed in an oscillating incubator at 65 ºC for 24 hours. Once mussel tissue was observed as dissolved (100% of samples after 24 hours), 400 ml of hyper-saturated salt solution (1.2 g cm^{-3}) was added and flasks stood at ambient room temperature for an additional 24 hours. Particles with a density greater than 1.2 g cm-3 sank while particles less than 1.2 g cm^{-3} floated to the top. Once samples settled with the hyper-saturated salt solution for 24 h, the top 200 ml of solution was vacuum filtered over a 5 µm cellulose nitrate membrane filter inside a fume hood. Each filter was subsequently rinsed with 50 ml DI water to clean the sides of the funnel as well as wash away remaining H_2O_2. Filters were placed in sterile petri dishes and sealed with Parafilm. Filters were left to dry for at least seven days before visual quantification.

Contamination prevention and control

To reduce ambient MP contamination, all equipment underwent extensive cleaning prior to sampling and processing. All glassware was acid washed (1 M HCl) and triple DI water rinsed before use and was covered with aluminum foil at all times. Researchers wore white 100% cotton lab coats in the lab at all times when processing samples. A paired process control with no mussel accompanied each set of digestions. A clean filter (in an open petri dish) was placed on the lab counter while processing samples to control for ambient MP that were present in the air.

MP Visual Quantification

Dry filters were examined under a compound microscope for particles. All particles were photographed using a Nikon Eclipse Ni camera and either the 4× or 10× objective. The scaled photos were processed with the software ImageJ. The particles were analyzed for length, width, morphotype (fiber, fragment, film, or sphere), and color. Length was measured as the longest dimension, with width being the next longest dimension. Measurements were made using the freehand line feature of ImageJ. The four morphotypes and color of debris were classified based on appearance. Particle color was recorded as the primary color found on the majority of the particle (some particles had multiple colors, but only one color was recorded for the purpose of analyses). Rare colors (<1% of total observations) were categorized as "other."

Polymer Identification

Plastic and organic particles can only be differentiated and identified by chemical identification. Chemical analysis was completed on 35 (10%) individual MPs found on the filter papers with a Renishaw inVia Raman microspectrometer equipped with a 785 nm laser. Two objectives, 10× and 50×, were used to optimize the analytical laser focus for analysis, and the laser power and acquisition times were varied depending on each particle's sensitivity to thermal damage. Following imaging, each MP's Raman spectrum was individually and manually matched to a known plastic Raman spectrum in the Renishaw Raman Database of Polymers library, containing 267 polymer identifications. Each spectrum was also subjected to data processing depending on the signal-to-noise ratio and fluorescent interference (which produced a curved, sloped baseline). Baseline correction allows for the removal of a distorted spectrum before comparing the sample spectrum to a known reference spectrum. A match was determined when all the characteristic

Raman peaks, corresponding to the main active functional groups in the polymer appeared in the sample spectrum.

Data Analysis

All data analyses and graphs were made with computing software R for Mac OS X (version 3.6.2, R Core Team, 2019, Dark and Stormy Night). Level of significance was set at $\alpha < 0.05$. Mussel contamination (MP g^{-1} wet mussel tissue) was not normally distributed and homogeneity of variance was not confirmed, as determined by Bartlett and Shapiro-Wilks tests, respectively. The effect of site on the proportion of mussels containing MP was evaluated with a generalized linear model (GLM) with a binomial distribution. The effect of site and basin were evaluated with the Kruskal-Wallis rank sums test, a non-parametric test. Differences in mussel MP concentration between sites and between basins were evaluated by pairwise post-hoc tests (Mann-Whitney test). The effect of site on mussel MP concentration and fiber length was evaluated with a Kruskal-Wallis rank sums test, a non-parametric test. Multivariate analyses of variance (MANOVA) was used to evaluate the effect of site on particle morphotype and color composition.

3.2.3 Results

The proportion of mussels containing microparticles (MPs) was not dependent on site, nor was there a difference in the proportion of mussels containing MPs compared to control filters ($p < 0.05$; GLM). Microparticles were found in 63% of mussels sampled, where Glacier and Simon's Landing (Tatoosh Island) had the fewest and Mukilteo had the most mussels containing MP (30% and 100%, respectively; Figure 3.2.2). A similar proportion of MP was found in controls where 82% of process control filters and 98% of ambient control filters contained MPs.

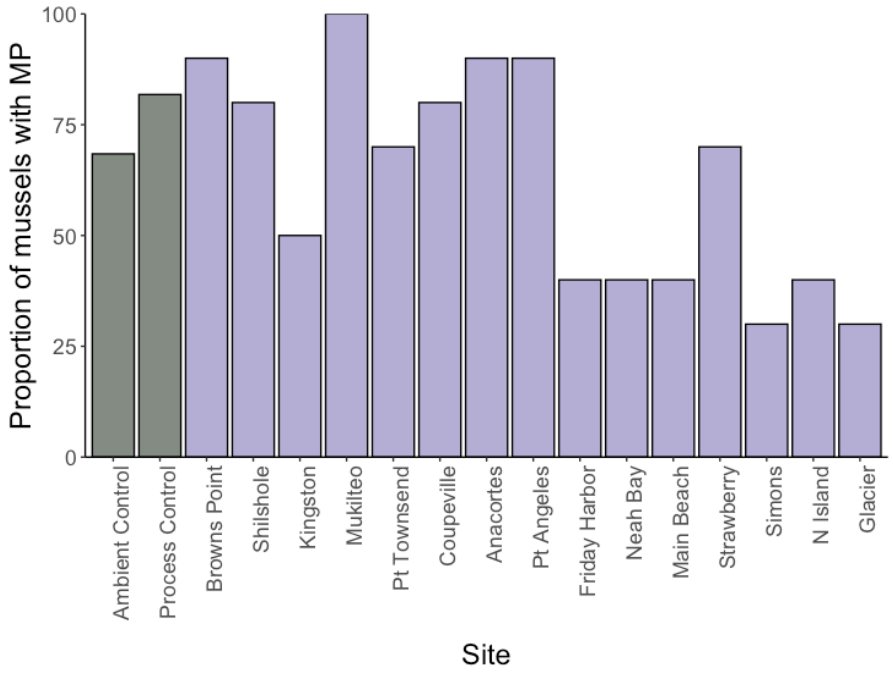

Figure 3.2. 2 Proportion of mussels containing MP at each site, from South Salish Sea on the left, moving towards the Pacific Ocean on the right. Grey bars represent control filters and purple bars represent sampling sites.

Microparticle concentrations ranged 0 – 12 per mussel and 0 – 6 MP g^{-1} wet tissue across the Salish Sea (Figure 3.2.3). Mussel and control filter MP concentrations were dependent on site ($p = 2.98 \times 10^{-8}$; Kruskal-Wallis; Table 3.2.2; Figure 3.2.3) where mussels from Coupeville had the highest concentration, with an average of 2 MP g^{-1} wet tissue and mussels from Tatoosh Island sites (Main Beach, Strawberry, Simons, North Island, and Glacier) had the lowest concentration, with averages ranging 0.11 – 0.48 MP g^{-1} wet tissue. All five Tatoosh sites had significantly fewer MP than the process controls (and were the only sites to do so; $p = 0.01 – 0.02$; Mann-Whitney test). Mussel MP concentration was dependent on which basin ($p = 1.44 \times 10^{-6}$; Kruskal-Wallis; Figure 3.2.4a) and number of dock slips in the marina mussels were collected from ($p = 0.04$; ANOVA; excluding largest marina; Table 3.2.2; Figure 3.2.4b).

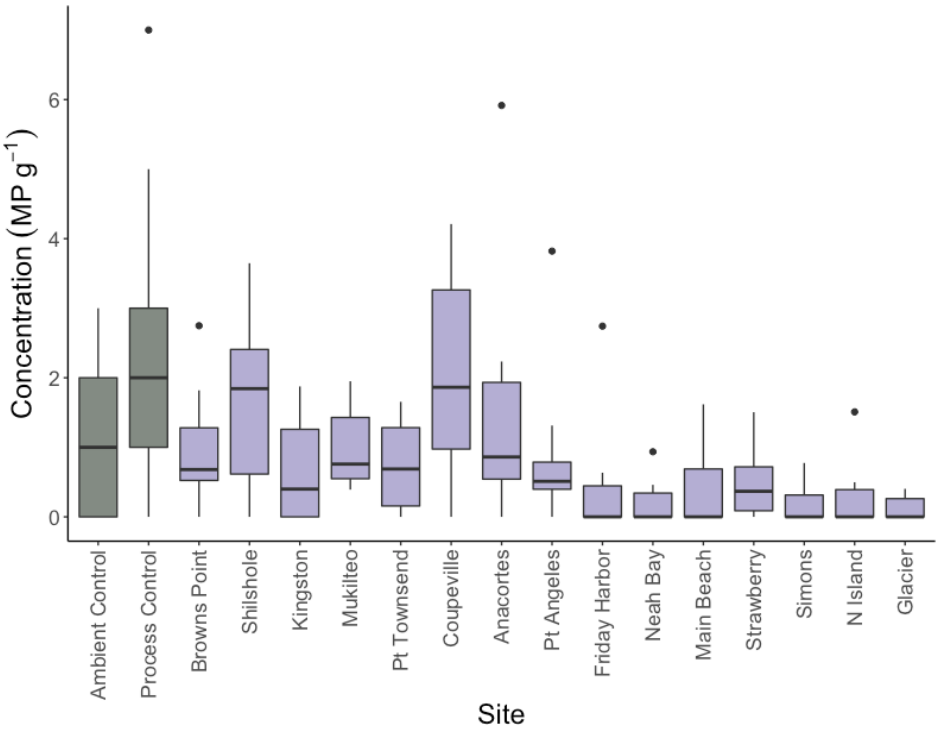

Figure 3.2. 3 Mussel microparticle contamination (MP g^{-1}) at each site, from South Salish Sea on the left, moving towards the Pacific Ocean on the right. Grey bars represent control filters and purple bars represent sampling sites. Boxes represent upper and lower quartiles and dots represent outliers; solid lines within boxes represent median values.

Table 3.2. 2 Kruskal-Wallis rank sum test on mussel MP concentration (MP g^{-1} wet tissue) across sites and basins. Summary table for analysis of variance (ANOVA) on mussel MP concentration (MP g^{-1} wet tissue) across number of slips in the marina or site where mussels were collected. Bold type and asterisk (*) indicates statistical significance ($p < 0.05$)

A)

Variable	X^2	**df**	**p-value**
Site	**67.3**	**16**	**< 0.0001***
Basin	**32.79**	**5**	**< 0.0001***

B)

Variable	**df**	**Sum sq**	**Mean Sq**	**F value**	**p-value**
Slips	**1**	**4.11**	**4.11**	**4.28**	**0.04***
Residuals	118	113.13	0.959		

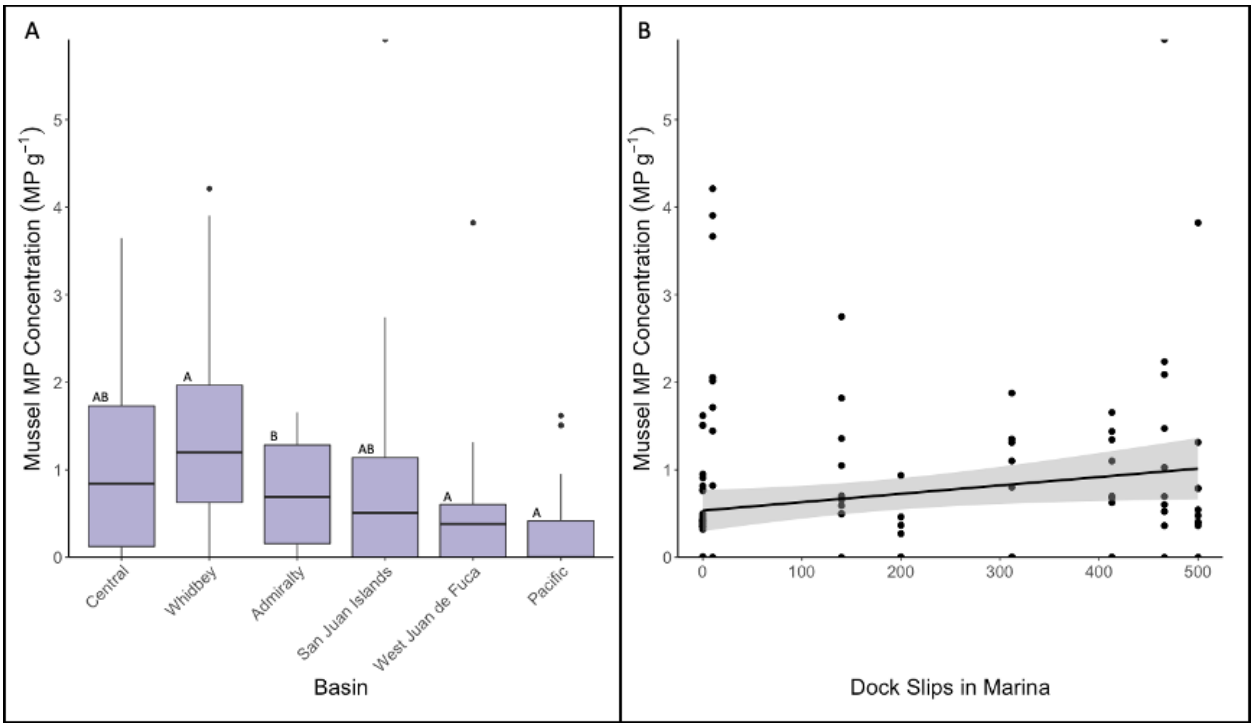

Figure 3.2. 4 Mussel MP concentration (MP g^{-1}) with respect to A) each basin and B) the number of docks in a marina.

The proportion of MP morphologies found in mussels differed by site (p = 6.7×10^{-5}; MANOVA; Figure 3.2.5A; Table 3.2.3). Specifically, fibers, films, and fragments were significantly different between sites (p = 0.0002, 0.017, 0.007, respectively; MANOVA). Fibers were the dominant morphotype, accounting for 42–100% of total MP morphologies at each site. Fiber lengths averaged 587 ± 37 μm (mean ± standard error) and did not differ across sites (p = 0.1; Kruskal-Wallis; Figure 3.2.6; Table 3.2.4). The proportion of MP colors color found in mussels differed by sites (p = 0.0001; MANOVA; Figure 3.2.5B; Table 3.2.3) where blue, clear, and "other" colored MP proportions were significantly different between sites (p = 0.03, <0.0001, 0.005, respectively; MANOVA). Blue and clear-colored MP accounted for 13–67% and 30–75% of colors observed at each site, respectively.

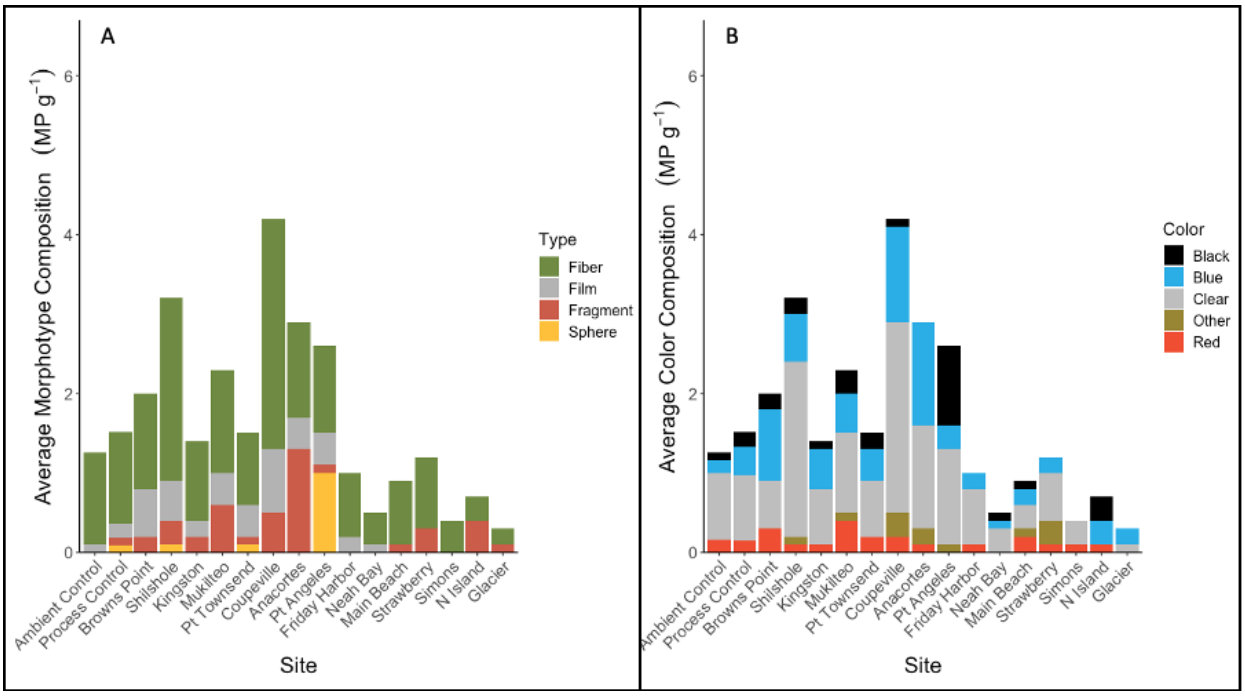

Figure 3.2. 5 Composition of average microparticle A) morphotype and B) color composition per gram of wet mussel tissue (MP g^{-1}) across sites. The first two bars on the left of each graph represent ambient and process control filters. Sites are ordered from the South Salish Sea on the left, moving towards the Pacific Ocean on the right.

Table 3.2. 3 Multivariate analysis of variance (MANOVA) on microparticle morphology and color composition across sites. Bold type and asterisk (*) indicates statistical significance ($p < 0.05$).

Variable	**df**	**Num df**	**Den df**	**p-value**
Morphology	**16**	**64**	**740**	**< 0.0001***
Residuals	185	–	–	–
Color	**16**	**80**	**925**	**0.0001***
Residuals	185	–	–	–

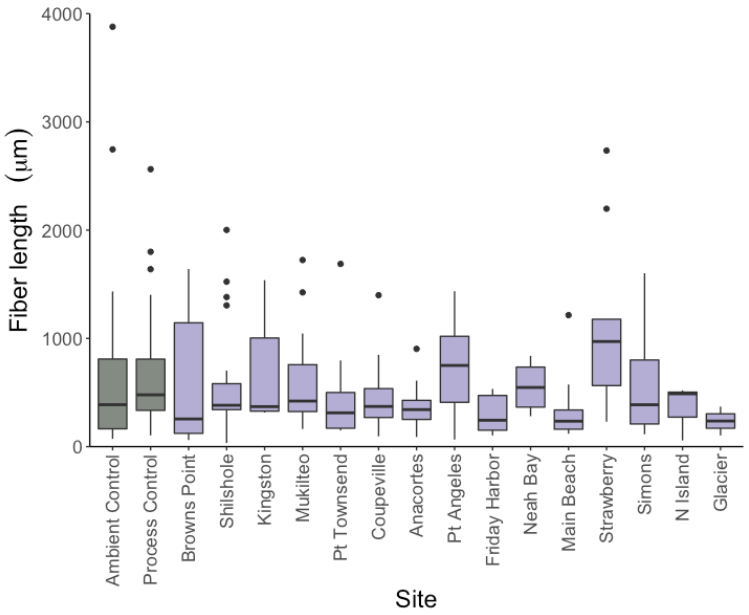

Figure 3.2. 6 Average fiber length (um) at each site, from South Salish Sea on the left, moving towards the Pacific Ocean on the right. Grey bars represent control filters and purple bars represent sampling sites. Boxes represent upper and lower quartiles and dots represent outliers; solid lines within boxes represent median values.

Table 3.2. 4 Kruskal-Wallis rank sum test on microparticle fiber length.

Variable	X^2	**Df**	**p-value**
Fiber length	23.36	16	0.10

Particle Identification

A total of 35 MPs were selected randomly and chemically identified. There was a significant amount of fluorescence interference, possibly from a layer of biofilm, that made the polymer identification process challenging. Seven, or 20%, of the identified MPs were synthetic materials, which include polyethylene terephthalate (PET), polypropylene (PP), polystyrene (PS), and nylon. Examples of the identified microplastics and corresponding Raman spectra are shown in Figure 3.2.7. Approximately 48% of visually identified MP were not anthropogenic, where 31% of the particles were identified as minerals such as orthoclase or quartz and another 17% of the particles

were graphitic materials (carbon fiber). Figure 3.2.8 illustrates the categorization of abundance, size and identification of particles found inside mussels.

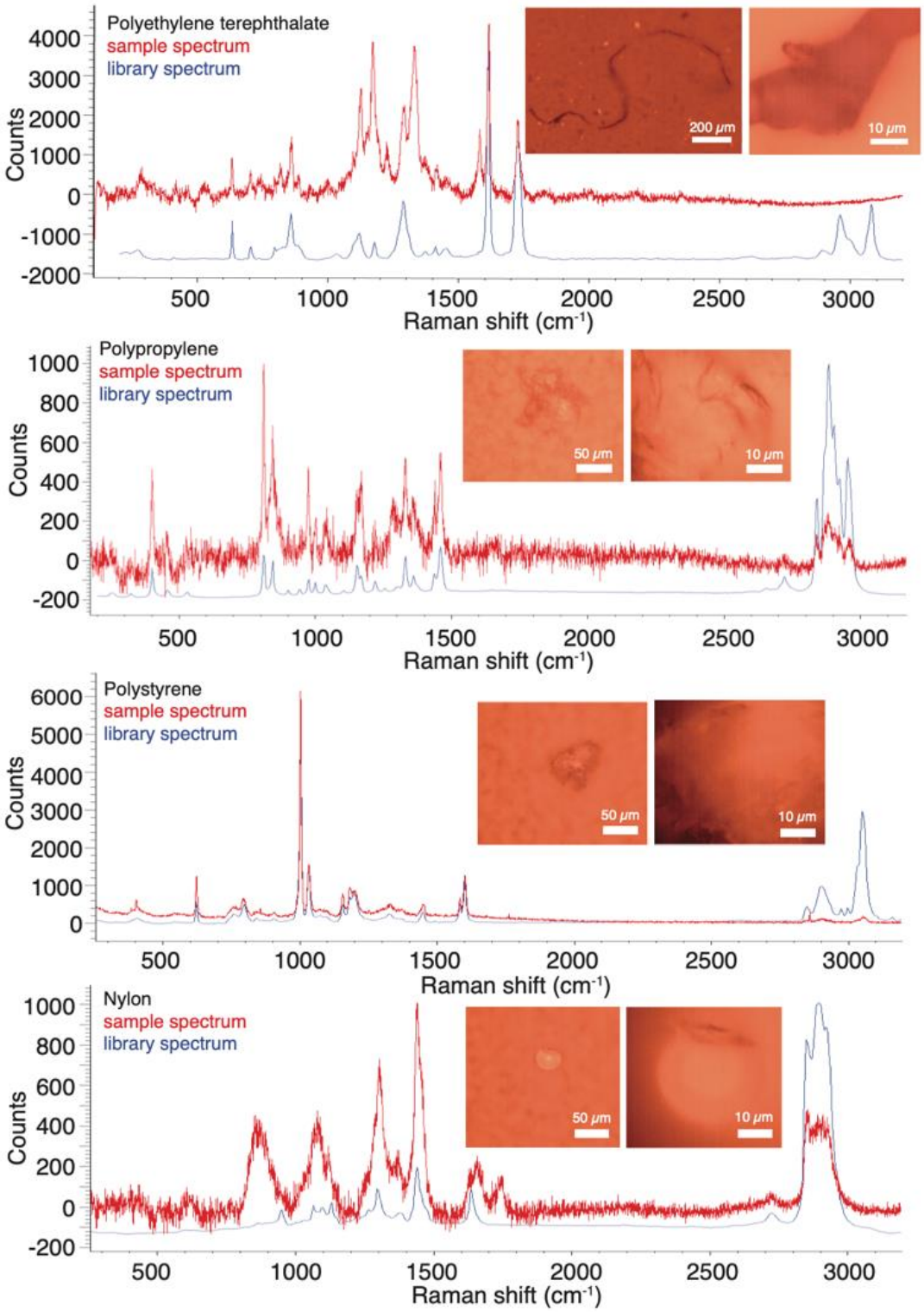

Figure 3.2. 7 Raman spectra for microplastics identified in mussel samples.

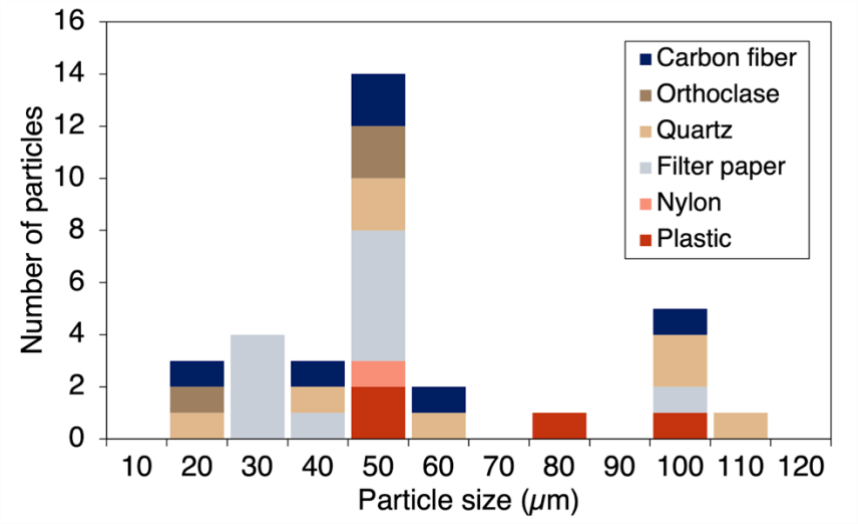

Figure 3.2. 8 Abundance of identified microparticles by size. Note that two plastics larger than 800 µm were omitted for clarity. Synthetic materials consist of three types of plastics, polyethylene terephthalate (PET), polypropylene (PP), polystyrene (PS), as well as nylon.

3.2.4 Discussion

This study demonstrated a consistent proportion of mussels containing microparticles (MP) across all sites, where concentrations ranged 0 – 6 MP g^{-1} wet mussel tissue, and MP morphologies were primarily fibers. Both concentration and morphology types are similar to previously observed concentrations and morphologies: sea surface tows observed MP concentrations of 0.00 – 0.2 MP L^{-1} in the Salish Sea (extrapolated from Davis III and Murphy 2015)[126] and 0.007 – 3.8 MP L^{-1} in the Strait of Georgia,[127] water at depth observed MP concentrations of 0 – 0.64 MP L^{-1} in Elliot Bay,[135] and oysters observed MP concentrations of 0.02–0.14 MP g^{-1} oyster tissue in the South Salish Sea.[40] Fibers are consistently the prominent morphology in sea surface tows, depth samples, oysters, and mussels in the Salish Sea.[133, 126, 40, 135] Further, the average fiber length observed here, 587 ± 37 µm, was consistent with previously observed fiber lengths in the region, 606 – 657.09 μm.[133, 135]

The Salish Sea is composed of many basins with varying water residence times (Table 3.2.1). Mahoney (2017) found that surface basin times correlated positively with plastic load in surface waters of the Salish Sea.[136] Here, mussels were sampled along an urban gradient as well as across multiple basins. Generally, the Salish Sea has a cumulative water residence time of 327 days,[137] where basins closer to the Pacific Ocean (Juan de Fuca Strait and Whidbey Basin) have shorter residency times (1–2 months) while basins further from the Pacific Ocean (Hood Canal and South Puget Sound) have longer water residence times (1–4 months).[137, 138, 40] Longer basin residency times indicate water remains in the same area for longer and there is less water movement. While basin residence times had an effect on mussel MP contamination, there was no observable trend as water basin residency times increased. Basin water residence times and water movement could affect the low rates of MP detected through changing MP encounter rate and/or causing MP to collect in places where mussels may not be present or where not sampled.

Mussels were, when possible, collected from marinas which are areas of high anthropogenic activity and may not reflect the average Salish Sea contamination levels. The size of the marina, or number of slips, had an effect on mussel contamination, where marinas with more slips and thus more anthropogenic activity had higher MP levels. Differences in MP contamination between sites and basins may instead be an artifact of marina size. Notably, Tatoosh sites had the lowest average MP levels (0.11–0.48 MP g^{-1} wet mussel tissue), and while these sites represent the least populated region, they also are located in the Pacific Ocean and were not collected from a marina. Further, only Tatoosh mussel MP concentrations were statistically different from process and ambient control samples, suggesting measured MP concentrations at other sites did not differ from background or contamination concentrations.

Only mussels from the Tatoosh sites were statistically different from either type of control filters, indicating contamination detected in other sites is no different than background noise or that mussels generally do not contain many particles. While mussel MP contamination was higher than oysters in the same region, they may predict lower MP concentrations than that which actually exist in the water column.[135] At the time of data collection for this study, there was little published research on the use of Mussels as MP bioindicators; now however, there is controversy surrounding their usefulness.[139–141] Research that advises against their use argues that the ingestion selection mechanisms are too complicated and egestion too rapid to ever accurately show MP water concentrations.[139, 142] These studies show, in controlled laboratory experiments, that mussel MP ingestion is biased towards small particles and fibers, and that most MP are rejected or quickly egested resulting in significantly lower MP water concentration predictions.[139, 142]

Differences in MP sources, heterogeneous transport thus leading to low or non-existent MP encounter rates, and mussel feeding biases are likely entangled, prohibiting a clear picture of Salish Sea MP contamination. These three differences (sources, transport, and biases need to be examined separately and in factorial analyses to begin to untangle Salish Sea MP contamination. Additionally, the quantity of MP particles found in each mussel (0–12) may not be enough to detect local or regional differences. While both Ward *et al.* (2019)[139] and Dimitrijevic (2018)[142] advise that mussels are not the best bioindicator for detecting MP contamination, other studies acknowledge these challenges, but argue that the information mussels can provide is still valuable.[140, 141] Mussels are ubiquitous, important to human consumption, already used globally to monitor other marine contaminants, accessible, and the ingestions mechanisms are understood.[139–141] Therefore, mussels could be more successful at understanding MP contamination at a larger or global scale rather than a regional or local scale, with standardized protocols.[140]

While MP found in mussels were composed of 20% plastic, quartz and orthoclase minerals were also found in mussel samples. Microplastic analysis performed on coastal surface water samples from the subtropical island of Okinawa, Japan found that together with plastic materials, quartz and other minerals such as calcite were also found, likely due to high river input in the region.[143] In the Salish Sea region, it is reasonable to infer that the mussel samples show quartz and orthoclase because of river input from the Duwamish and Fraser Rivers (Figure 3.2.1).

About 20% of the MP found in mussels were synthetic material and contained four different types of plastic: PET, PP, PS, and nylon. Given the proportion of chemically identified MP in mussels, it is estimated that 0–1.2 MP wet g^{-1} are plastics. Compared to Martinelli *et al.* (2020),[40] the mussel specimens were found to have nearly ten times more plastics than the oysters samples (where 2.6% of chemically identified MP were plastic) and more types of synthetic particles (oyster samples consisted of PE, PP, and PS). Seawater samples from Okinawa, Japan found plastic materials that were identified as PP, poly(vinyl) chloride, PS, and nylon[143] while seawater from the broader Northwestern Pacific Ocean contained fewer plastic types, PE, PP, and nylon. Notably, both Pacific seawater and both Salish Sea Shellfish studies found that PE was present,[90, 144, 134, 40] however, MP analyzed from mussels in this study did not contain PE. This result is interesting considering that PE is one of the most widely used commodity plastics.[144, 90] Nylon was found in the Salish Sea mussel samples as well as Pacific oyster near coastal British Columbia, Canada,[134] but was not found in Pacific Oysters in South Salish Sea.[40]

Physical characteristics of microplastics are known to dictate fate and transportation in marine systems.[10] Examining the material properties of MP found in mussels (e.g. density in g mL^{-1}) may offer an explanation on mussel MP concentrations (morphotype, polymer type, and quantities). The most common commodity plastics are PE, PP, and PS are similar in density as

seawater (1.025 g/mL) while PET and nylon are denser (Table 3.2.5). Mussels in this study were collected from docks or rocks relatively near the sea surface, so it is likely that PE is available due to its low density, high buoyancy, and relatively high production, highlighting a selection bias of mussels described by Ward *et al.* (2019).[139] While it is possible that the Salish Sea surface waters have low levels of PE, oysters collected in the Salish Sea by Martinelli *et al.* (2020) were found to contain PE.[40] Another possibility is that PE were biofouled, causing an increase in density, bypassing mussel filter zones and landed in benthic substrate, available for oysters. Morét-Ferguson *et al.* (2010) found that low-density polymers such as polyethylene were found on beaches with higher densities than pristine counterparts, concluding that the increase in density resulted from biofouling at sea.[90] There is still little research on the mechanisms of biofouling and how that contributes to the distribution of microplastics in the water column.

3.2.5 Conclusion

This research shows no microplastic contamination differences across an urban gradient. However, there is obviously more microplastic contamination in urban sites (e.g., Seattle and Tacoma) compared to more rural sites such as Tatoosh Island. About 20% of the microparticles analyzed with Raman microspectroscopy confirmed the presence of synthetic or plastic material such as PET, PP, and PS. These results indicate that mussel contamination is about ten times higher than that of Pacific oysters studied by Martinelli *et al.* (2020).[40] Interestingly, PE was not among the microplastics found and may indicate possible biofouling on PE microplastics.

3.3 Microplastics in Orcas

3.3.1 Introduction

Marine mammals are important indicators of the well-being of marine ecosystems because of their longevity, migratory behavior, and their role as apex predators.[145] Monitoring marine mammals provide a window into the global trends of persistent organic pollutants, which are known to bioaccumulate within their tissues.[146] Some examples of persistent organic pollutants are polychlorinated biphenyls, polycyclic aromatic hydrocarbons, and organochlorine pesticides such as dichlorodiphenyltrichloroethane (DDT).**Error! Reference source not found.** These chemicals are sorbed by plastic particles and can leech into tissues once ingested.[146] Killer whales along the Pacific coast of British Columbia in Canada and the state of Washington in the US are recognized as some of the most contaminated animals in the world.[145] The highest levels of persistent organic pollutants are found at the top of the food chain such as orcas as a result of biomagnification, which is when larger organisms feed on contaminated lower trophic organisms.[147, 148]

Orca whales inhabit large habitation ranges and preferentially feed on salmonoids.[149] Orcas also serve as a sentinel species that shed light about marine ecosystem health and are particularly relevant to human health because of their shared resources of Chinook salmon.[150] The eastern North Pacific Ocean is home to three contiguous populations of orcas.[149] The Southern resident orcas, the southern-most population, is listed as an endangered species in 2005 under the Endangered Species Act and considered depleted under the Marine Mammal Protection Act. The current population consists of about 70 individuals. The factors that are causing the decline in the Southern resident orcas are complicated but are identified as (1) a reduced quality and quantity of prey, (2) persistent organic pollutants that cause immune or reproductive dysfunction, and (3) noise disturbances from vessels.[151] In contrast, another population is the southern Alaskan resident orcas

which has experienced an increase of 3% in population for the past 25 years (currently with 700 individuals).[152] Endocrine-disrupting chemicals present in plastics mimic hormones naturally present in organisms. Plastic additives that are added plastics to increase their performance, such as styrene or phthalates, are also chemicals with endocrine-disrupting properties and are a major concern for marine organisms.[153, 154] The effects of endocrine-disrupting chemicals include impaired reproduction, metabolism, thyroid function, increased risk for hormone-sensitive cancers, and overall cause life-long cellular issues.[154] The effects of endocrine-disrupting chemicals are amplified through transmission to offspring during gestation and lactation because marine mammals have high milk fat percentages and long lactation periods.[155] These factors highlight the significant risk to orcas from these plastic-borne chemicals.

These two orca populations occupy different regions that may influence their health and population numbers. Alaskan resident orcas occupy less urbanized and populated regions around Prince William Sound and around Kenai Fjords, Cook Inlet, and possibly Anchorage.[152] The Southern resident orcas, however, are found primarily in the inland waters of the Salish Sea during the summer, but also from southern British Columbia to California.[151] The water and area around the Salish Sea are more urbanized and affected by chemical run-off and contaminants associated with anthropogenic activities compared to the Gulf of Alaska.[151] This study investigates the prevalence of microplastic pollution in the two North Pacific resident orca populations; the Southern Alaskan and Southern resident orcas.

3.3.2 Methods

Fecal collection

All fecal samples were collected under permit to conduct marine mammal research granted by United States National Marine Fisheries Service (NMFS), Marine Mammal Protection Act research permit # 781-1824, 16163, and 21348 issued to the NW Fisheries Science Center. Fecal samples were collected from both the Southern Resident (in 2007–2019) and the Alaska Resident killer whales (2016–2018). The location for samplings were selected by seasonal patterns of killer whale populations on nearshore waters in the Salish Sea for the Southern residents and the Gulf of Alaska for the Alaskan residents (Figure 3.3.1). Samples were collected using a 4 m long-handled fine-mesh net, initially stored in clear polyethylene plastic bags or 50 mL tubes on ice, and then later transferred to long-term storage at -20 °C or -80 °C before analyses.

Quality control

Fecal samples were collected and archived prior to the conception of the microplastic study and the large microplastic contamination in the environment was unknown at the time of collection. Therefore, there were no controls or efforts to mitigate plastic contamination of samples during field collection. Many possible contaminations of the fecal samples may have occurred during collection (e.g., nets, synthetic clothing) or may have been collected with the samples from surface water. One liter water samples collected at the same time as the fecal samples (2019) was used to understand the possible contamination.

Fecal selection

Fecal samples were selected from the archived killer whale samples at the Northwest Fisheries Science Center (NOAA Fisheries, Seattle, WA) based on sample volumes larger than 5 mL. All

samples were genotyped to genetically assign individual whale identifications to the fecal sample based on a reference of vouchered killer whale nuclear genotypes.

Microplastic isolation

To isolate microplastics form the fecal samples, 1 L glass flasks were rinsed with filtered DI water, dried in a dedicated microplastics incubating oven at 60°C and weighed. Fecal samples were then thawed and 3–4 mL was transferred into the cleaned pre-weighed flasks. The flasks were covered with aluminum foil and dried at 60 °C for 24–48 h until dry. The dry weight of fecal matter was measured to normalize the samples by dry weight because of the varying volumes of fecal samples. Filtered 30% hydrogen peroxide as added to the flasks, covered with foil, and placed in an oscillator incubator at 60 °C and 80 rpm for 24–48 h. If the samples appeared to be digested after 24 h, the heat was turned off and allowed to continue oscillate for 24–36 h. Following digestion, 800 mL of filtered 0.25 g mL^{-1} sodium chloride solution was added to the flasks and then covered overnight for density separation. Lower density material would float (including microplastics) while the higher density materials would sink. Each solution was then filtered through 1µm pore size nitrocellulose-filter-membrane (Whatman, GE Healthcare). Finally, each filter paper was placed in labeled Petrislides (MilliporeSigmaTM PetriSlideTM) and left to dry for 48 h.

Visual observation and validation of microplastics

Dried filter samples and control samples were visually inspected with Nikon SMZ745 stereomicroscope and photographed with an attached Nikon 5300 camera. All microparticles were classified by shape (fragment, fiber, film, or other) and color.

A sub-sample of 10% of all particles found by the dissecting microscope from 14 fecal samples and three procedural controls (17 filters) were analyzed with Raman microspectroscopy to validate microplastics, identify polymer type, and measured in the size. The method for identification was similar to that described in Chapter 3.1.2 and 3.2.2 previously.

Statistical analysis

R software (R Core Team, 2013) was used for statistical data analysis. A t-test was performed to test for a difference in total microparticle abundance between the two orca populations and potential differences between the types of microplastics in the two orca populations. T-tests and ANOVA were used to determine the statistical significance for control samples.

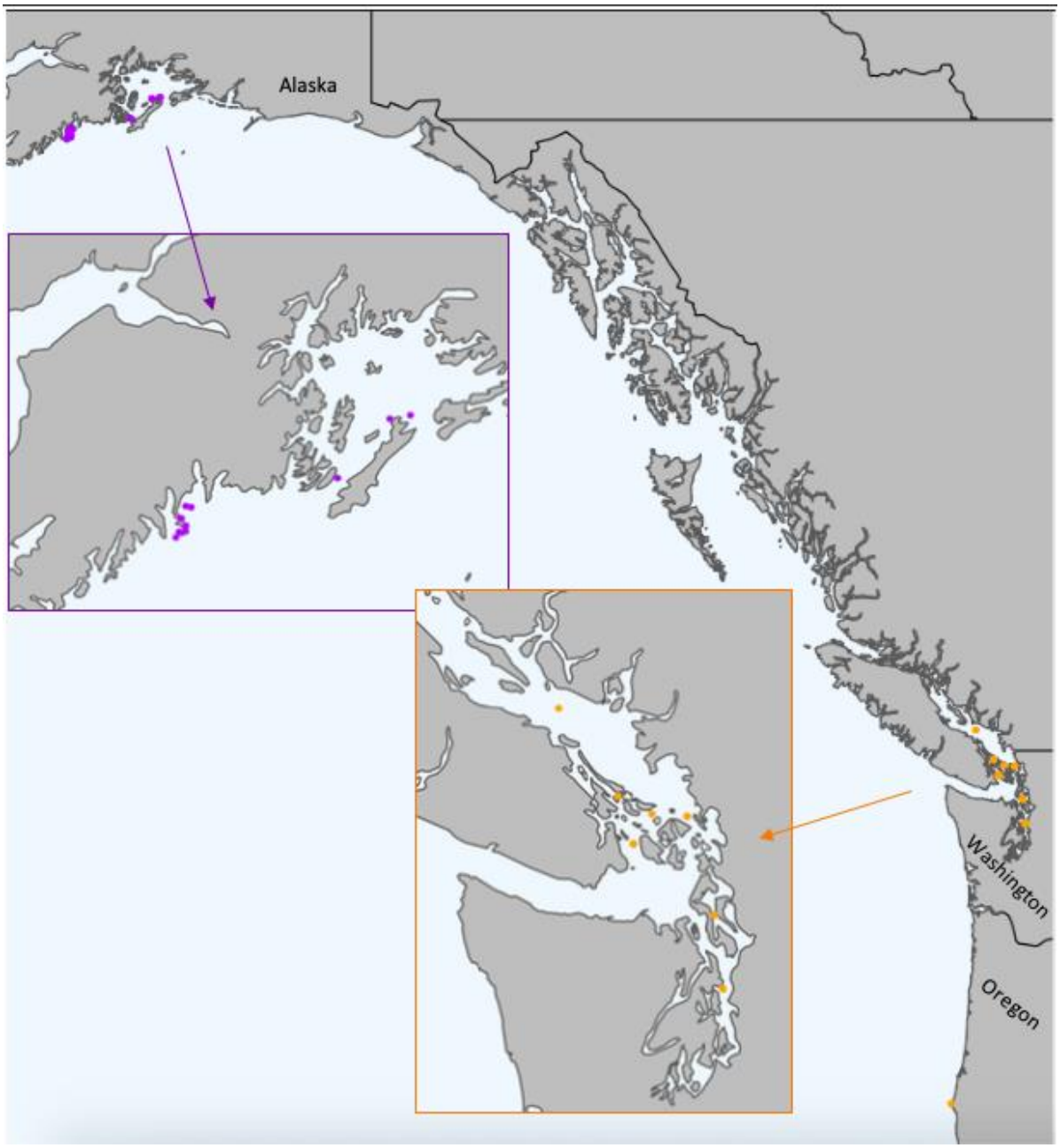

Figure 3.3. 1 Sample locations for orca fecal samples. Alaskan resident samples are in purple and Southern resident samples are in orange.[156]

3.3.3 Results

A total of 248 microparticles from orca and control filters were analyzed with RMS; the size distribution and identification of each particle is shown in Figure 3.3.2. The number of microparticles analyzed per filter were pre-determined as a percentage based on the total number

of particles broadly observed and categorized using a dissecting microscope. Out of the 248 microparticles examined, 37.5% were unable to be identified due to fluorescence masking the structured Raman signal. More information about this phenomenon is discussed in Section D. Despite this challenge, a total of 16.9% microparticles were found to be synthetic, consisting of 6.8% particles as PE, 0.4% as polyethylene terephthalate (PET), 0.4% as PVC, and 9.3% as nylon. An example spectrum of a particle found in the orca samples identified as PE and two reference spectra (of polyethylene and polyvinyl stearate) is shown in Figure 3.3.3. Statistical analysis was completed and reported by Harlacher, but overall found no significant difference in the microparticle burden between the two orca populations.[156]

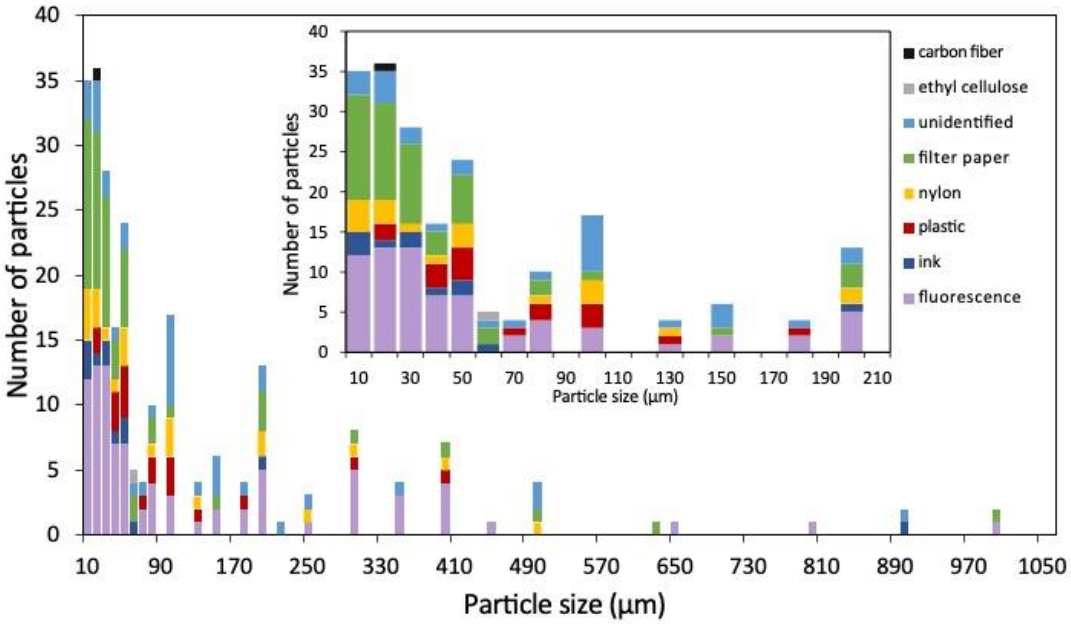

Figure 3.3. 2 Size distribution and identification of microparticles from orca samples using RMS. The identity of the particle is color coded according to the key in the top right-hand corner of the image. Five fluorescent microparticles larger than 1050 µm were omitted for clarity.

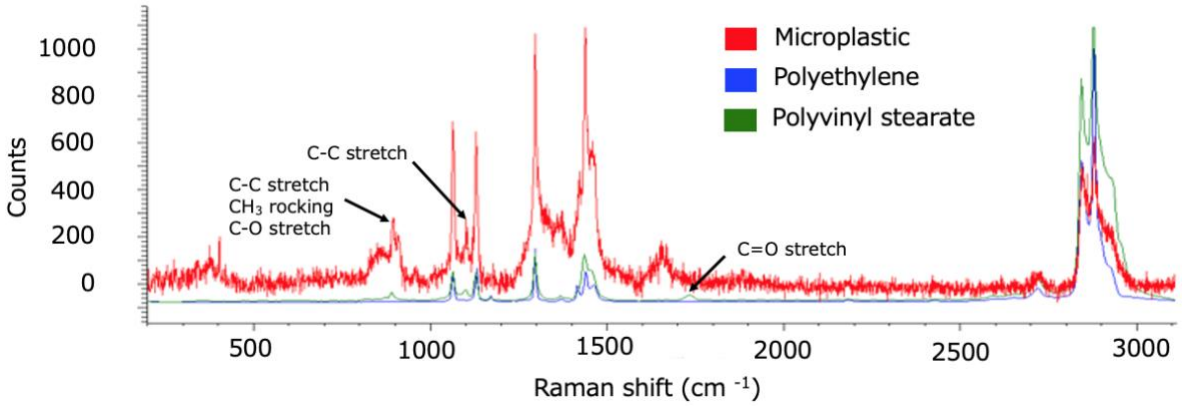

Figure 3.3. 3 Example microplastic particle spectrum found in orca sample (after baseline correction, red) and reference spectrum of polyethylene (blue).

3.3.4 Discussion

The Alaskan resident orca population range is near small human communities and open ocean, the Gulf of Alaska. However, the Southern resident orca population is much closer to dense human populations in the Salish Sea. Microplastics were found in both orca populations, but because of the small portion of samples identified with Raman microspectroscopy, there was no obvious difference in the type of polymers found between the populations. Every fecal sample examined contained microparticles, except one, implicating the extensive contamination in the marine environment. The most abundant microplastic type that was found in the orca samples was polyethylene; considering the abundance and versatility of PE products, this result was unsurprising. Polyolefins, such as PE and PP, dominate the world's plastic production.[1] High- and low-density PE are used for milk and juice jugs, plastic bags, six pack rings, netting, and drinking straws.**Error! Reference source not found.** The lower occurrence of PVC and PET found in the orca samples may be related to the lower commonality of these plastics in the global market compared to PE or possibly due their greater density, sinking behaviors, and ability to be ingested by prey.[1, 157, 158] Nylon was also another polymer found in orca samples. The presence of PE and nylon

microplastics is well-known in coastal areas and highlights the contamination in orca populations.[143]

Considering the two geographically different locations and level of urbanization between the Alaskan and Southern resident orcas, it was surprising there was no difference in microplastic occurrence. Cities that are upstream to urbanized rivers may contribute to potential microplastics throughout the Southern resident orca population range.[159] Studies also examining the relationship of microplastic contamination and costal area use find higher microplastic abundance in more urbanized areas compared to urban sites.[143] Chinook salmon is a prey common to both resident orca populations and may explain the similarities in microplastic occurrence. Salmon mature in the mid-Pacific Ocean and feed the most during this time,[160] possibly also ingesting microplastics at this time.[33] So even though the Alaskan and Southern resident orcas may prey on different salmon stocks, the stocks may overlap in their distribution in the mid-Pacific.[156] Another possibility is that microplastics are originating from the fishing industry. Alaska produces 60% of the US commercial fisheries and so may contribute microplastic contamination to the Alaskan resident orcas.[156]

Careful analysis of each Raman spectrum in crucial for proper identification. In Figure 3.3.3, an example microplastic Raman spectrum, the most prominent peaks that correlate between the sample and reference spectra are 1080 cm^{-1} and 1280 cm^{-1} (which correspond to the C-C stretch in the backbone) and 1306 cm^{-1}, 1416 cm^{-1}, 1460 cm^{-1} (which correspond to CH_2 twisting and bending). However, two interesting peaks appear at 1100 cm^{-1} and 890 cm^{-1} that do not appear in the reference polyethylene spectrum. Upon further analysis, the peak at 1100 cm^{-1} corresponds to C-C stretches while the peak at 890 cm^{-1} is related to C-C stretches, methyl rocking, and C-O stretches. Therefore, another possible identification for the microplastic is polyvinyl stearate.

Considering the low global production levels of polyvinyl stearate, it is unlikely that the particular microplastic found in the sample is polyvinyl stearate, but rather PE, or a result of oxidation of polyethylene.[161, 162] Another possibility, and more likely outcome, is that this microplastic contains a phthalate additive such as di(2-ethylhexyl)phthalate. This particular additive is concerning, because it is known as an endocrine disruptor.[163] Common peaks associated with amides in lipids occur between 1645 – 1670 cm^{-1} and proteins between 1500 – 1700 cm^{-1}, and so the broader peak around 1650 cm^{-1} is suspected to be residual biological material.[164, 165] About 14.1% of particles remain unidentified as their spectra do not match entries in the Renishaw polymer library and are require individual and manual analysis with available Raman spectral literature and open-source libraries. Efforts for individual matching led to the identification of one particle as carbon fiber and one particle as ethyl cellulose.

3.3.5 Conclusion

This study is the first to identify the presence of microplastics in orca feces and compare microplastics in two populations of orcas. The isolation and identification of microplastics in orca feces provides strong evidence for microplastics in the gut of killer whales, particularly PE and nylon. Raman analysis determined that 16.9% of the particles identified were synthetic materials. The detection and quantification of microplastics is a critical in understanding the potential health effects microplastics may have on killer whale populations. An important next step is to analyze the fecal samples for xenoestrogenic compounds.

Chapter 4. Weathering effects on microplastics

4.1 Introduction

Identification of microplastics is challenging because of the variety of polymers and chemicals used to produce plastics and the numerous weathering processes that chemically change them. Early microplastic studies relied on visual recognition and discernment of particles as microplastic or non-microplastic; however, this inaccurately estimates the true amount of microplastics found in the environment as visual inspection leads to a misleading amount of actual plastic particles. [32, 33] As stated in Chapter 2, two common non-destructive methods for microplastic analysis is Fourier transform infrared microspectroscopy (μ-FTIR) and Raman microspectroscopy (RMS).[8, 3, 31–36] Considering the thousands of polymers, additives, copolymers used in plastics, identification requires the usage of an extensive polymer library for spectral matching.[31, 8, 39, 40] Unfortunately, environmentally weathered microplastics can differ significantly from their un-weathered counterparts, thus complicating the identification of microplastics.[5, 39, 37, 41] Additionally, different plastics undergo different degradation pathways making individual studies of plastic types necessary.[166] Challenges in microplastic identification have pushed researchers to call for weathered polymer spectra to be included in polymer libraries.[31, 37, 39–41] Most weathered spectra are included in in-house polymer libraries, but few if any have been included in commercial libraries for widespread use.[51] Considering the many variations of polymer type and weathering environment, it may even be impractical to include all possible weathered spectra for a comprehensive library.

Some recent studies have subjected commodity polymers to artificial degradation in efforts to understand weathering effects more systematically.[5, 39, 167] These studies have primarily focused of IR, understandably as IR depends on changes in dipole moment and can detect more drastic

changes in microplastics such as oxidation by the formation of hydroxyl and carbonyl groups. However, Raman spectroscopy in microplastic identification is becoming increasingly popular as it is more sensitive to additives and can detect smaller particles than IR.[42] Raman spectroscopy relies on detecting changes in polarizability and thus allows for greater understandings between the interactions of nonpolar atoms and molecules. The difference between the techniques is that IR can elucidate oxidative end functional groups while Raman is more capable in characterizing the polymer backbone. Both IR and Raman methods are complimentary and while they are comparable for smaller molecules, they become more complementary as the molecule becomes larger, such as the case in polymers.[41, 168, 169] UV exposure of various polymers conducted by Lenz *et al.* reported that UV-exposure unhindered Raman polymer identification,[37] but microplastic identification studies using Raman spectroscopy still observe weathering effects that hinder microplastic identification.[49] Currently, there are few studies that explore weathering of microplastics influence their Raman spectra in conjunction with IR spectra.

This work involves a systematic investigation of the influence of weathering on both Raman and IR spectroscopy chemical identification of plastics, specifically polyethylene and polypropylene. The findings highlight the different strengths of Raman spectroscopy and IR spectroscopy as identification techniques for microplastics. Raman spectroscopy retains great fidelity of weathered polymer spectra and show little variation with increasing exposure to sunlight which allows for easy identification of the original polymer. In contrast, IR spectroscopy allows for better monitoring of microplastic degradation, however, may be a more difficult tool for identifying weathered microplastics. Finally, our study shows that weathering environments (e.g., different seawater) influence various degradation pathways that can produce different oxidative products for the same polymer. The authors hope that this study will provide new information for

future studies in identification of microplastics, predicting weathering patterns, and the degradation of microplastics.

4.2 Methods

Materials

All plastic samples (pellets or powder) that were used for this study were purchased in pure form and unaltered from Sigma Aldrich. Low-density polyethylene (LDPE) was in pellet form with a density of 0.925 g mL^{-1} at 25 °C, and melting temperature of 116 °C. Ultra-high molecular weight polyethylene (UHMW) was in powder form with an average molecular weight of 3,000,000–6,000,000 g mol^{-1}, density of 0.94 g mL^{-1} at 25 °C, and melting temperature of 138 °C. Isotactic polypropylene (PP) was in pellet form with an average molecular weight of 12,000, density of 0.9 g mL^{-1} at 25 °C, and at melting temperature of 157 °C. Sea salts (NutriSelect® Basic) was also purchased from Sigma-Aldrich as an artificial seawater mix. Water collected directly from the Puget Sound (Seattle, Washington) without any filtration or treatment was also used for the studies.

Experimental procedure

The objective in this study was to investigate the influence of sunlight and water environments on different types of microplastics without other effects such as temperature or mechanical abrasion. Therefore, a limited number of plastic pellets or amount of plastic was added together in one vial avoid possible abrasion effects. Six plastic pellets (approximately 0.025 grams) or 0.025 g of powder was placed into a glass vial. The glass vials were then filled with either nothing (for an air environment), deionized water (DI), artificial seawater (AS), or seawater collected from the Puget Sound (PSS). An AS solution was made with 35 g of NutriSelect® Basic in 1 L of DI water. Once

the glass vials were filled with water and plastic, they were sealed with a glass coverslip to prevent foreign particles from entering the vial and to reduce water evaporation. The vials were then placed on an automatic rocker to mimic light ocean waves and more importantly ensure homogenous temperature within the vials.

The lightbulbs that served as the light source for solar irradiation were 120 W SoluX Eiko 4700K halogen lightbulbs. The lightbulbs were connected to a lightbulb socket, transistor, and mechanical timer. The lightbulbs were chosen to mimic ambient sunlight as much as possible. The mechanical timer allowed for 12 hours of continuous light irradiation and 12 hours in the without irradiation from the lightbulbs, to mimic a typical day. The temperature was controlled to 25–30 °C to avoid thermodegradation. Figure 4.1 shows a schematic of the experimental setup. Aliquots of each sample were taken out every 2 weeks for 10 weeks and one final sample was taken after 26 weeks of irradiation. After each aliquot was taken, copious amounts of DI water were used to rinse the particles and then the particles were dried under air. In the case of the artificial seawater and Puget Sound seawater samples, this was necessary to rinse off any excess salt before drying and characterization.

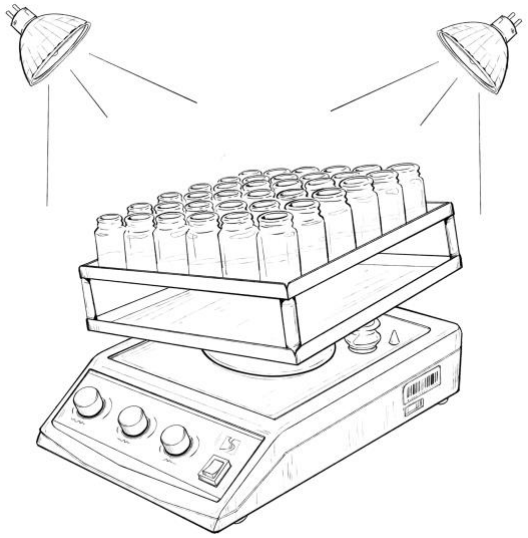

Figure 4. 1 Experimental setup for microplastic study

Instrumentation and data processing

Raman spectra were collected with a Renishaw inVia Raman microspectrometer equipped with a 785 nm laser. Two objectives, 10× and 50×, were used to optimize the analytical laser focus for analysis on the microplastic surface. All measurements were collected for 5 accumulations at 5% laser power. After collection, each spectrum was subjected to data processing depending on the signal-to-noise ratio and fluorescent interference (which produced a curved, sloped baseline). Baseline correction was completed using a reweighted penalized least squares algorithm developed by Zhang *et al.* to create a consistent baseline correction and avoid microscope objective interference signals.[170] After baseline correction, each spectrum was normalized according to a reference peak that was known to be consistent regardless of polymerization or degradation. Table 4.1 describes the reference peaks used for normalization in each polymer.

A Nicolet iN10 infrared microscope from ThermoFisher Scientific was used to measure the IR spectra of the polymers. The microplastic pellets had a thickness that was too large (> 100 μm) for the microscpectrometer transmission or reflectance mode to be measured effectively. For that reason, attenuated total reflectance Fourier Transform infrared spectroscopy (ATR-FTIR) equipped with a germanium tip-ATR crystal applied with a standard pressure of "15" was used to measure the IR spectra. According to manufacturers the standard pressure of "15" did not correspond to a standard pressure unit. This pressure was low enough to avoid breaking or fragmenting the microplastic samples tested.

Table 4. 1 Polymer peaks used for Raman spectral normalization and assigned vibrational mode

Polymer	Peak position (cm^{-1})	Vibrational mode
PE	1298	CH_2 twist[171]
PP	1460	Asymmetric CH_3 bend[172, 173]

4.3 Results and Discussion

Like other microplastic studies, there were slight variations in Raman peaks associated with the crystalline and amorphous regions as the microplastics were exposed to sunlight over time.[171, 37] Raman spectral analysis of the microplastics revealed little influence from increasing sunlight and different weathering environments (air, DI water, artificial sweater, and Puget Sound seawater) as there was no disappearance in characteristic Raman peaks associated with each plastic. This indicates that Raman spectral analysis may be more reliable for microplastic identification despite various weathering conditions (not considering fluorescence interferences). Considering the different vibrational modes of each unique polymer and careful analysis, these Raman peak variations indicated slight polymer backbone modifications.

IR spectroscopy revealed the extent of weathering more readily as significant changes were observed through the evolution of various oxidative functional groups with increasing sunlight exposure and across the different environments. In the case of LDPE, antioxidant leeching was also observed. Air samples exposed to sunlight across all the polymers show relatively low weathering degradation effects compared to their pristine counterparts which was observed by little change in the IR spectra. On the other hand, water weathered microplastics show higher extents of weathering compared to air samples and showed different oxidative products in depending on the type of water. Water can react slowly with polymer chains *via* hydrolysis which results in chain cleavage.[174] With increasing sunlight exposure, the formation of oxidative functional groups become more prevalent in the water weathered samples based on the IR spectra.

Both Raman and IR spectra indicating that weathering is a non-linear process across all microplastics, and an overall trend could not be observed with increasing sunlight exposure or different weathering conditions. Raman and IR analysis is explained further in the following

sections for low-density polyethylene (LDPE) and polypropylene (PP). Ultra-high molecular weight polyethylene (UHMW) results are provided in the supplemental information.

4.3.1 Raman analysis

Low-density polyethylene

LDPE has been the subject of extensive study because of its importance in many industrial sectors and consumer products.[1, 95] LDPE is highly branched at irregular intervals compared to its high-density PE counterpart and therefore is more susceptible to weathering effects. The major differences in the LDPE Raman spectra with increasing sunlight exposure across all the environments were observed around the 1130, 1418, 1440, 1460, 2852, 2884 cm^{-1} bands, which are associated with the LDPE amorphous and crystalline phases (Figure 4.2, Table 4.2). The Raman spectra (focused on these regions exhibiting the greatest variation in intensity) of LDPE exposed to sunlight over the course of 10 weeks and 26 weeks in different environments are shown in Figure 4.2. Full LDPE Raman spectra can be found in Appendix B, supplementary information for Chapter 4.

The most popular Raman bands associated with LDPE crystallinity are within the 1100 and 1450 cm^{-1} regions are usually studied in photodegradation studies.[37, 171] However, there was no obvious trend indicated from the Raman peak intensity changes in these regions following increasing sunlight exposure in any environment (Figure 4.2, columns a and b). Thus, no correlation is drawn regarding the crystallinity or amorphous phases of the weathered microplastics based on the intensity or intensity ratios of the bands normally analyzed for crystallinity. The 1418 cm^{-1} band is assigned to CH_2 bending and wagging in crystalline regions, the 1440 cm^{-1} band corresponds to CH_2 deformation of the amorphous trans regions, and the 1463

cm^{-1} band is due to CH_2 bending from amorphous regions of polyethylene (Table 4.2).[171, 175] It is expected that with increasing UV exposure, LDPE undergoes microscopic structural changes and changes in crystallinity.[175] The lack of an overall trend implies that the weathering of microplastics is a non-linear process and chemical spectra inadequately age microplasics.[14] With increasing sunlight exposure both air and DI water samples showed similar variation in intensity over time in the Raman peaks in the 1440 cm^{-1} region while the artificial seawater and Puget Sound seawater samples exhibited slightly more variation of intensity in the same region (Figure 4.2, column b),. This may suggest that microplastics weathered in seawater may experience more changes following sunlight exposure to the surface than in air or DI water, but it may also simply highlight the heterogeneous nature of microplastic surfaces. Overall, there is little LDPE Raman spectral difference between the different environments following increasing sunlight exposure of the most popular bands associated with crystallinity.

Table 4. 2 Selected Raman bands and associated vibrational modes of PE[175, 176–178]

Peak position (cm^{-1})	Vibrational mode	Phase or associated features
830	C-C-H, C-O-C stretch	–
853	C-C-H, C-O-C stretch	–
988	C-O stretch	–
1763	C=O stretch	Ester
1063	Anti-symmetric C-C stretch	Trans chain
1130	Symmetric C-C stretch	Trans chain
1418	CH_2 bend and CH_2 wag	Crystalline (orthorhombic)
1440	CH_2 bend	Amorphous trans
1460	CH_2 bend	Amorphous
2852	Symmetric C-H stretch	Sensitive to crystallinity
2884	Antisymmetric C-H stretch	Sensitive to crystallinity

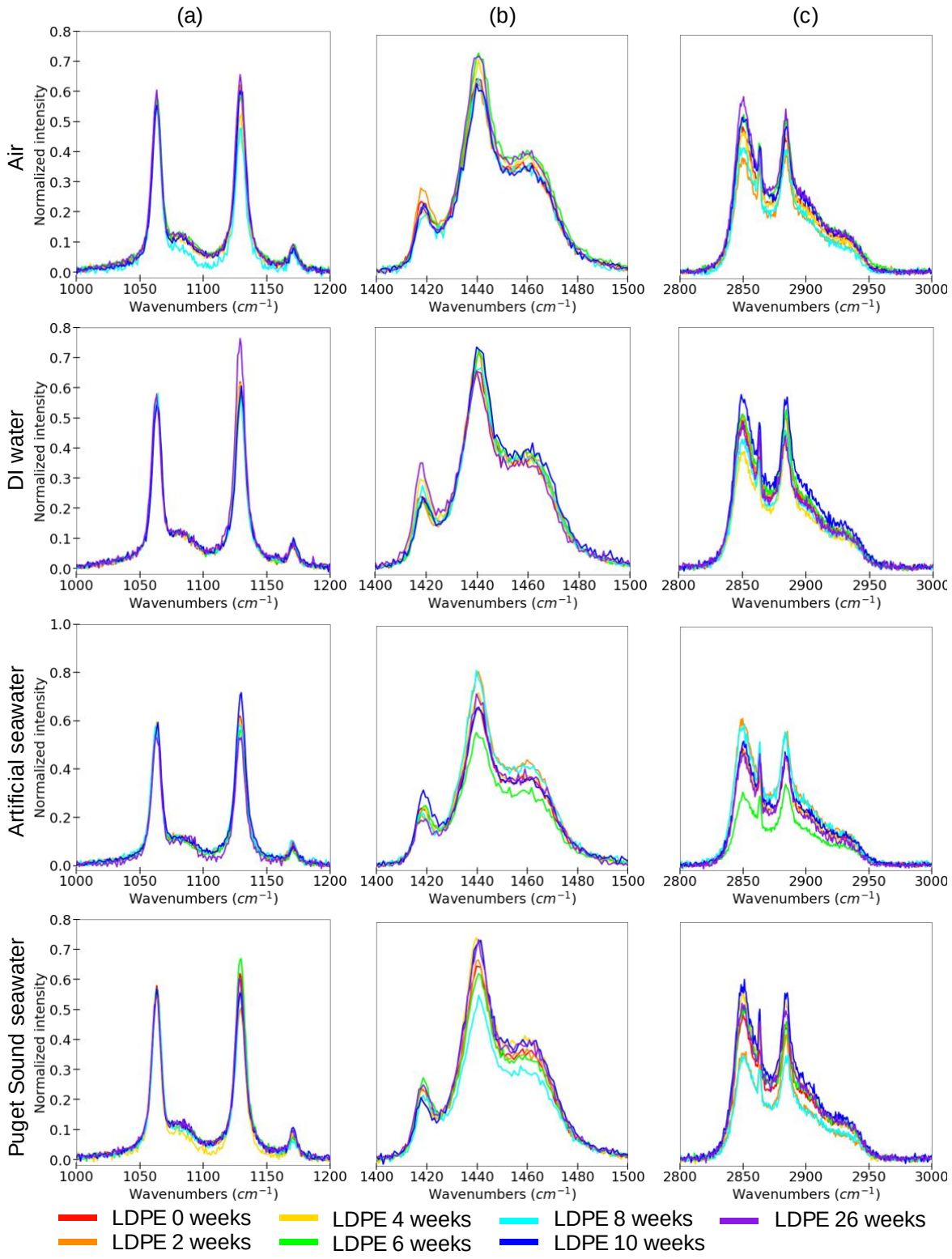

Figure 4. 2 Truncated Raman spectra of LDPE with increasing sunlight exposure times in Air, DI water, Artificial seawater, and Puget Sound seawater environments. The truncation highlights the (a) 1100, (b) 1450, and (c) 2850 cm^{-1} regions which exhibit the greatest variability in normalized Raman intensity.

The C-H stretch region is particularly sensitive to crystallinity can indicate small structural changes that go undetectable in the C–C stretch (around 1100 cm^{-1}) regions.[176, 177, 179] Larsson *et al.* proposed that this is due to intermolecular interactions influencing C-H stretching vibrations more than C-C stretches along the carbon chain.[179] Inspecting the LDPE Raman spectral changes, the C-H region (Figure 4.2, column c) does show more significant changes than the 1100 and 1440 cm^{-1} regions (Figure 4.2, column a and b). The air, artificial seawater, and Puget Sound seawater samples showed more variation in the C-H stretches compared to DI water samples. The ratio of peak intensities of 2890 and 2850 cm^{-1} (I_{2890}/I_{2850}) is used in studying structure and structural changes in polyethylene as it is sensitive to lateral packing and extended chains and to conformational disorder.[177] Disruption in polymer chain packing results in a decrease in intensity of the 2890 cm^{-1} band relative to the 2850 cm^{-1} band.[177, 174] This implied that a decrease in the I_{2890}/I_{2850} ratio results in a decrease in crystallinity, which can be monitored in the weathered microplastics. Figure 4.3 shows the I_{2890}/I_{2850} ratios of each environment with increasing sunlight exposure for each LDPE sample (Appendix B Supplementary Table 4.1 for Chapter 4 show the numerical values of the ratios). Overall, across all the environments, with increasing sunlight exposure the ratio initially increases then decreases over time compared to the pristine samples. This indicates an initial increase in crystallinity then, as other atoms are incorporated into the backbone, a decrease in crystallinity for LDPE in all environments. The initial increase is indicative of chain scission which allow polymer chains to have higher mobility to crystallize.[180]

Although Raman spectroscopy is less sensitive to polar functional groups such as C-O bonds, we do observe some evolution of increasing intensity 382, 400, 830, 853, and 988, 1763 cm^{-1} for LDPE in all environments. The peak at 1763 cm^{-1} is attributed to the C=O stretching of

esters, indicating a higher content of oxygen in weathered PE.[181] However, IR spectroscopy is much more efficient at observing oxidative products and is discussed in the IR analysis section.

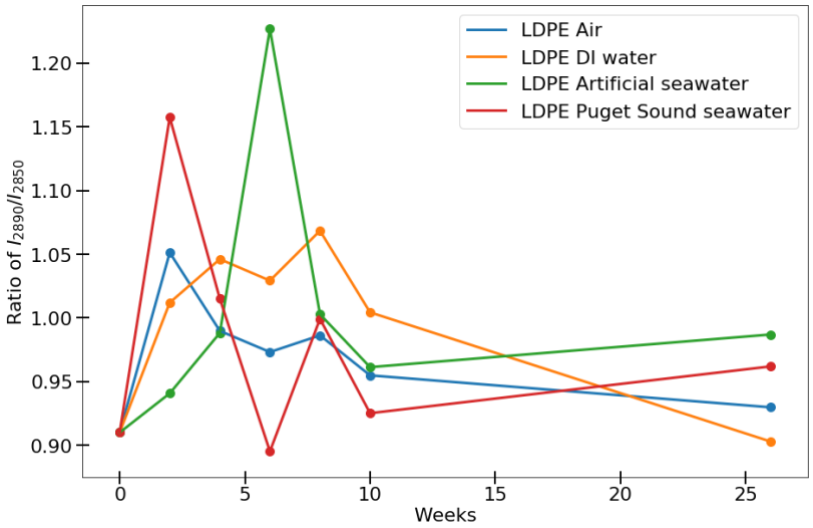

Figure 4. 3 Ratios of I_{2890}/I_{2850} bands of weathered LDPE in different environments with increasing sunlight exposure

Polypropylene

PP is used in many different types of packaging like PE. However, PP is less stable than PE because of tertiary carbon available in its backbone.[38] The major difference in the PP with increasing sunlight exposure were observed around the 809, 841, 973, 998, 1152, and 1167 cm^{-1} bands (Table 4.3). The Raman spectra (focused on these regions exhibiting the greatest variation in intensity) of PP exposed to sunlight over the course of 10 weeks and 26 weeks in different environments are shown in Figure 4.4. Full PP Raman spectra can be found in Appendix B, supplementary information.

In contrast to PE, there is little variation in the C-H stretch regions of PP with increasing sunlight exposure across all the environments (Figure 4.4, column c). However, PP Raman spectra do exhibit more significant changes in the peak intensities assigned to the PP amorphous and

crystalline phases with increasing sunlight exposure in all environments (Figure 4.4 columns a and b, Table 4.3). Puget sound seawater samples show the most variation in intensity with more sunlight exposure in the C-H region, at about 2963 cm^{-1}, compared to the air, DI water, and artificial seawater (Figure 4.4, column c). The Raman peak at 809 cm^{-1} is assigned to the vibrations of isostatic PP helical chains in the crystalline phases and the peak at 841 cm^{-1} is assigned to the vibrations of isotactic PP helical chains with significant amount of conformational defects which is localized in the amorphous phase.[173] The intensity ratios between the 809 and 841 cm^{-1} peaks (I_{809}/I_{841}) is used as a measure of the degree of crystallinity of isotactic PP.[173, 182, 183] Figure 4.5, shows the I_{809}/I_{841} ratios of each environment with increasing sunlight exposure for each PP sample (Appendix B, Supplementary Table 4.2 show the numerical values of the ratios). In the air and Puget Sound seawater samples, there is an initial increase then decrease at the 808 cm^{-1} peak and an initial decrease then increase in the 840 cm^{-1} peak, from 0 to 10 weeks, this indicates an initial increase of crystallinity then decrease as weathering continues like PE. At 26 weeks however, both air and Puget Sound seawater samples show increases in crystallinity compared to PP weathered until 10 weeks. The DI water and artificial seawater samples show much more variation the ratio I_{809}/I_{841} with increasing sunlight exposure, but no trend was observed over time which highlights the inability for spectral analysis in aging microplastics. Interestingly, all the water samples show the appearance of a small shoulder-type peak at 998 cm^{-1} with more sunlight exposure. The peak at 998 cm^{-1} is related to the isotactic segments in a helix confirmation with a minimum length of 5–10 monomer units, which indicate the evolution of smaller chains of PP as a result from chain scission or branching.[185, 187] This is also supported with the decrease in intensity of the 840 cm^{-1} band, associated with the helix confirmation with a minimum length of 12–14 monomer units, with increasing sunlight exposure seen in all environments.

Table 4. 3 Selected vibrational modes and phases of Raman bands of PP[173, 182–186]

Peak position (cm^{-1})	Vibrational mode	Phase or associated features
809	CH_2 rock, C-C stretch, C-CH_3 stretch	Crystalline
840	CH_3 rock	Amorphous, 12–14 helix segments
973	CH_3 rock	2–4 helix segments
998	CH_3 rock	5–10 helix segments
1152	C-C stretch	–
1167	C-C stretch	Crystalline
1463	Asymmetric CH_3 bend	–
2963	Asymmetric CH stretch	–

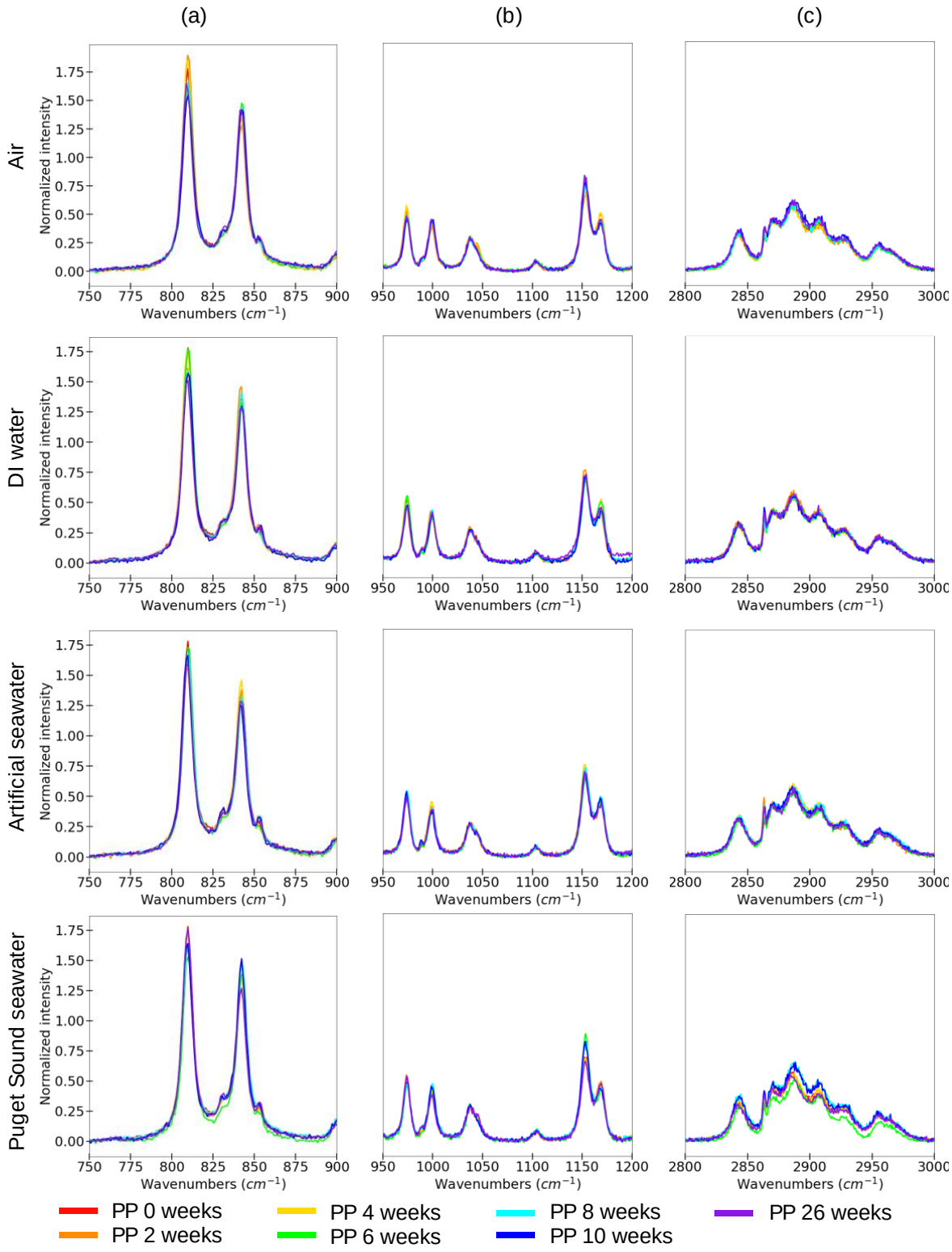

Figure 4. 4 Truncated Raman spectra of PP with increasing sunlight exposure times in Air, DI water, Artificial seawater, and Puget Sound seawater environments. The truncation highlights the (a) 820, (b) 1100, and (c) 2900 cm^{-1} regions which exhibit the greatest variability in normalized Raman intensity.

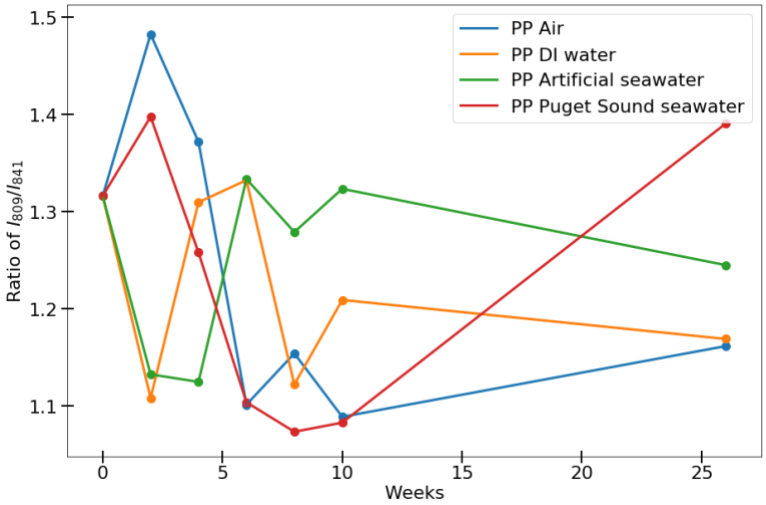

Figure 4. 5 Ratios of I_{809}/I_{841} bands of weathered PP in different environments with increasing sunlight exposure

4.3.2 IR analysis

Low-density polyethylene

The IR spectra of LDPE, shown in Figure 4.6, indicated that air samples exhibited less weathering and oxidative product formation over time compared to the water samples. Peaks appearing at 3392, 3189, 1580, 1545 cm^{-1} are antioxidant peaks from hindered amine light stabilizers (HALs).[188] This was surprising, because when LDPE was received from Sigma-Aldrich, there was no mention antioxidant content. HALs act to inhibit degradation of the polymer by continuously and cyclically removing free radicals that are produced by photooxidation of the polymer.[189] This explains why air samples of LDPE did not exhibit major changes in the IR spectra. Only 20% of oxygen that reacts with HALs-stabilized polymer is converted to CO and CO_2 while the other 80% is not chemically bound or converted into carbon-containing oxidation products.[189] HALs also appear in the IR spectra for DI water samples and remain in the spectra even after 26 weeks of sunlight exposure. The artificial seawater IR spectra indicates that trace amounts of HALs are sometimes present but can disappear, most likely leeching into the surrounding water, as in the

samples of LDPE at 6, 8, and 10 weeks. What is particularly alarming is that none of the Puget Sound seawater samples exhibit any indication of HALs present, indicating that they may have leeched into the water. HALs, such as TINUVIN® and CHIMASSORB®, are very toxic to aquatic life and can cause long lasting adverse effects.[190, 191]

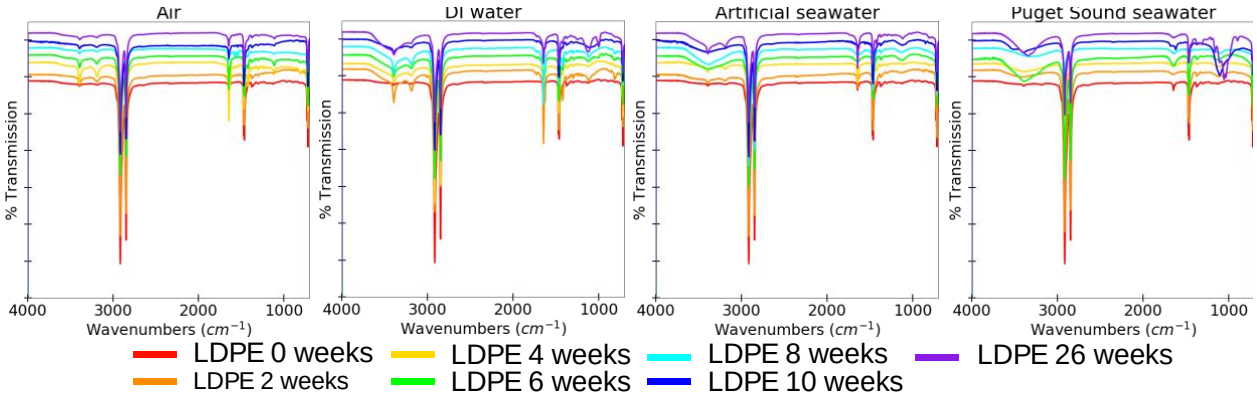

Figure 4. 6 IR spectra of LDPE after sunlight exposure over time in four different environments in a staggered overlay to observe the emergence of functional groups.

The IR spectra of weathered LDPE also showed the formation of new functional groups with increasing sunlight exposure, represented by peaks centered at 3385, 1725, 1645, 1420, 1122, 1057, 1035, 1000, 898, and 820 cm^{-1} (Table 4.4). The hydroxyl content of LDPE indicated by the band 3385 cm^{-1} remained relatively the same in the air samples but evolved much more in the water samples. Interestingly, only DI water samples showed the presence of C=O stretching at 1725 cm^{-1} from carbonyl groups, a common indicator of oxidation.[5, 39] The most obvious change in the weathered LDPE was the increase in the 1645 cm^{-1} peaks, assigned to the C=C stretches, as a result from chain scission. DI water samples exhibited the greatest formation of carbonyl and vinyl groups, followed by air, artificial seawater, and then Puget Sound seawater. While oxidative bands around 1800–1600 and 1400–1000 cm^{-1} were structured or sharper in air, artificial seawater, and DI water like the study conducted by Fernandez-Gonzalez *et al.*, the weathered LDPE in Puget

Sound seawater becomes more broadened like as seen in Da Costa *et al.*'s work.[5, 39] This indicates that depending on the weathering environment and water type, LDPE can undergo different degradation pathways that modify the polymer resulting in different IR spectra.

Table 4. 4 Selected vibrational modes of IR bands of weathered PE samples[39, 175, 179]

Peak position (cm^{-1})	Vibrational mode	Environment band present
3514*	R-O-OH	PSS
3385*	O-H stretch	Air, DI, AS, PSS
2915	CH_2 asymmetric stretch	Air, DI, AS, PSS
2848	CH_2 symmetric stretch	Air, DI, AS, PSS
1725*	C=O stretch (Aldehyde[36])	DI
1645*	C=C stretch	Air, DI, AS, PSS
1471, 1463	CH_2 Bending deformation	Air, DI, AS, PSS
1420*	Aldehyde	Air, DI, AS
1377	CH_3 symmetric deformation	Air, DI, AS, PSS
1122*	C-O-C asymmetric bend	Air, DI, AS, PSS
1162, 1107, 1057, 1035*	C-O stretch[63]	PSS
1000*	Unknown	DI
898*	C-O-C stretch	Air, DI, PSS
820*	O-O stretch	Air, DI, AS
720	CH_2 (deformation) rock	Air, DI, AS, PSS

* Indicates new band formation. DI = deionized water, AS = artificial seawater, PSS = Puget Sound seawater.

When focusing on the 1800–800 cm^{-1} regions, artificial seawater and Puget Sound seawater samples showed smaller and broader 1645 cm^{-1} peaks than DI water and air samples. However, Puget Sound seawater and DI water samples exhibited significant changes in the C-O bending regions compared to air and artificial seawater samples. Both Puget Sound seawater and DI water samples show broad bands between 1200 and 900 cm^{-1} from C-O bonds, but their IR spectra appear drastically different. There appears to be a greater variety of C-O environments in LDPE weathered in PSS compared to DI water as indicated by the multiple peaks found after 26 weeks of weathering. This is possibly due to PE crosslinking creating various C-O-C or C=C structures in the polymer.[192]

The formation of new functional groups in the weathered LDPE also led to a decrease in peak intensities of the 2915, 2848, 1471, and 1463 cm^{-1}, peaks associated with CH_2 stretches, indicating chain scission of LDPE and formation of tertiary carbons.[192]

Polypropylene

The IR spectra of weathered PP, in Figure 4.7, indicated the formation of various new functional groups, represented by peaks listed in Table 4.5; primarily located in the hydroxyl, carbonyl, and C-O IR regions. The IR spectrum of air samples show low hydroxyl groups content, while the water samples show significantly more hydroxyl content indicated by the greater increase at 3390 cm^{-1}. Puget Sound seawater samples also showed the presence of additional peaks in this region, which may indicate the presence of polymer hydroperoxides.[193] Air, artificial seawater, and Puget Sound seawater samples showed presence of peaks at 1785 or 1735 cm^{-1} and thus the presence of different carbonyl containing products in the weathered PP. Air, artificial seawater, and Puget Sound seawater weathered PP samples indicate the formation of C=O groups though artificial seawater carbonyls showed at slightly higher wavenumbers than air and Puget Sound seawater (1785 vs 1735 cm^{-1} respectively). This may indicate that artificial seawater samples show the formation of vinyl esters while air and Puget Sound seawater show the formation of aliphatic esters.[192] However, DI water samples did not show peaks in this region but did show evidence of ketone formation at 1545 cm^{-1}. The difference in these peaks indicate different carbonyl containing products formed among the different environments. All samples expectedly exhibited evidence of carbon double bonds at 1645 cm^{-1} because of chain scission, the main degradation mechanism of PP.[193] Moreover, Puget Sound seawater samples showed the presence of conjugated double bonds,

which may indicate a greater level of chain scission and higher olefin formation compared to the other environments.

A major difference in the PP IR spectra of the different environments is between the region 1300 to 900 cm-1, the region assigned to C-O-C or O-O stretches (Figure 4).[192] Puget Sound seawater samples showed the appearance of multiple unique peaks not found in the other environments. The presence of these multiple peaks may indicate the various crosslinking bonds found in Puget Sound seawater weathered PP. Considering this and revisiting the unique Puget Sound seawater peaks between 3200 and 3550 cm^{-1}, it is likely that the multiple peaks around 1300 cm^{-1} are from polymer hydroperoxides as these groups are the primary product of PP photooxidation.[193] Hydroperoxides are considered the main product in photooxidation which result from attack at primary, secondary, or tertiary C-H bonds.[194] The significance of this is that Puget Sound seawater weathered PP showed the evolution of more hydroperoxides compared to the other environments. The greater level of hydroperoxides can influence more chain scission and crosslinking, as identified by both Raman and IR, which can accelerate the aging of PP and result in higher crystallinity, thus making PP more susceptible to fragmentation.

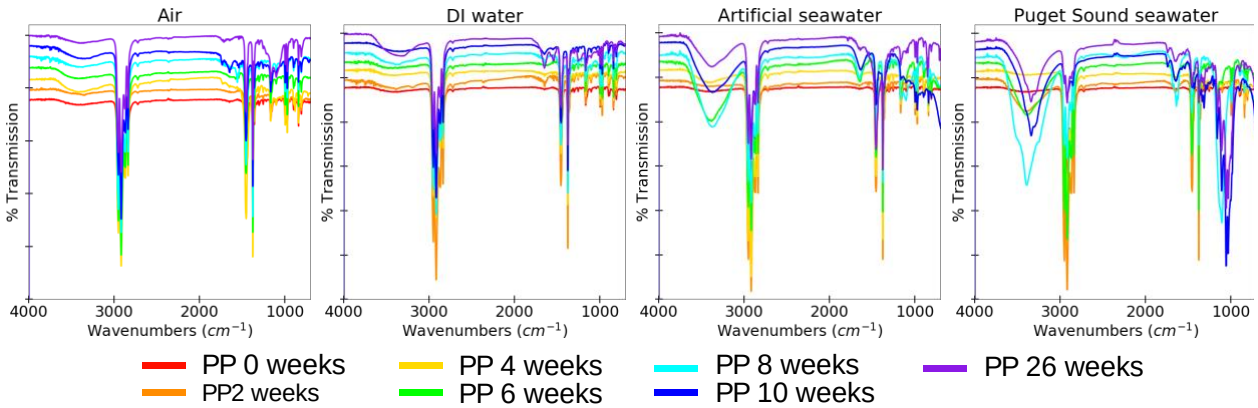

Figure 4. 7 IR spectra of PP after sunlight exposure over time in four different environments in a staggered overlay to observe the emergence of functional groups

Table 4. 5 Selected vibrational modes of IR bands of weathered PP samples[193, 195, 197]

Peak position (cm^{-1})	Vibrational mode	Environment band present
3530, 3338, 3265, 3245*	R-O-OH	PSS
3390*	O-H stretch	Air, DI, AS, PSS
1785*	C=O stretch	AS
1735*	C=O stretch	Air, PSS
1681*	Unknown	PS
1645*	C=C	Air, DI, AS, PSS
1619*	C=C, conjugated	PSS
1545*	C=O, ketone	DI
1454*	Unknown	PS
1430	C-O-H, Carboxylic acid	AS (sort of), PSS
1334, 1315	CH bend, CH2 twist	PSS
1261	CH bend, CH2 twist, CH3 rock	DI
1110	C-C stretch, CH2 wag, CH twist	Air, AS, PSS
1160, 1031, 1016*	C-C bend, CH3 rock, CH bend C-O-C, ether	PSS
900	CH3 rock, CH2 rock, CH bend	PSS

* Indicates new band formation. DI = deionized water, AS = artificial seawater, PSS = Puget Sound seawater.

4.3.3 Weathering environment differences

Across all polymers, the weathering conducted with Puget Sound seawater show different weathering byproducts compared to air, DI water, and artificial seawater weathering. What's particularly interesting is that artificial seawater showed different products compared to the Puget Sound seawater, indicating that simulated laboratory techniques does not account for all the degradation byproducts and microplastic pollution effects. The results from IR clearly show different functional groups formed from weathering in different environments which are summarized in Table 4.4 and Table 4.5. In this section we explore the different products that form in LDPE and PP in the four environmental weathering conditions and what that may implicate regarding degradation pathways.

The polymer backbone of PE is constructed of exclusively C-C single bonds that are highly resistant to photooxidative degradation. However, in the case of LDPE a small number of

unsaturated C=C bonds can exist. These groups are readily oxidized and can be converted into more stable UV-absorbing carbonyl groups.[198] Based on the IR spectrum of pristine LDPE, there are C=C bonds already present indicated by the peak at 1645 cm^{-1}. With increasing sunlight exposure, the intensity of this band increases then decreases in air and DI water. Both air and DI water samples also show increases in the 3385 (hydroxyl), 1420 (aldehyde), and 1122 (secondary alcohol or ketone) cm^{-1} bands. These band changes my indicate Norrish type I and II reactions that primarily result in aldehyde/ketone and alkene containing byproducts.[199] The Raman data indicated changes in the lateral packing of polymer chains which hinted at chain scission. Considering both IR and Raman data, both Norrish type processes contribute to the carbonyl and vinyl group formation via chain scission.[199] DI water samples, in contrast to the air samples, show broadening of the 1122 cm^{-1} band after 8 weeks and the presence of a new 1000 cm^{-1} band at 26 weeks. The broadening of IR peaks is associated with different types of hydrogen bonding influencing the stretching frequencies. DI water samples are the only environment to exhibit a 1725 cm^{-1} peak, indicative of carbonyl from carboxylic acid derivatives, which may implicate at more Norrish Type II reactions with hydroxy radical formation.[39, 199]

Interestingly, Puget Sound seawater LDPE shows various unique peaks in the C-O region around 1200 and 900 cm^{-1} after compared to artificial seawater LDPE. LDPE weathered in Puget Sound seawater exhibit a broadening of the 1645 and 1122 cm^{-1} peaks, while LDPE in AS shows a combination of increasing and broadening of these bands. Peaks around 1645 cm^{-1} correspond to the formation of both carbonyl and C=C bonds while peaks around 1122 cm^{-1} correspond to C-O groups.[1, 200] The multiple peaks unique to Puget Sound seawater samples from 1162 – 1035 cm-1, may indicate different C-O containing degradation products,[201] but may also indicate phosphate ions or aliphatic phosphates.[202, 203] However, the Raman spectra showed no obvious peaks

corresponding to phosphates and therefore the different C-O degradation products or crosslinking is more likely.[204, 205] The unique products found in Puget Sound seawater samples requires more with microbial environments and environmental seawater to fully elucidate.

The degradation reaction mechanisms of PP are like PE, though the tertiary carbon in the PP backbone makes PP more unstable to abiotic attack.[51] The main mechanism for PP degradation is chain scission.[166, 193] In the water samples, there is more chain scission occurring is indicated appearance of the Raman 989 cm^{-1} peak, associated with isotactic segments in a helix confirmation with a minimum length of 5–10 monomer units. IR spectroscopy similarly shows the effects of photooxidation by the presence of 1645 cm^{-1} bands, associated with C=C bonds, in all the environments. PP expectedly showed greater formation of oxidative groups than LDPE indicated by the greater intensity in IR bands around 3390, 1600, and 1100 cm^{-1}. Air weathered PP samples showed little changes in the O-H stretch region followed by DI water, artificial seawater, and Puget Sound seawater samples with the most. Like LDPE, Puget Sound seawater showed various products not shown in the other environments, most notably hydroperoxides. Hydroperoxide acts as the major source of free radicals for chain scission during photodegradation.[194] As stated previously, the higher formation of hydroperoxides in Puget Sound seawater demonstrates that PP weathered in the Puget Sound seawater is more suspectable to weathering and fragmentation than other environments. Based on these findings, artificial seawater does not adequately describe weathering that occurs in the environment.

4.4 Conclusion

The following conclusions can be drawn from this study:

1. Raman spectroscopy retains great fidelity of weathered polymer spectra and show little variation with increasing exposure to sunlight and may serve as a more accurate and versatile tool for microplastic identification compared to IR spectroscopy.
2. Slight variations in notable Raman peaks of each polymer indicate slight polymer structural changes such as crystallinity and chain length.
3. Raman and IR spectral indices comparing the formation of oxidized groups are inadequate in quantifying the age of microplastics as their weathering and aging does appears to be non-linear.
4. Weathering is effects were most obvious in the water samples, with Puget Sound seawater showing the significantly different spectra compared to pristine polymer samples.
5. Weathering conducted with Puget Sound seawater show different weathering byproducts compared to air, DI water, and artificial seawater weathering. This implies that studies with environmental water is needed to further understand degradation mechanisms and microplastic pollution effects.
6. Considering the varied spectra collected from each environment and polymers, a comprehensive IR spectral library containing weathered polymer spectra may be inadequate in facing the microplastic identification challenge.

Chapter 5. Computer vision tools for microplastic analysis

5.1 Introduction

Computer vision and machine learning is used by various disciplines to extract digital features from an image and used for classification problems with high accuracy.[206–208] These approaches have been used by diverse disciplines to automatically identify features from digital images for categorization problems.[207, 208] The wide variety of different microplastic morphologies and composition coupled with the dynamic environmental forces involved make understanding the transport process of microplastics extremely challenging. Microplastic research can benefit from a fast and reliable methodology that can facilitate automatic monitoring of microplastics less than 1 mm.[209] Most microplastic studies focus on collecting data on the abundance and spatiotemporal distribution of microplastics and their categorization by size, shape, and color.[7] One limitation is the ability to categorize and label the large data sets of particles found in the environment quickly and accurately. Categorization and imaging are time-intensive and completed by human experts with ample experience in microplastic analysis.[42] Current methods to sort and classify microplastics are time-intensive and can result in human-error-based mislabeling and biases that negatively affect the representativeness of the sample; which ultimately impedes scientific understanding of microplastic accumulation and transport.[5] Few tools can classify microplastics automatically and those that do focus on particles 1 – 5 mm in size, drastically reducing smaller microplastics that need to be analyzed.[210–212] Increasing computing power and machine learning algorithms offer an opportunity for researchers to understand microplastic distribution patterns quickly and quantitatively track the accumulation of microplastic types.

The understanding of morphological features of microplastics can aid current computer vision programs in particle selection before chemical identification. The development of an

automated computer vision and machine learning algorithm that can classify microplastics crucially speeds up and standardizes the research process. As the microplastic pollution increases, the bottleneck becomes not only the ability for researchers to identify and image microplastics, but also to quickly classify and analyze microplastics.[213] With the application of computer vision techniques and microplastic chemical identification data it may be possible to identify specific features that are common in all microplastics and visually distinguish microplastics from non-microplastics. Only recently have correlations between particle shape and polymer identity been studied in the laboratory setting.[6] This study probes the potential of computer vision and machine learning to recognize morphological features to classify the shape of microplastics <100 µm and distinguish microplastics from non-microplastics.

5.2 Methods

Materials

An image database consisting of 562 images of classified and labeled microparticles (microscopy images of both 145 microplastics and 417 non-microplastics) is used to train and test the computer vision algorithms. The microparticle images were collected from marine organisms around the Puget Sound and Salish Sea and from simulated weathering studies.[40] The majority of microparticles found in the environment were non-microplastics and therefore to avoid major sample bias additional microplastic images from weathering studies were included. The microplastic samples were collected on filter membranes and analyzed using a Renishaw inVia Raman microscope equipped with a Leica DMIRBE inverted optical microscope with 514 nm and 785 nm excitation lasers. The imaging, classification, and Raman spectral identification of over 500 microparticles was completed by human researchers. The imaging and identification involved

using different objective (10× and 50×) to locate and select particles from the background (filter membrane). Each microparticle is photographed, measured in major axis, and classified into four shape classes (fiber, spheroid, fragment, or irregular). All images in the database were taken with a 10× objective as the lower magnification allowed for the entire particle morphology to be captured. A Renishaw Inc. spectral reference library consisting of 267 commodity polymers was used as reference for the identification of polymer type. Each microplastic image consisted of one particle and its corresponding morphological and chemical identification labels.

Semantic segmentation and processing

One challenge in microplastic analysis is the ability to distinguish microparticles against a background since the complexity and heterogeneous nature of the filter membranes–the background–can be mistaken as microplastics.[215] Without proper segmentation of the object of interest, important variables such as shape, size, or color from the samples cannot be derived which can yield information about microplastic origins and fate.[10, 210, 211] Image segmentation methods can be classified into classical computer vision methods or neural network techniques; both techniques were explored in this study. Additionally, some minor pre-processing was completed to extract microplastic size from the images. The Raman microscope images contained microscope scale bars in the bottom right corner corresponding to the physical size of the microplastics. Resolution information was extracted which corresponded to the number of pixels in the scale bar to the physical size of the microplastics in μm. This parameter is then used in the decision trees to aid in microplastic shape classification.

Unsupervised semantic segmentation

Considering the myriad of microplastic morphologies, unsupervised semantic segmentation is ideal in classifying each pixel to derive insights from microplastic quickly and accurately. Unsupervised segmentation does not require users to train the model with pre-segmented microplastic images, therefore frees up significant researcher time. Additionally, unsupervised methods allow for the collection of unknown patterns in data which may aid in microplastic identification unknown to researchers. Unsupervised semantic segmentation was based on outlier extraction and morphological clean-up to discern the microparticle from the background and generate an unsupervised mask of the particle of interest. Outlier extraction used information based on the z-score of RGB component variability of each pixel in the entire image to identify outlier pixels associated with the particle compared to the background. Z-scores are multiples of standard deviation from the mean of a normally distributed population, in this case the pixel colors of the image. Morphological image clean-up was performed using the Scikit-learn morphology module which included remove_small_objects, binary_closing, binary_opening, binary_dilation, and binary_erosion. These morphological operations were necessary to ensure that pixels associated with small background anomalies from the filter paper were disregarded and that the pixels extracted properly represent the particle region.

This segmentation method can result in the identification of multiple regions in some images and post-processing was needed to select one object. Post-processing applies connected component analysis to the outlier detections to label connected components, a collection of pixels or region.[214] The total RGB variance across each component was compared and the component with the largest variance was selected as the object of interest. The selected connected component

was then saved as an unsupervised segmentation mask for each image (Figure 5.1 “Training mask”).

Pixel segmentation

In a comparison to unsupervised segmentation, a neural network model was also developed to segment microplastic images by detecting every pixel that belongs to an object class. Unsupervised segmentation may give less accurate results compared to supervised segmentation but can discover new data patterns. Pixel segmentation, on the other hand, uses a ground truth of binary masks to train and ultimately predict new segmentations. Using these two methods allow for comparison of how well each segmentation model is performing in extracting the metrics necessary for classification and which is more accurate for researchers to implement in analysis. Pixel segmentation was carried out based a U-Net architecture to label each pixel as the microparticle or the background. Convolutional Neural Networks (CNNs) are a class of deep learning algorithms most popularly used for computer vision image analysis by learning the optimal extracted features in vast amounts of images. U-Net is composed of contraction (encoder) and expansion (decoder) paths with concatenation between the paths at each model depth. The concatenation at each level allows the model to combine feature maps with the images for more precise feature localization. The unsupervised binary masks generated in the previous section were used as the “Training mask” or ground truth to train the supervised pixel segmentation neural network to generate the “Predicted mask” shown in Figure 5.1. Manual binary masks of 100 microplastic images generated by human researchers using ImageJ were used to compare the accuracy of segmentation of both methods and listed as “True mask” in Figure 5.1.

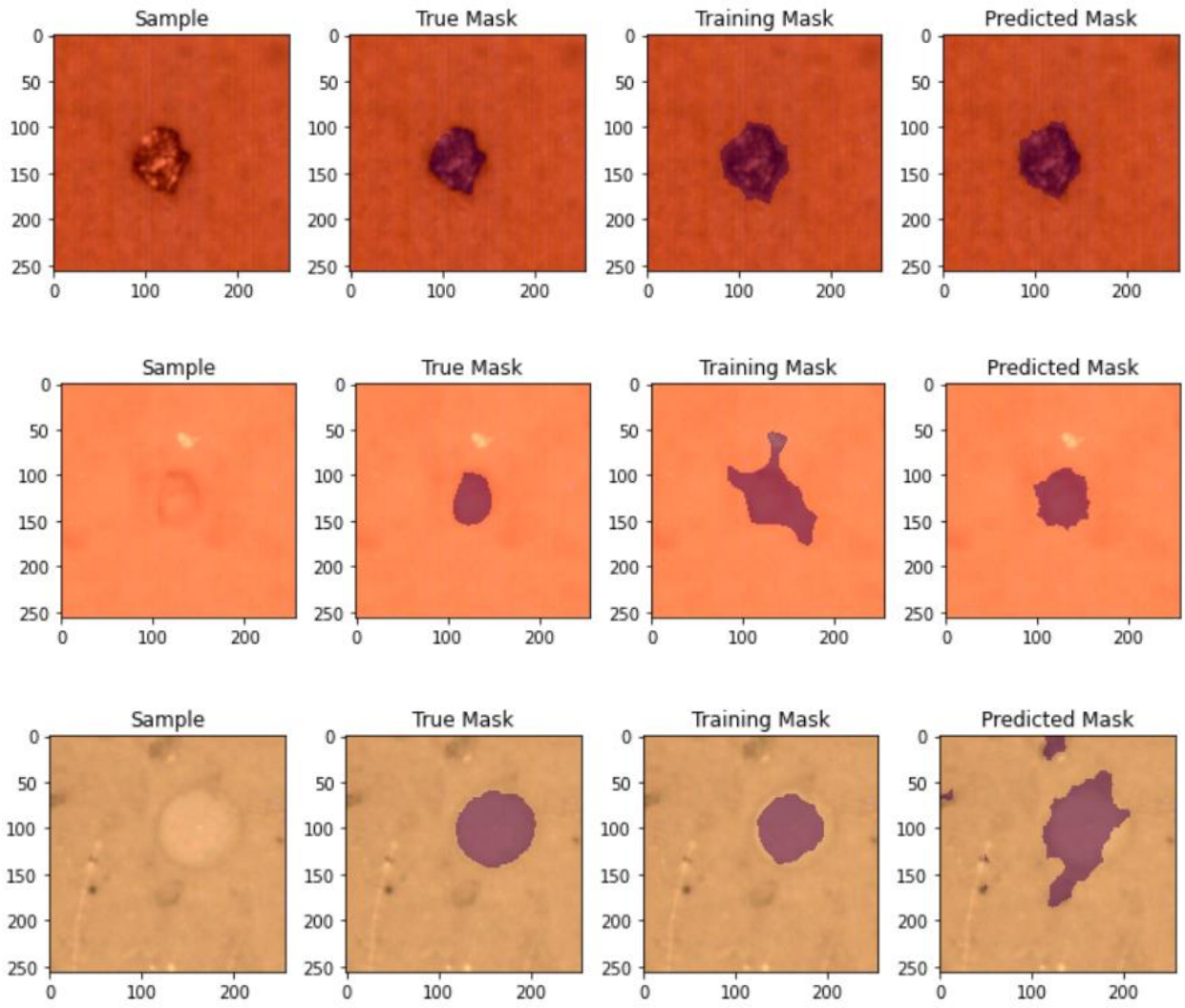

Figure 5. 1 Microparticle images from dataset (sample), and binary image masks created by human researchers (True Mask), unsupervised image segmentation (Training Mask), and neural network segmentation (Predicted Mask).

Properties of samples from masks

Measured properties of the unsupervised and pixel segmentation masks representing the size and shape of microplastics were computed with Scikit-learn feature and measure modules. The physical size (in µm) and other numerical representations of image properties describing the microplastic shape were measured using the segmented masks. Table 5.1 describes the image properties and basic formulas used to measure microplastic samples.

Table 5. 1 Image properties, formulas, and descriptions

Metrics	Formula	Description[216]
Extent	area/bbox_area	Ratio of pixels in the region to pixels in the total bounding box.
Eccentricity	minor_axis_length / minor_axis_length	The ratio of focal distance (distance between focal points or minor distance) over the major axis. Can distinguish spheroids.
Compactness	4*pi*area / perimeter^2	The ratio of the area of an object to the area of a circle with the same perimeter. Measures the elongation of shapes. Can distinguish fibers.
Solidity	area / convex_area	Ratio of pixels in the region to pixels of the convex hull image. Can distinguish fragments (also labeled shards) from irregulars.

Supervised image classification

Once the microplastic particles were segmented by the two methods, we used a decision tree classified each particle into shape classes. After the properties were measured from both unsupervised and pixel segmentation masks, the features were fed into a decision tree classifier to determine the microplastic shape classifications as fiber, irregular, fragment (also called shard), or spheroid. Figure 5.2 shows a plot of the decision tree generated with the measured metrics. Additionally, we explored a neural network approach that attempted to classify the microplastic shapes without any measured mask/shape features. In this aspect, we also used a CNN for image classification in which the model was trained on the same set of images and microplastic shape labels.

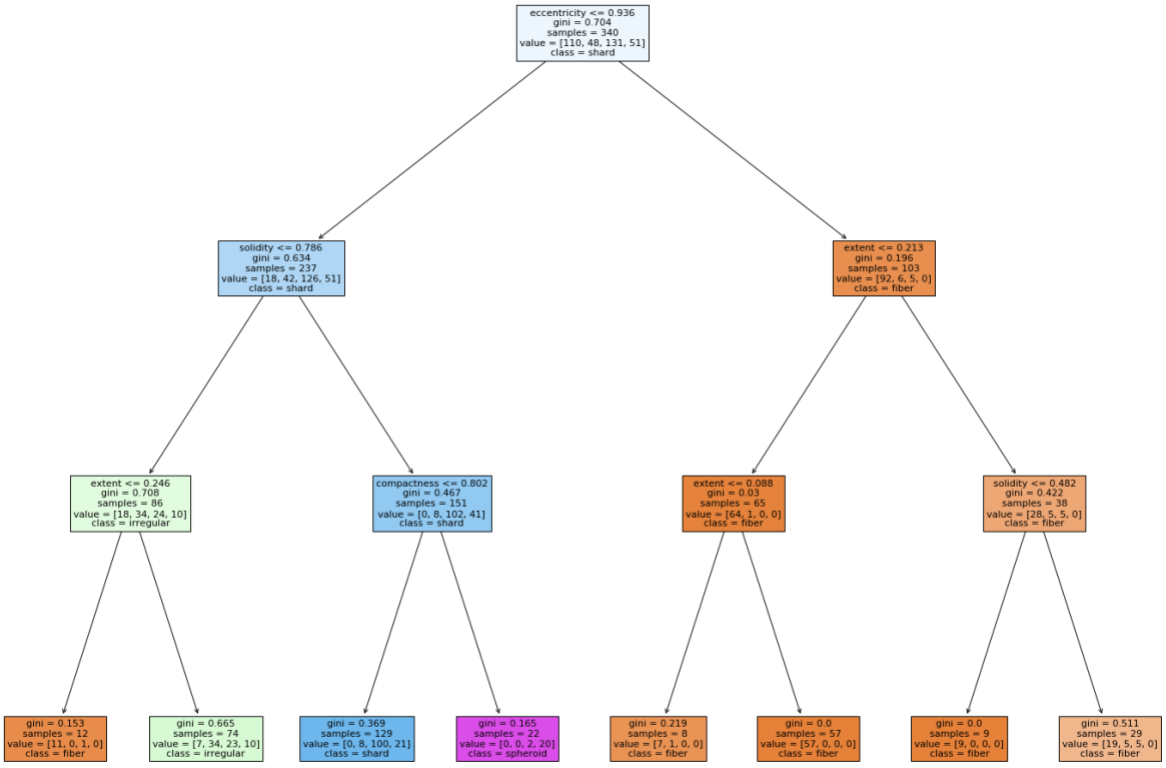

Figure 5. 2 Binary decision tree for classifying microplastic shape

5.3 Results and discussion

Segmentation

When evaluating a model, predictions are classified as true positives, false positives, true negatives, and false negatives. In semantic segmentation, each pixel in an image is predicted as a class of either the particle or the background. The quality of segmentation for the unsupervised and supervised neural-network-generated masks were measured by the performance metrics of precision, recall, and f1-score in relation to the true labeled masks (True Mask). Definitions and descriptions of these metrics are listed in Table 5.2. In some cases, both unsupervised segmentation

and neural network approach results in accurate and inaccurate segmentation as seen in Figure 5.1. Table 5.3 summarizes the calculated metrics from each approach. The top row in Figure 5.1 shows how both models predict an accurate mask for the microplastic image compared to the True Mask. The second row shows the weakness of unsupervised segmentation in which the model predicts extraneous features as part of the microplastic, but the neural network was successful. And the third row shows weakness of the neural network segmentation in which it merges multiple features, compared to the unsupervised segmentation model. Unsupervised segmentation masks (Training Mask, Figure 5.1) when compared to the True Mask had a precision of 0.86 while the neural network segmentation (Prediction Mask) had a precision of 0.78. The higher precision for the unsupervised mask is expected since outlier extraction specifically selects pixels that are related to the object of interest whereas the neural network is trained on binary masks and can select pixels unrelated to the object of interest. The recall for the unsupervised segmentation model is 0.65 and the recall for neural network segmentation is 0.84. And finally, the F1-score is 0.61 for unsupervised segmentation and 0.78 for neural network segmentation. This indicates that although unsupervised segmentation has higher precision, it is also missing other features that may be representative of the microplastic. The neural network has a lower precision, but higher true positive rate (recall) and has a less likely chance of missing important features of the microplastics. However, a lower chance of missing important features also means that the masks may pick up extraneous features that can reduce the accuracy of shape classification.

Table 5. 2 Quality metrics for segmentation, formulas, and descriptions

Accuracy metric	Formula	Description
Precision	True positives / (True positives + False positives)	Describes the purity of positive detections relative to the ground truth. (How well the objects match the ground truth)
Recall	True positives / (True positives + False Negatives)	Describes the completeness of positive predictions relative to the ground truth. (How many objects captured as positive predictions)
F1-score	2(Precision * Recall) / (Precision + Recall)	Weighted average recall and precision. Important for uneven class distributions.

Table 5. 3 Metrics for unsupervised and neural network segmentation

	Precision	Recall	F1-score
Unsupervised segmentation	0.86	0.65	0.61
Neural network supervised (pixel) segmentation	0.78	0.84	0.78

Classification

Image classification uses image-wide annotations to classify microplastic shapes into four different classes (e.g. fiber, irregular, fragment/shard, or spheroid). There were three approaches for shape classification in which metrics measured from the (1) unsupervised binary masks and (2) pixel segmentation were fed into decision trees and also (3) using a CNN. From the unsupervised and supervised masks, metrics related to the shape and size of the microplastics were measured and input into a decision tree (Figure 5.2). Decision trees predict the shape classes derived from the features that are input into it. The accuracy of image classifications was calculated based the F1-score for each microplastic shape class. Since there are a different number of microplastic shapes that are classified, to have a more representative quality assessment the F1-score provides a geometric average of the precision and recall. A CNN uses less pre-processing and does not require

the metrics measured from masks. CNN work by extracting features from images and eliminates the need for manual feature extraction (in contrast to the decision tree methods).

Current accuracy results reveal that the supervised decision tree classifications are more accurate than the neural network classifications. This is important as this reveals that properties from the microplastic images is necessary for accurate shape classifications. The decision tree classification method has another benefit in which it informs the user which features (e.g. extent, solidity, etc.) are important. This highlights the usefulness of traditional computer vision and feature extraction. In the case of deep learning, the pixels of the imagery are used for classification and there are no refined features extracted as what is needed in the decision trees. Additionally, with the neural network, there is no obvious microplastic features in which researchers can identify for additional studies. Statistical analysis of each of the microplastic features are underway.

5.4 Conclusion

The current tool for segmentation and classification of microplastics will be valuable for experts and non-experts to advance studies in microplastics. The development of an automated classification tool will allow quick and accurate microplastic identification under 100 µm, greatly increasing the range of microplastics that can be classified. The tools developed allow for unsupervised segmentation and a neural network approach for segmentation. Regarding both methods, the segmentation accuracy is similar. Finally, the decision tree method for microplastic shape classification is about 80% using unsupervised segmentation methods. And while the model predicts microplastic shapes as fibers well, it does have more difficulty with classifying spheroids and fragments.

5.5 Future work

The results from the algorithm's microplastic classification can be used to map the occurrence of microplastic types efficiently. Furthermore, the features extracted from the microplastic masks can reveal different properties about microplastics that hint about the commonalities between microplastics and non-microplastics. Early studies on microplastics relied primarily on visual identification of microplastics; however, this inaccurately estimates the actual amount of microplastics found in the environment as visual inspection leads to both false positives and false negatives. The pre-sorting and classification performed by human researchers results in human-error-based mislabeling and biases that yield less than representative results. An approach to increase representativeness and accuracy of environmental microplastic occurrence is to analyze every particle in a sample, but such an approach involves even more operator time than pre-sorting. Recent developments of imaging techniques can locate many particles on a sample for chemical identification.[6] The algorithms developed critically speed up and standardizes the process of classifying microplastics. As the occurrence of microplastics types change over time and more microplastic images are collected, the collected images will be used to train the algorithm further to recognize more detailed features. Understanding the pattern between the types of microplastic types in a certain region will elucidate the patterns of accumulation and transport as well as will offer a method to monitor the development of microplastics in the environment.

Chapter 6. References

1. PlasticsEurope, Plastics – the Facts 2019: An analysis of European plastics production, demand and waste data. https://www.plasticseurope.org/application/files/9715/7129/9584/FINAL_web_version_Plastics_the_ facts 2019 _14102019.pdf Accessed 29 July 2020.
2. R. Geyer, J. R. Jambeck, K. L. Law, Production, use, and fate of all plastics ever made. *Sci. Adv.* 3 (2017) 1700782.
3. Z. Sobhani, M. A. Amin, R. Naidu, M. Megharaj, C. Fang, Identification and visualization of microplastics by Raman mapping. *Anal. Chim. Acta* 1077 (2019) 191–199.
4. O. O. Fadare, E. D. Okoffo, Covid-19 face masks: A potential source of microplastic fibers in the environment. *Sci Total Environ*. 737 (2020) 140279.
5. J. P. Da Costa, A. R. Nunes, P. S. M. Santos, A. V. Girão, A. C. Duarte, T. Rocha-Santos, Degradation of polyethylene microplastics in seawater: Insights into the environmental degradation of polymers. *J. Environ. Sci. Health A* 53 (2018) 866–875.
6. F. Julienne, N. Delorme, F. Lagarde, From macroplastics to microplastics: Role of water in the fragmentation of polyethylene. *Chemosphere* 236 (2019) 124409.
7. Z. Akdogan, B. Guven, Microplastics in the environment: A critical review of current understanding and identification of future research needs. *Environ. Pollut.* 254 (2019) 113011.
8. C. F. Araujo, M. M. Nolasco, A. M. P. Ribeiro, P. J. A. Ribeiro-Claro, Identification of microplastics using Raman spectroscopy: Latest developments and future prospects, *Water Res.* 142 (2018) 426–440.
9. J. Gigault, A. ter Halle, M. Baudrimont, P.-Y. Pascal, F. Gauffre, T.-L. Phi, H. E. Hadri, B. Grassl, S. Reynaud, Current opinion: What is a nanoplastic? *Environ. Pollut.* 235 (2018) 1030–1034.
10. H. Zhang, Transport of microplastics in coastal seas. *Estuar. Coast. Shelf Sci.* 199 (2017) 75–86.
11. A. N. Genc, N. Vural, L. Balas, Modeling transport of microplastics in enclosed coastal waters: A case study in the Fethiye Inner Bay. *Mar. Pollut. Bull.* 150 (2020) 110747.
12. S. Allen, D. Allen, V. R. Phoenix, G. L. Roux, P. D. Jiménez, A. Simonneau, S. Binet, D. Galop, Atomspheric transport and deposition of microplastics in a remote catchment. *Nat. Geosci.* 12 (2019) 339–344.
13. O. S. Alimi, J. F. Budarz, L. M. Hernandez, N. Tufenkji, Microplastics and Nanoplastics in Aquatic Environments: Aggregation, Deposition, and Enhanced Contaminant Transport. *Environ. Sci. Technol.* 52 (2018) 1704−1724.
14. R. W. Obbard, Microplastics in Polar Regions: The role of long range transport. *Curr Opin Environ Sci Health.* 1 (2018) 24–29.
15. Ward, J.E., Shumway, S.E., 2004. Separating the grain from the chaff: particle selection in suspension-and deposit-feeding bivalves. J. Exp. Mar. Biol. Ecol. 300 (1–2), 83–130.
16. Ward, J.E., Newell, R.I., Thompson, R.J., MacDonald, B.A., 1994. In vivo studies of suspension-feeding processes in the eastern oyster, Crassostrea virginica (Gmelin). Biol. Bull. 186 (2), 221–240.
17. Paul-Pont, I., Lacroix, C., Fernández, C.G., Hégaret, H., Lambert, C., Le Goïc, N., ... Guyomarch, J., 2016. Exposure of marine mussels Mytilus spp.to polystyrene microplastics:

toxicity and influence on fluoranthene bioaccumulation. Environmental Pollution 216, 724–737.
18. Sussarellu, R., Suquet, M., Thomas, Y., Lambert, C., Fabioux, C, Pernet, M.E.J., ... Corporeau, C., 2016. Oyster reproduction is affected by exposure to polystyrene microplastics. Proceedings of the National Academy of Sciences 113 (9), 2430–2435.
19. Welden, N.A., Cowie, P.R., 2016. Long-term microplastic retention causes reduced body condition in the langoustine, Nephrops norvegicus. Environ. Pollut. 218, 895–900.
20. Harris, L.S., Carrington, E., 2019. Impacts of microplastic vs. natural abiotic particles on the clearance rate of a marine mussel. Limnology and Oceanography Letters 1–8.
21. Farrell, P., Nelson, K., 2013. Trophic level transfer of microplastic: Mytilus edulis (L.) to Carcinus maenas (L.). Environ. Pollut. 177, 1–3.
22. Au, S.Y., Lee, C.M., Weinstein, J.E., van den Hurk, P., Klaine, S.J., 2017. Trophic transfer of microplastics in aquatic ecosystems: identifying critical research needs. Integr. Envi- ron. Assess. Manag. 13 (3), 505–509.
23. Cole, M., Lindeque, P., Halsband, C., Galloway, T.S., 2011. Microplastics as contaminants in the marine environment: a review. Mar. Pollut. Bull. 62 (12), 2588–2597.
24. Siegfried, M., Koelmans, A.A., Besseling, E., Kroeze, C., 2017. Export of microplastics from land to sea. A modelling approach. Water Res. 127, 249–257.
25. Horton, A.A., Dixon, S.J., 2018. Microplastics: an introduction to environmental transport processes. Wiley Interdiscip. Rev. Water 5 (2), e1268.
26. Miller, R.Z.,Watts, A.J., Winslow, B.O., Galloway, T.S., Barrows, A.P., 2017. Mountains to the sea: river study of plastic and non-plastic microfiber pollution in the northeast USA. Mar. Pollut. Bull. 124, 245–251.
27. Wessel, C.C., Lockridge, G.R., Battiste, D., Cebrian, J., 2016. Abundance and characteristics of microplastics in beach sediments: insights into microplastic accumulation in northern Gulf of Mexico estuaries. Mar. Pollut. Bull. 109 (1), 178–183.
28. F. Wang, C. S. Wong, D. Chen, X. Lu, F. Wang. E. Y. Zheng, Interaction of toxic chemicals with microplastics: A critical review. *Water Res.* 139 (2018) 208–219.
29. C. Campanale, C. Massarelli, I. Savino. V. Locaputo, V. F. Uricchio, A Detailed Review Study on Potential Effects of Microplastics and Additives of Concern on Human. *Health. Int. J. Environ. Res. Public Health* 17 (2020) 1212.
30. X. Guo, X. Wang, X. Zhou, X. Kong, S. Tao, B. Xing, Sorption of Four Hydrophobic Organic Compounds by Three Chemically Distinct Polymers: Role of Chemical and Physical Composition. *Environ. Sci. Technol.* 46 (2012) 7252−7259.
31. W. J. Shim, S. H. Hong, S. E. Eo, Identification methods in microplastic analysis: a review. *Anal. Methods* 9 (2017) 1384.
32. A. M. Elert, R. Becker, E. Duemichen, P. Eisentraut, J. Falkenhagen, H. Sturm, U. Braun, Comparison of different methods for MP detection: what can we learn from them, and why asking the right question before measurements matters? *Environ. Pollut.* 231 (2017) 1256–1264.
33. J. Wagner, Z.-M. Wang, S. Ghosal, C. Rochman, M. Gassel, S. Wall, S., Novel method for the extraction and identification of microplastics in ocean trawl and fish gut matrices. *Anal. Methods* 9 (2017) 1479–1490.
34. Y. Pico, A. Alfarhan, D. Barcelo, Nano- and microplastic analysis: Focus on their occurrence in freshwater ecosystems and remediation technologies. *Trends Anal. Chem. 113 (2019) 409–425.*

35. W. Fu, J. Min, W, Jiang, Y. Li, W. Zhang, Separation, characterization and identification of microplastics and nanoplastics in the environment. *Sci. Total Environ*. 721 (2020) 137561.
36. L. Frère, I. Paul-Pont, J. Moreau, P. Soudant, C. Lambert, A. Huvet, E. Rinnert, A semi-automated Raman micro-spectroscopy method for morphological and chemical characterizations of microplastic litter. *Mar. Pollut. Bull.* 113 (2016) 461–468.
37. R. Lenz, K. Enders, C. A. Stedmon, D. M. Mackenzie, T. G. Nielsen, T.G., A critical assessment of visual identification of marine microplastic using Raman spectroscopy for analysis improvement. *Mar. Pollut. Bull.* 100 (2015) 82–91.
38. F. J. Medela, C. M. Rimnacb, S. M. Kurtza, On the assessment of oxidative and microstructure changes after in vivo degradation of historical UMHWPE knee components by means of vibrational spectroscopies and nanoindentation, *J. Biomed. Mater. Res. A.* 89 (2009) 530–538.
39. V. Fernandez-Gonzalez, J.M. Andrade-Garda, P. Lopez-Mahía , S. Muniategui-Lorenzo, Impact of weathering on the chemical identification of microplastics from usual packaging polymers in the marine environment. *Analytica Chimica Acta* 1142 (2021) 179–188.
40. J. C. Martinelli, S. Phan, C. K. Luscombe, J. L. Padilla-Gamiño, Low incidence of microplastic contaminants in Pacific oysters (Crassostrea gigas Thunberg) from the Salish Sea, USA. *Sci Total Environ*. 715 (2020) 136826.
41. X. Wu, P. Liu, H. Shi, H. Wang, H. Huang, Y. Shi, S. Gao, Photo aging and fragmentation of polypropylene food packaging materials in artificial seawater. *Water Research* 188 (2021) 115456.
42. P. M. Anger, L. Prechtl, M. Elsner, R. Niessner, N. P. Ivleva, Implementation of an open source algorithm for particle recognition and morphological characterisation for microplastic analysis by means of Raman microspectroscopy. *Anal. Methods* 11 (2019) 3483–3489.
43. L. T. Kerr, H. J. Byrne, B. M. Hennelly, Optimal choice of sample substrate and laser wavelength for Raman spectroscopic analysis of biological specimen, *Anal. Methods* 7 (2015) 5041–5052.
44. D. Wei, S. Chen, Q. Liu, Review of Fluorescence Suppression Techniques in Raman Spectroscopy. *Appl. Spectrosc. Rev.* 50 (2015) 387–406.
45. C. D. Rummel, A. Jahnke, E. Gorokhova, D. Kühnel, M. Schmitt-Jansen, Impacts of biofilm formation on the fate and potential effects of microplastic in the aquatic environment. *Environ. Sci. Technol. Lett.* 4 (2017) 258–267.
46. R. E. Carlson, J. Shapiro, Dissolved humic substances: a major source of error in fluorometric analyses involving lake waters. *Limnol. Oceanogr.* 26 (1981) 785–790.
47. B. G. Mitchell, D. A. Kiefer, Chlorophyll α specific absorption and fluorescence excitation spectra for light-limited phytoplankton. *Deep Sea Res. Part A: Oceanogr. Res. Pap.* 35 (1988) 639–663.
48. J. N. Hahladakis, C. A.Velis, R. Weber, E. Iacovidou, P. Purnell, An overview of chemical additives present in plastics: Migration, release, fate and environmental impact during their use, disposal and recycling, *J. Hazard. Mater.* 344 (2018) 179–199.
49. M. Dong, Q. Zhang, X. Xing, W. Chen, Z. She, Z. Luo, Raman spectra and surface changes of microplastics weathered under natural environments, *Sci. Tot. Environ.* 739 (2020) 139990.
50. V. P. Ranjan, S. Goe, Degradation of Low-Density Polyethylene Film Exposed to UV Radiation in Four Environments. *J. Hazard. Toxic Radioact. Waste*, 23 (2019) 04019015.

51. W. Cowger, Z. Steinmetz, A. Gray, K. Munno, J. Lynch, H. Hapich, S. Primpke, H. D. Frond, C. Rochman, O. Herodotou, Microplastic Spectral Classification Needs an Open Source Community: Open Specy to the Rescue! *Anal. Chem.* 93 (2021) 7543−7548.
52. Van Cauwenberghe, L., Janssen, C.R., 2014. Microplastics in bivalves cultured for human consumption. Environ. Pollut. 193, 65–70.
53. Mathalon, A., Hill, P., 2014. Microplastic fibers in the intertidal ecosystem surrounding Halifax Harbor, Nova Scotia. Mar. Pollut. Bull. 81 (1), 69–79.
54. Rochman, C.M., Tahir, A., Williams, S.L., Baxa, D.V., Lam, R., Miller, J.T., ... Teh, S.J., 2015. An- thropogenic debris in seafood: Plastic debris and fibers from textiles in fish and bivalves sold for human consumption. Scientific Reports 5, 14340.
55. Li, J., Qu, X., Su, L., Zhang, W., Yang, D., Kolandhasamy, P., ... Shi, H., 2016. Microplastics in mussels along the coastal waters of China. Environmental Pollution 214, 177–184.
56. Baechler, B.B., Stienbarger, C.D., Horn, D.A., Joseph, J., Taylor, A.R., Granek, E.F., 2019. Microplastic occurrence and effects in commercially harvested North American fin- fish and shellfish: current knowledge and future directions. Limnology and Oceanog- raphy Letters 1–24 (Special Issue: Microplastics inmarine and freshwater organisms: Presence and potential effects).
57. Granek, E.F., Brander, S.M., Holland, E.B., 2020. Microplastics in aquatic organisms: improving understanding and identifying research directions for the next decade. Lim- nology and Oceanography Letters 1–4.
58. Davidson, K., Dudas, S.E., 2016. Microplastic ingestion by wild and cultured Manila clams (Venerupis philippinarum) from Baynes Sound, British Columbia. Arch. Environ. Contam. Toxicol. 71 (2), 147–156.
59. Murphy, C.L., 2018. A Comparison of Microplastics in Farmed and Wild Shellfish Near Vancouver Island and Potential Implications for Contaminant Transfer to Humans. Masters dissertation. Royal Roads University, Victoria, British Columbia, Canada.
60. Shumway, S.E., Ward, J.E., Mladinich, 2018. Themicroplastics and shellfishmedia frenzy – stop the train, we want to get off! East Coast Shellfish Growers Newsletter 26–27 (August 2018).
61. Coen, L.D., Brumbaugh, R.D., Bushek, D., Grizzle, R., Luckenbach, M.W., Posey, M.H., ... Tolley, S.G., 2007. Ecosystem services related to oyster restoration. Marine Ecology Progress Series 341, 303–307.
62. Washington Sea Grant, 2015. Shellfish Aquaculture in Washington State. Final Report to the Washington State Legislature (84 p).
63. Andrady, A.L., 2011. Microplastics in the marine environment. Mar. Pollut. Bull. 62 (8), 1596–1605.
64. Cózar, A, Echevarría, F, González-Gordillo, JI, Irigoien, X, Úbeda, B, Hernández-León, S, ... Fernández-de-Puelles, ML, 2014. Plastic debris in the open ocean. Proceedings of the National Academy of Sciences 111 (28), 10239–10244.
65. Lebreton, L., Slat, B., Ferrari, F., Sainte-Rose, B., Aitken, J., Marthouse, R., ... Noble, K., 2018. Evidence that the Great Pacific Garbage Patch is rapidly accumulating plastic. Scientific reports 8 (1), 4666.
66. Encyclopedia of Puget Sound. https://www.eopugetsound.org/articles/puget-sounds-physical-environment, Accessed date: 1 May 2019.

67. Finlayson, D., 2006. The geomorphology ofPuget Sound beaches (No. 2006–02). University of Washington, School of Oceanography.
68. United States Census Bureau (2016).
69. Masura, J., et al., 2015. Laboratory Methods for the Analysis of Microplastics in the Marine Environment: Recommendations for Quantifying Synthetic Particles in Waters and Sediments.
70. Eshom-Arzadon, F., 2017. Concentration ofMicroplastics in Beach Sediments Surrounding Seattle, Washington in the Puget Sound Estuary. Undergraduate dissertation for an Oceanography degree. University of Washington.
71. Li, J., Yang, D., Li, L., Jabeen, K., Shi, H., 2015. Microplastics in commercial bivalves from China. Environ. Pollut. 207, 190–195.
72. Foekema, E.M., De Gruijter, C., Mergia, M.T., van Franeker, J.A., Murk, A.J., Koelmans, A.A., 2013. Plastic in north sea fish. Environmental Science & Technology 47 (15), 8818–8824.
73. Torre, M., Digka, N., Anastasopoulou, A., Tsangaris, C., Mytilineou, C., 2016. Anthropogenic microfibres pollution in marine biota. A new and simple methodology to minimize airborne contamination. Mar. Pollut. Bull. 113 (1–2), 55–61.
74. Frias, J.P.G.L., Nash, R., 2019. Microplastics: finding a consensus on the definition. Mar. Pollut. Bull. 138, 145–147.
75. Hidalgo-Ruz, V., Gutow, L., Thompson, R.C., Thiel, M., 2012. Microplastics in the marine environment: a review of the methods used for identification and quantification. Environmental Science & Technology 46 (6), 3060–3075.
76. R Core Team, 2019. R: A Language and Environment for Statistical Computing. R Foundation for Statistical Computing, Vienna, Austria URL. https://www.R-project.org/.
77. Enders, K., Lenz, R., Stedmon, C.A., Nielsen, T.G., 2015. Abundance, size and polymer composition of marine microplastics ≥ 10 μm in the Atlantic Ocean and their modelled vertical distribution. Marine Pollution Bulletin 100 (1), 70–81.
78. Löder, M.G., Gerdts, G., 2015. Methodology used for the detection and identification of microplastics—a critical appraisal. Marine Anthropogenic Litter. Springer, Cham, pp. 201–227.
79. Tagg, A.S., Sapp, M., Harrison, J.P., Ojeda, J.J., 2015. Identification and quantification of microplastics in wastewater using focal plane array-based reflectancemicro-FTIR imaging. Anal. Chem. 87 (12), 6032–6040.
80. Imhof, H.K., Laforsch, C., Wiesheu, A.C., Schmid, J., Anger, P.M., Niessner, R., Ivleva, N.P., 2016. Pigments and plastic in limnetic ecosystems: a qualitative and quantitative study on microparticles of different size classes. Water Res. 98, 64–74.
81. Hind, A.R., Bhargava, S.K., McKinnon, A., 2001. At the solid/liquid interface: FTIR/ATR—the tool of choice. Adv. Colloid Interf. Sci. 93 (1–3), 91–114.
82. Käppler, A., Fischer, D., Oberbeckmann, S., Schernewski, G., Labrenz, M., Eichhorn, K.J., Voit, B., 2016. Analysis of environmental microplastics by vibrational microspectroscopy: FTIR, Raman or both? Anal. Bioanal. Chem. 408 (29), 8377–8391.
83. Browne, M.A., Crump, P., Niven, S.J., Teuten, E., Tonkin, A., Galloway, T., Thompson, R., 2011. Accumulation of microplastic on shorelines worldwide: sources and sinks. Environmental Science & Technology 45 (21), 9175–9179.

84. Gallo, F., Fossi, C., Weber, R., Santillo, D., Sousa, J., Ingram, I., ... Romano, D., 2018. Marine litter plastics and microplastics and their toxic chemicals components: the need for urgent preventive measures. Environmental Sciences Europe 30, 1–14.
85. Eriksen, M., Lebreton, L.C., Carson, H.S., Thiel, M., Moore, C.J., Borerro, J.C., ... Reisser, J., 2014. Plastic pollution in the world's oceans: more than 5 trillion plastic pieces weighing over 250,000 tons afloat at sea. PloS one 9 (12), e111913.
86. Li, J., Green, C., Reynolds, A., Shi, H., Rotchell, J.M., 2018a. Microplastics in mussels sampled from coastal waters and supermarkets in the United Kingdom. Environ. Pollut. 241, 35–44
87. Li, J., Lusher, A., Rotchell, J.M., Company, S.D., Turra, A., Bråte, I.L.N., ... Shi, H., 2018b. Using mussel as a global bioindicator of coastal microplastic pollution. Environmental Pollution 244, 522–533.
88. Qu, X., Su, L., Li, H., Liang, M., Shi, H., 2018. Assessing the relationship between the abundance and properties of microplastics in water and in mussels. Sci. Total Environ. 621, 679–686.
89. Santana, M.F.M., Ascer, L.G., Custódio, M.R., Moreira, F.T., Turra, A., 2016. Microplastic contamination in natural mussel beds from a Brazilian urbanized coastal region: rapid evaluation through bioassessment. Mar. Pollut. Bull. 106 (1–2), 183–189.
90. S. Morét-Ferguson, K. L. Law, G. Proskurowski, E. K. Murphy, E. E. Peacock, C. M. Reddy, The size, mass, and composition of plastic debris in the western North Atlantic Ocean. *Mar. Pollut. Bull.* 60 (2010) 1873–1878.
91. Woodall, L.C., Sanchez-Vidal, A., Canals, M., Paterson, G.L., Coppock, R., Sleight, V., Thompson, R.C., 2014. The deep sea is a major sink for microplastic debris. R. Soc. Open Sci. 1 (4), 140317.
92. Courtene-Jones, W., Quinn, B., Gary, S.F., Mogg, A.O., Narayanaswamy, B.E., 2017. Microplastic pollution identified in deep-sea water and ingested by benthic invertebrates in the Rockall Trough, North Atlantic Ocean. Environ. Pollut. 231, 271–280.
93. Rios, L.M., Moore, C., Jones, P.R., 2007. Persistent organic pollutants carried by synthetic polymers in the ocean environment. Mar. Pollut. Bull. 54 (8), 1230–1237.
94. Zhao, J., Ran, W., Teng, J., Liu, Y., Liu, H., Yin, X., ... Wang, Q., 2018. Microplastic pollution in sediments from the Bohai Sea and the Yellow Sea, China. Science of The Total Environment 640, 637–645.
95. M. Smith, D. C. Love, C. M. Rochman, R. A. Neff, R.A., Microplastics in seafood and the implications for human health. *Curr. Environ. Health Rep.* 5 (2018) 375–386.
96. Bobin, M.F., Michel, V., Martini, M.C., 1999. Study of formulation and stability of emulsions with polymeric emulsifiers. Colloids Surf. A Physicochem. Eng. Asp. 152, 53–58.
97. Nielloud, Francoise, Marti-Mestres, Gilberte, 2000. Pharmaceutical Emulsions and Suspensions. Marcel Dekker, Inc, New York, NY.
98. European Food Safety Authority, 2015. Scientific opinion on the re-evaluation of polyoxyethylene sorbitan monolaurate (E432), polyoxyethylene sorbitan monooleate (E433), polyoxyethylene sorbitan monopalmitate (E434), polyoxyethylene sorbitan monostearate (E435)and polyoxyethylene sorbitan tristearate (E436) as food additives. ESFA Journal 3 (7), 4152.
99. Andrady, A.L., 2015. Persistence of plastic litter in the oceans. Marine Anthropogenic Litter. Springer, Cham, pp. 57–72.

100. Quaranta, E., Sgherza, D., Tartaro, G., 2017. Depolymerization of poly(bisphenol A carbon- ate) under mild conditions by solvent-free alcoholysis catalyzed by 1,8-diazabicyclo [5.4.0]undec-7-ene as a recyclable organocatalyst: a route to chemical recycling of waste polycarbonate. Green Chem. 19, 5422–5434.
101. Siddiqui, M.N., Redhwi, H.H., Antonakou, E.V., Achilias, D.S., 2018. Pyrolysis mechanism and thermal degradation kinetics of poly(bisphenol Acarbonate)-based polymers originating in waste electric and electronic equipment. J. Anal. Appl. Pyrolysis 132, 123–133.
102. Artham, T., Doble, M., 2012. Bisphenol A and metabolites released by biodegradation of polycarbonate in seawater. Environ. Chem. Lett. 10 (1), 29–34.
103. Luo, W., Su, L., Craig, N.J., Du, F., Wu, C., Shi, H., 2019. Comparison ofmicroplastic pollution in different water bodies from urban creeks to coastal waters. Environ. Pollut. 246, 174–182.
104. Im, J., Loffler, F.E., 2016. Fate of bisphenol A in terrestrial and aquatic environments. Environmental Science & Technology 50 (16), 8403–8416.
105. Silva, A.B., Bastos, A.S., Justino, C.I.L., da Costa, J.P., Duarte, A.C., Rocha-Santos, T.A.P., 2018. Microplastics in the environment: challenges in analytical chemistry - a review. Anal. Chim. Acta 1017, 1–19.
106. Fredericks, P.M., 2012. Forensic analysis offibres by vibrational spectroscopy. Infrared and Raman Spectroscopy in Forensic Science, pp. 153–169.
107. Araya, R., Tani, K., Takagi, T., Yamaguchi, N., Nasu, M., 2003. Bacterial activity and community composition in stream water and biofilm from an urban river determined by fluorescent in situ hybridization and DGGE analysis. FEMS Microbiol. Ecol. 43 (1), 111–119.
108. Thompson, Richard C., et al. "Lost at sea: where is all the plastic?." *Science(Washington)* 304.5672 (2004): 838.
109. Wright, Stephanie L., Richard C. Thompson, and Tamara S. Galloway. "The physical impacts of microplastics on marine organisms: a review." *Environmental pollution* 178 (2013): 483-492.
110. Frias, João P., et al. "Microplastics in the Marine Environment: Sources, Distribution, Biological Effects and Socio-Economic Impacts." (2021).
111. Avio, Carlo Giacomo, Stefania Gorbi, and Francesco Regoli. "Plastics and microplastics in the oceans: from emerging pollutants to emerged threat." Marine environmental research 128 (2017): 2-11.
112. Palmer, Jacinta, and Sunil Herat. "Ecotoxicity of Microplastic Pollutants to Marine Organisms: a Systematic Review." *Water, Air, & Soil Pollution* 232.5 (2021): 1-21.
113. O. Setälä, J. Norkko, M. Lehtiniemi, Feeding type affects microplastic ingestion in a coastal invertebrate community. *Mar. Pollut. Bull.* 102 (2016) 95–101.
114. Sussarellu, Rossana, et al. "Oyster reproduction is affected by exposure to polystyrene microplastics." Proceedings of the national academy of sciences 113.9 (2016): 2430-2435.
115. Pedersen, Adam F., et al. "Microplastic ingestion by quagga mussels, Dreissena bugensis, and its effects on physiological processes." Environmental Pollution 260 (2020): 113964.
116. Mendrik, F. M., et al. "Species-specific impact of microplastics on coral physiology." Environmental Pollution 269 (2021): 116238.

117. Mallik, Abhijit, et al. "Ecotoxicological and physiological risks of microplastics on fish and their possible mitigation measures." Science of The Total Environment 779 (2021): 146433.
118. Franzellitti, Silvia, et al. "Microplastic exposure and effects in aquatic organisms: A physiological perspective." Environmental toxicology and pharmacology 68 (2019): 37-51.
119. National Centers for Coastal Ocean Science, 2021: National Status and Trends: Mussel Watch Program, https://www.fisheries.noaa.gov/inport/item/39400.
120. J. Widdows, C. Nasci, V. U. Fossato, Effects of Pollution on the Scope for Growth of Mussels (Mytilrcs galloprovincialis) from the Venice Lagoon, Italy. *Mar. Environ. Res.* 43 (1997) 69–79.
121. B. De Whitte, L. Devrise, K. Bekaert, S. Hoffman, G. Vandermeersch, K. Cooreman, J. Robbens, Quality assessment of the blue mussel (Mytilus edulis): Comparison between commercial and wild types. *Mar. Poll. Bull.* 85 (2014) 146–155.
122. J. A. Lanksbury, L. A. Niewolny, A. J. Carey, J. E. West, Toxic Contaminants in Puget Sound's Nearshore Biota: A Large-Scale Synoptic Survey Using Transplanted Mussels (Mytilus trossulus). Washington Department of Fish and Wildlife Publication #FPT 14-08. (2014) 180.
123. E. Carrington, J. H. Waite, G. Sarà, K. P. Sebens, Mussels as a Model System for Integrative Ecomechanics. *Annu. Rev. Mar. Sci.* 7 (2015) 443–69.
124. Harris, Lyda ST, Harsimran Gill, and Emily Carrington. "Microplastic changes the sinking and resuspension rates of marine mussel biodeposits." *Marine Pollution Bulletin* 165 (2021): 112165.
125. R. J. Uncles, P. E. Frickers, A. E. Easton, M. L. Griffiths, C. Harris, R. J. M. Howland, R. S. King, A. W. Morris, D. H. Plummer, A. D. Tappin, Concentrations of suspended particulate organic carbon in the tidal Yorkshire Ouse River and Humber Estuary. *Sci. Tot. Environ.* 251–252 (2000) 233–242.
126. W. Davis III, A. G. Murphy, Plastic in surface waters of the Inside Passage and beaches of the Salish Sea in Washington State. *Mar. Poll. Bull.* 97 (2015) 169–177.
127. Desforges, Jean-Pierre W., Moira Galbraith, and Peter S. Ross. "Ingestion of microplastics by zooplankton in the Northeast Pacific Ocean." *Archives of environmental contamination and toxicology* 69.3 (2015): 320-330.
128. Choy, C. Anela, et al. "The vertical distribution and biological transport of marine microplastics across the epipelagic and mesopelagic water column." *Scientific reports* 9.1 (2019): 1-9.
129. A. Kinjo, K. Mizukawa, H. Takada, K. Inouea, Size-dependent elimination of ingested microplastics in the Mediterranean mussel *Mytilus galloprovincialis. Mar. Poll. Bull.* 149 (2019) 110512.
130. S. Avery-Gomm, P. D. O'Hara, L. Kleine, V. Bowes, L. K. Wilson, K. L. Barry, Northern fulmars as biological monitors of trends of plastic pollution in the eastern North Pacific. *Mar. Poll. Bull.* 64 (2012) 1776–1781.
131. S. Avery-Gomm, J. F. Provencher, K. H. Morgan, D. F. Bertram, Plastic ingestion in marine-associated bird species from the eastern North Pacific. *Mar. Poll. Bull.* 72 (2013) 257–259.
132. V. A. Lindborg, J. F. Ledbetter, J. M. Walat, C. Moffett, Plastic consumption and diet of Glaucous-winged gulls (*Larus glaucescens*). *Mar. Poll. Bull.* 64 (2012) 2351–2356.

133. Desforges, Jean-Pierre W., et al. "Widespread distribution of microplastics in subsurface seawater in the NE Pacific Ocean." *Marine pollution bulletin* 79.1-2 (2014): 94-99.
134. G. A. Covernton, K. Cox, Commentary on: Abundance and distribution of microplastics within surface sediments of a key shellfish growing region of Canada. *PLoS One.* 14 (2019) e0225945.
135. Harris *et al.* In Review
136. Mahoney, Ty. *The concentration of microplastics compared to relative population proximity and basin residence times in Hood Canal and Whidbey Basin in Puget Sound, WA*. Diss. 2017.
137. MacCready, Parker, et al. "Estuarine circulation, mixing, and residence times in the Salish Sea." *Journal of Geophysical Research: Oceans* 126.2 (2021): e2020JC016738.
138. Sutherland, David A., et al. "A model study of the Salish Sea estuarine circulation." *Journal of Physical Oceanography* 41.6 (2011): 1125-1143.
139. Ward, J. Evan, et al. "Selective ingestion and egestion of plastic particles by the blue mussel (Mytilus edulis) and eastern oyster (Crassostrea virginica): implications for using bivalves as bioindicators of microplastic pollution." *Environmental science & technology* 53.15 (2019): 8776-8784.
140. Li, Jiana, et al. "Using mussel as a global bioindicator of coastal microplastic pollution." *Environmental pollution* 244 (2019): 522-533.
141. Ding, Jinfeng, et al. "Microplastics in four bivalve species and basis for using bivalves as bioindicators of microplastic pollution." *Science of The Total Environment* 782 (2021): 146830.
142. Dimitrijevic, Julie. *Application of the Blue Mussel (Mytilus edulis) as an indicator of microplastic pollution within the Salish Sea*. Diss. Science: Biological Sciences Department, 2018.
143. C. Ripken, D. G. Kotsifaki, S. N. Chormaic, Analysis of small microplastics in coastal surface water samples of the subtropical island of Okinawa, Japan. *Sci Total Environ.* 760 (2021) 143927
144. G. Grause, M.-F. Chien, C. Inoue, Changes during the weathering of polyolefins. Polymer Degradation and Stability 181 (2020) 109364.
145. M.M. Krahn, M. B. Hanson, R. W. Baird, R. H. Boyer, D. G. Burrows, C. K. Emmons, J. K. B. Ford, L. L. Jones, D. P. Noren, P. S. Ross, G. S. Schorr, T. K. Collier. Persistent organic pollutants and stable isotopes in biopsy samples (2004/2006) from Southern Resident Killer Whales. *Mar. Poll. Bull.* 54 (2007) 1903–1911.
146. S. E. Nelms, J. Barnett, A. Brownlow, N. J. Davison, R. Deaville, T. S. Galloway, P. K. Lindeque, D. Santillo, B. J. Godley, Microplastics in marine mammals stranded around the British coast: Ubiquitous but transitory? *Sci. Rep.* 9 (2019) 1075.
147. Pierce, G. J., Santos, M. B., Murphy, S., Learmonth, J. A., Zuur, A. F., Rogan, E., Bustamante, P., Caurant, F., Lahaye, V., Ridoux, V., Zegers, B. N., Mets, A., Addink, M., Smeenk, C., Jauniaux, T., Law, R. J., Dabin, W., López, A., Alonso Farré, J. M., ... Boon, J. P. (2008). Bioaccumulation of persistent organic pollutants in female common dolphins (Delphinus delphis) and harbour porpoises (Phocoena phocoena) from western European seas: Geographical trends, causal factors and effects on reproduction and mortality. *Environmental Pollution (Barking, Essex: 1987)*, *153*(2), 401–415.
148. Vinzant, A. (2017, February 7). Bioaccumulation and Biomagnification: Increasingly Concentrated Problems! *CIMI School*. https://cimioutdoored.org/bioaccumulation/

149. K. M. Parsons, K. C. Balcomb III, J. K. B. Ford, J. W. Durban, The social dynamics of southern resident killer whales and conservation implications for this endangered population. *Anim. Behav.* 77 (2009) 963–971.
150. A. Riera, J. F. Pilkington, J. K. B. Ford, E. H. Stredulinsky, N. R. Chapman, Passive acoustic monitoring off Vancouver Island reveals extensive use by at-risk Resident killer whale (Orcinus orca) populations. *Endang. Species Res.* 39 (2019) 221–234.
151. T. M. Mongillo, G. M. Ylitalo, L. D. Rhodes, S. M. O'Neill, D. P. Noren, Exposure to a mixture of toxic chemicals: Implications for the health of endangered southern resident killer whales. *U.S. Department of Commerce, National Oceanic and Atmospheric Administration* (2016) *National Marine Fisheries Service, Northwest Fisheries Science Center*.
152. M. M. Muto, V. T. Helker, R. P. Angliss, P. L. Boveng, J. M. Breiwick, M. F. Cameron, P. J. Clapham, S. P. Dahle, M. E. Dahlheim, B. S. Fadely, M. C. Ferguson, L. W. Fritz, R. C. Hobbs, Y. V. Ivashchenko, A. S. Kennedy, J. M. London, S. A. Mizroch, R. R. Ream, E. L. Richmond, K. E. W. Shelden, K. L. Sweeney, R. G. Towell, P. R. Wade, J. M. Waite, A. N. Zerbini, Alaska marine mammal stock assessments, 2018. NOAA Technical Memorandum NMFS-AFSC-393.
153. Bang, D. Y., Kyung, M., Kim, M. J., Jung, B. Y., Cho, M. C., Choi, S. M., Kim, Y. W., Lim, S. K., Lim, D. S., Won, A. J., Kwack, S. J., Lee, Y., Kim, H. S., & Lee, B. M. (2012). Human Risk Assessment of Endocrine-Disrupting Chemicals Derived from Plastic Food Containers. *Comprehensive Reviews in Food Science and Food Safety*, *11*(5), 453–470.
154. Gallo, F., Fossi, C., Weber, R., Santillo, D., Sousa, J., Ingram, I., Nadal, A., & Romano, D. (2018). Marine litter plastics and microplastics and their toxic chemicals components: The need for urgent preventive measures. *Environmental Sciences Europe*, *30*(1).
155. H. Godfray, J. Charles, A. E. A. Stephens, P. D. Jepson. S. Jobling, A. C. Johnson, P. Matthiessen, J. P. Sumpter, C. R. Tyler, A. R. McLean, A restatement of the natural science evidence base on the effects of endocrine disrupting chemicals on wildlife. *Proceedings of the Royal Society B: Biological Sciences*, *286* (1897) 20182416
156. J. Harlacher, Whale, what do we have here? Evidence of microplastics in top predators: analysis of two populations of Resident killer whale fecal samples. Masters dissertation. University of Washington, Seattle, USA.
157. J. Daily, M J. Hoffman, Modeling the three-dimensional transport and distribution of multiple microplastic polymer types in Lake Erie. *Mar. Pollut. Bull.* 154 (2020) 111024.
158. N. Kowalski, A. M. Reichardt, J. J. Waniek, Sinking rates of microplastics and potential implications of their alteration by physical, biological, and chemical factors. *Mar. Pollut. Bull.* 109 (2016) 310–319.
159. Ecology and King County, 2011. Control of Toxic Chemicals in Puget Sound: Assessment of Selected Toxic Chemicals in the Puget Sound Basin, 2007-2011. Washington State Department of Ecology, Olympia, WA and King County Department of Natural Resources, Seattle, WA. Ecology Publication No. 11-03-055.
160. K. Y. Aydin, G. A. McFarlane, J. R. King, B. A. Megrey, K. W. Myers, Linking oceanic food webs to coastal production and growth rates of Pacific salmon (Oncorhynchus spp.), using models on three scales. *Deep Sea Research Part II: Topical Studies in Oceanography*, *52* (2005) 757–780.
161. J. W. Gooch, Encyclopedic Dictionary of Polymers: Polyvinyl Stearate (2011) Springer, New York, NY.

162. G. Suaria, C. G. Avio, A. Mineo, G. L. Lattin, M. G. Magaldi, G. Belmonte6, C. J. Moore, F. Regoli, S. Aliani, The Mediterranean Plastic Soup: synthetic polymers in Mediterranean surface waters, *Sci. Rep.* 6 (2016) 37551.
163. I. A. Sheikh, M. Abu-Elmagd, R. F. Turki, G. A. Damanhouri, M. A. Beg, M. Al-Qahtani, Endocrine disruption: In silico perspectives of interactions of di-(2-ethylhexyl)phthalate and its five major metabolites with progesterone receptor. *BMC Struct. Biol* 16 (2016) 16.
164. S. Dochow, N Bergner, C. Krafft, J. Clement, M. Mazilu, B. B. Praveen, P. C. Ashok, R. Marchington, K. Dholakiac, J. Popp, Classification of Raman Spectra of Single Cells with Autofluorescence Suppression by Wavelength Modulated Excitation, Anal. Methods 5 (2013) 4608.
165. H. J Butler, L. Ashton, B. Bird, G. Cinque, K. Curtis, J. Dorney, K. Esmonde-White, N. J. Fullwood, B. Gardner, P. L. Martin-Hirsch, M. J. Walsh, M. R. McAinsh, N. Stone, F. L. Martin, Using Raman spectroscopy to characterize biological materials, Nat. Protoc. 11 (2016) 664-687.
166. B. Gewert, M. M. Plassmann, M. MacLeod, Pathways for degradation of plastic polymers floating in the marine environment. *Environ. Sci.: Processes Impacts* 17 (2015) 1513–1521.
167. L. Cai, J. Wang, J. Peng, Z. Wu, X. Tan, Observation of the degradation of three types of plastic pellets exposed to UV irradiation in three different environments. *Sci Total Environ.* 628–629 (2018) 740–747.
168. C. Farber, J. Li, E. Hager, R. Chemelewski, J. Mullet, A. Y. Rogachev, D. Kurouski, Complementarity of Raman and Infrared Spectroscopy for Structural Characterization of Plant Epicuticular Waxes. ACS Omega 4 (2019) 3700-3707.
169. P.C. Cross, J. Burnham, P. A. Leighton, The Raman Spectrum and the Structure of Water. *J. Am. Chem. Soc.* 59 (1937) 1134–1147.
170. Z. Zhang, S. Chen, Y. Liang, Baseline correction using adaptive iteratively reweighted penalized least squares. *Analyst* 135 (2010) 1138–1146.
171. W. Lin, M. Cossar, V. Dang, J. Teh, The application of Raman spectroscopy to three-phase characterization of polyethylene crystallinity. *Polym. Test.* 26 (2007) 814–821.
172. J. Zhao, Z. Peng, J. Zhang, In situ FT-IR spectroscopy study on the conformational changes of quenched isotactic polypropylene during stepwise heating. *Polym. Bull.* 67 (2011) 1649–1659.
173. G. Y. Nikolaeva, E. A. Sagitova, K. A. Prokhorov, P. P. Pashinin, P. M. Nedorezova, A. N. Klyamkina, M. A. Guseva, V. A. Gerasin, Using Raman spectroscopy to determine the structure of copolymers and polymer blends. *J. Phys.: Conf. Ser.* 826 (2017) 012002.
174. B. P. Gaber, W. L. Peticolas, On the quantitative interpretation of biomembrane structure by Raman spectroscopy. *Biochim. Biophys. Acta* 465 (1977) 260–274.
175. Y. Hiejima, T. Kida, K. Takeda, T. Igarashi, K. Nitta, Microscopic structural changes during photodegradation of low-density polyethylene detected by Raman spectroscopy. *Polym. Degrad. Stab.* 150 (2018) 67–72.
176. M. J. Gall, P. J. Hendra, C. J. Peacock, M. E. A Cudby, H. A. Willis, The laser-Raman spectrum of polyethylene. The assignment of the spectrum to fundamental modes of vibration. *Spectrochim. Acta A* 28 (1971) 1485–1496.
177. R. G. Snyder, S. L. Hsu, S. Krimm, Vibrational spectra in the C–H stretching region and the structure of the polymethylene chain. *Spectrochim. Acta A* 34 (1977) 395–406.

178. G. Keresztury, E. Földes, On the Raman Spectroscopic Determination of Phase Distribution in Polyethylene. *Polym. Test*. 9 (1990) 329–339.
179. K. Larsson, R. P. Rand, Detection of changes in the environment of hydrocarbon chains by Raman spectroscopy and its application to lipid-protein systems. *Biochim. Biophys. Acta* 326 (1973) 245–255.
180. A. Gleadall, J. Pan, H. Atkinson, A simplified theory of crystallisation induced by polymer chain scissions for biodegradable polyesters. *Polym. Degrad. Stab.* 97 (2012) 1616-1620.
181. Z. Zhang, Rapid Discrimination of Cheese Products Based on Probabilistic Neural Network and Raman Spectroscopy. J. Spectrosc. Vol. 2020, Article ID 8896535, 7 pages, 2020.
182. M. Arruebarrena de Báez, P. J. Hendra, M. Judkins, The Raman spectra of oriented isotactic polypropylene. *Spectrochim. Acta A* 51 (1995) 2117–2124.
183. C. Minogianni, K. G. Gatos, C. Galiotis, Estimation of crystallinity in isotropic isotactic polypropylene with Raman spectroscopy. *Appl. Spectrosc.* 59 (2005) 1141–1147.
184. A. S. Nielsen, D. N. Batchelder, R. Pyrz, Estimation of crystallinity of isotactic polypropylene using Raman spectroscopy. *Polymer* 43 (2002) 2671–2676.
185. K. A. Prokhorov, G. Y. Nikolaeva, E. A. Sagitova, P. P. Pashinin, P. M. Nedorezova, A. N. Klyamkin, Regularity modes in Raman spectra of polyolefins: Part I. Propylene/ olefin copolymers. *Vib. Spectrosc.* 85 (2016) 22–28.
186. T. Furukawa, H. Sato, Y. Kita, K. Matsukawa, H. Yamaguchi, S. Ochiai, H. W. Siesler, Y. Ozaki, Molecular Structure, Crystallinity and Morphology of Polyethylene/Polypropylene Blends Studied by Raman Mapping, Scanning Electron Microscopy, Wide Angle X-Ray Diffraction, and Differential Scanning Calorimetry. *Polym. J.* 38 (2006) 1127–1136.
187. Y. V. Kissin, L. A. Rishina, Regularity bands in the I.R. spectra of C_3H_6–C_3D_6 copolymers. *Eur. Polym. J.* 12 (1975) 757–759.
188. J. V. Gulmine, P. R. Janissek, H. M. Heise, L. Akcelrud, Polyethylene characterization by FTIR. *Polym. Test.* 21 (2002) 557-563.
189. P. Gijsman, J. Hennekens, D. Tummers, The mechanism of action of hindered amine light stabilizers, *Polym. Degrad. Stab.* 39 (1993) 225-233
190. HALS 292. Dongguan Baoxu Chemical Technology., Ltd. [Online]; Caijin Business Bldg DongGuan CN. https://www.additivesforpolymer.com/wp-content/uploads/2019/11/light-stabilizer-tinuvin-292-765-msds-baoxu-chemical.pdf
191. Chimassorb® 2020 FDL. BASF SE. [Online]; Ludwigshafen, Germany. March 15, 2018. https://img.es1688.com/group1/M00/02/2B/Cg1Dp1w3ChOAVF3PAAHsMAjK-KA078.pdf
192. P. J. Larkin, IR and raman Spectroscopy: principles and spectral interpretation. Elsevier Inc. 2011. ISBN: 978-0-12-386984-5. http://www.chemistry.uoc.gr/lapkin/Infrared_and_Raman_Spectroscopy__Principles_and_Spectral_Interpretation.pdf
193. F. Gugumus, Re-examination of the role of hydroperoxides in polyethylene and polypropylene: chemical and physical aspects of hydroperoxides in polyethylene. *Polym. Degrad. Stab.* 49 (1995) 29–50.
194. D. J. Carlsson, D. M. Wiles, The Photodegradation of Polypropylene Films. III. Photolysis of Polypropylene hydroperoxides. *Macromolecules* 6 (1969) 597–606.
195. E. Andreassen, Propylene: Infrared and Raman spectroscopy of polypropylene. Karger-Kocsis, J., Ed.; Kluwer Publishers: Dordrecht, The Netherlands, 1999.

196. A. Nojiri, T. Sawasaki, Radiation crosslinking of polypropylene. *Radiat. Phys. Chem.* 26 (1985) 339–346.
197. A. Al-Khanbashi , M. Dhamdhere, M. Hansen, Application of In-Line Fiber-Optic Raman Spectroscopy to Monitoring Emulsion Polymerization Reactions. *Appl. Spectrosc. Rev.* 33 (1998) 115–131.
198. A. Chamas, H. Moon, J. Zheng, Y. Qiu, T. Tabassum, J.H. Jang, et al., Degradation rates of plastics in the environment. *ACS Sustainable Chem. Eng.* 8 (2020) 3494–3511.
199. A. Abdelhafidi, S. F. Shabira, W. Yagoubi, M. C. Mistretta, Sun radiation and temperature impact at different periods of the year on the photooxidation of polyethylene films. *Int. J. Heat Technol.* 35 (2017). 255-261.
200. H. Rajandas, S. Parimannan, K. Sathasivam, M. Ravichandran, L. S.Yin, A novel FTIR-ATR spectroscopy based technique for the estimation of low-density polyethylene biodegradation. *Polym. Test.* 31 (2012) 1094–1099.
201. M. Niaounakis, E. Kontou, S. Pispas, M. Kafetzi, D. Giaouzi, Aging of Packaging Films in the Marine Environment. *Polym. Eng. Sci.* 59 (2019) E432–E441.
202. J. Coates, Interpretation of Infrared Spectra, A Practical Approach, in: Encyclopedia of Analytical Chemistry, John Wiley & Sons, Ltd, 2006.
203. F. A. Miller, C. H. Wilkins, Infrared Spectra and Characteristic Frequencies of Inorganic Ions. *Anal. Chem.* 24 (1952) 1253–1294.
204. W. L. Marshall, G. M. Begun, Raman Spectroscopy of Aqueous Phosphate Solutions at Temperatures up to 450 ºC. *J. Chem. Soc., Faraday Trans.* 85 (1989) 1963–1978.
205. K. D. Litasov, N. M. Podgornykh, Raman spectroscopy of various phosphate minerals and occurrence of tuite in the Elga IIE iron meteorite. *J. Raman Spectrosc.* 48 (2017) 1518–1527.
206. S. M. Mastelini, M. G. A. Sasso, G. F. C. Campos, M. Schmiele, M. T. P. S. Clerici, D. F. Barbin, S. Barbon Jr. Computer vision system for characterization of pasta (noodle) composition. *J. Electron. Imaging* 27 (2020) 053021.
207. G. S. Ghyar, G. K. Birajdar, "Computer Vision Based Approach to Detect Rice Leaf Diseases using Texture and Color Descriptors." *Proceedings of the International Conference on Inventive Computing and Informatics.* IEEE Xplore Complaint, 2017, pp. 1074–1078.
208. V. P. Kour, S. Arora, Particle Swarm Optimization Based Support Vector Machine (P-SVM) for the Segmentation and Classification of Plants. *IEEE Access* 7 (2019) 29374–29385.
209. V. Bianco, P. Memmolo, P. Carcagnì, F. Merola, M. Paturzo, C. Distante, P. Ferraro, Microplastic Identification via Holographic Imaging and Machine Learning. *Adv. Intell. Syst.* 2 (2020) 1900153.
210. J. Lorenzo-Navarro, M. Castrillón-Santana, E. Santesarti, M. De Marsico, I. Martínez, E. Raymond, M. Gómez, A. Herrera, SMACC: A System for Microplastics Automatic Counting and Classification. *IEEE Access* 8 (2020) 25249–25261.
211. J. Lorenzo-Navarro, M. Castrillón-Santana, E. Sánchez-Nielsen, B. Zarco, A. Herrera, I. Martínez, M. Gómez, Deep learning approach for automatic microplastics counting and classification, *Sci Total Environ*. 765 (2021) 142728.
212. V. Wegmayr, A. Sahin, B. Sæmundsson, J. M. Buhmann, Instance segmentation for the quantification of microplastic fiber images. Proceedings of the 2020 Winter Conference on Applications of Computer Vision (WACV '20), USA, (2020) 2199–2206.

213. W. Wang, J. Wang, Investigation of microplastics in aquatic environments: An overview of the methods used, from field sampling to laboratory analysis. *Trends Anal. Chem.* 108 (2018) 195–202.
214. K. Wu, E. Otoo, A. Shoshani, Optimizing Connected Component Labeling Algorithms. *Lawrence Berkeley National Laboratory*. (2005) Retrieved from https://escholarship.org/uc/item/7jg5d1zn
215. B. E. Oßmann, G. Sarau, S. W. Schmitt, H. Holtmannspötter, S. H. Christiansen, W. Dicke, Development of an optimal filter substrate for the identification of small microplastic particles in food by micro-Raman spectroscopy. *Anal. Bioanal. Chem.* 409 (2017) 4099–4109
216. F. Y. Manik, Y. Herdiyeni, E. N. Herliyani, Leaf Morhpological Feature Extraction of Digital Image Anthocephalus Cadamba. *Telkomnika* 14 (2016) 630–637.

Appendix A. Supplementary information for Chapter 3.1

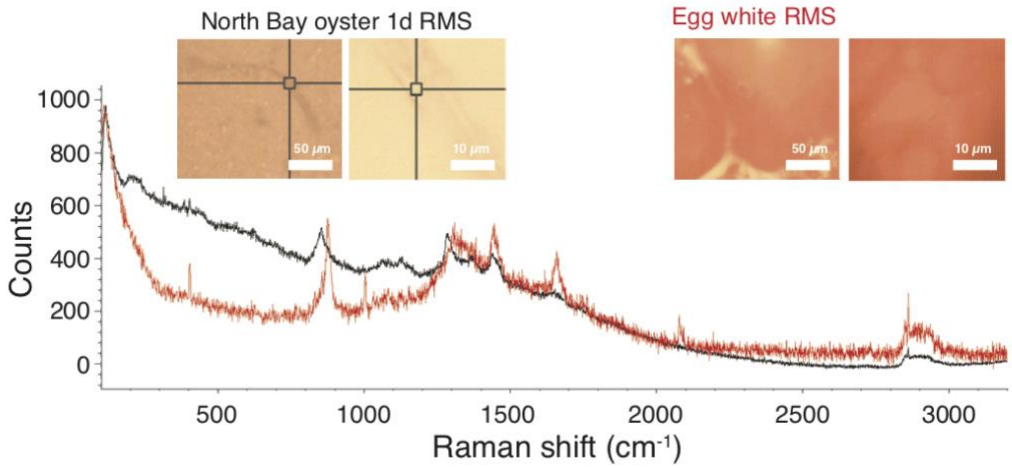

Supplementary Figure 3.1. 1 RMS spectrum for a chicken egg. This test was completed to determine whether the polyamide resin particles observed in the oysters were biological in nature. Since the spectrum matches well with the one observed in the oysters we suspect the polyamide resins identified by RMS in our samples are biological in nature.

Supplementary Table 3.1. 1 Supplementary Table 3.1.1 shows the results from the visual inspection of filters with a stereomicroscope. The columns indicate the site where the oyster came from, the oyster number from that site, the number of suspected plastics observed, the type or morphology of the suspected plastic, its color (if any) and the weight of the oyster. The numbers of suspected plastics need not necessarily match the numbers presented in Supplementary Table 2 as those were observed under the RMS microscope that has finer resolution.

site	oyster	n plastics	weight	type of plastic	color
heritage	1	3	29.37	fiber	3 clear

heritage	2	8	20.68	fiber and flake (3)	5 clear, black flakes
heritage	3	7	25.8	fiber	4 blue, clear, red, green
heritage	4	5	24.47	fiber and flake (1)	4 clear, black flake
heritage	5	2	15.04	fiber	2 amber
heritage	6	0	14.14	na	na
heritage	7	1	21.05	flake	clear
heritage	8	0	24.12	na	na
heritage	9	1	29.38	fiber	black
heritage	12	1	15.68	fiber	black
heritage	13	3	27.02	fiber	3 clear
heritage	14	1	23.32	fiber	blue
heritage	15	0	39.55	na	na
heritage	16	2	30.34	fiber	2 clear
heritage	19	1	15.45	fiber	blue
heritage	20	1	11.23	fiber	dark
heritage	21	3	19.82	fiber	3 blue/dark
heritage	22	0	23.1	na	na
heritage	23	0	22.73	na	na
heritage	24	2	15.87	fiber	2 clear
illahee	1	2	12.53	fiber and flake (1)	red and black
illahee	2	4	26.91	fiber and flake (3)	clear, 3 black
illahee	3	3	21.27	fiber	2 clear, dark
illahee	4	1	21.84	fiber	dark
illahee	5	2	13.5	fiber	blue, black
illahee	6	4	33.43	fiber	2 pink, blue, dark
illahee	7	10	26.08	fiber, flake and fragment (4,1)	5 black/dark, 4 black flakes, 1 clear fragm
illahee	9	0	48.91	na	na
illahee	10	2	34.83	fiber	2 black
illahee	11	0	52.06	na	na
illahee	12	0	45.38	na	na
illahee	13	0	56.74	na	na
illahee	15	2	15.38	fiber	2 black
illahee	19	0	32.76	na	na
illahee	20	0	25.36	na	na
illahee	21	4	35.68	fiber	3 blue, 1 dark
illahee	22	1	36.08	fiber	blue

illahee	23	1	25.84	fiber	clear
illahee	25	0	10.08	na	na
illahee	26	0	21.61	na	na
illahee	29	0	12.36	na	na
jacoby	1	3	11.96	fiber	clear
jacoby	2	0	22.92	na	na
jacoby	3	1	25.7	fiber	white
jacoby	4	1	37.13	fiber	black
jacoby	5	0	39.62	na	na
jacoby	6	0	20.11	na	na
jacoby	8	1	27.36	fiber	purple
jacoby	10	1	22.46	fiber	red
jacoby	12	0	19.29	na	na
jacoby	14	1	29.96	fiber	black
jacoby	15	1	29.19	fiber	black
jacoby	16	2	29.95	fiber	amber
jacoby	17	0	21.26	na	na
jacoby	18	1	15.59	fiber	black
jacoby	19	2	26.93	fiber	amber
jacoby	20	0	17.25	na	na
jacoby	21	0	16.89	na	na
jacoby	24	1	22.79	fiber	black
jacoby	25	0	25.58	na	na
jacoby	27	1	26.43	fiber	black
jacoby	29	0	39.31	na	na
jacoby	30	0	40.86	na	na
jacoby	31	0	10.48	na	na
kopachuck	1	1	20.38	fiber	na
kopachuck	2	1	16.76	fiber	na
kopachuck	3	1	16.28	fiber	na
kopachuck	4	1	15.47	fiber	na
kopachuck	5	0	16.58	na	na
kopachuck	6	1	18.05	fiber	na
kopachuck	7	2	19.34	fiber	blue
kopachuck	8	1	34.01	fiber	na
kopachuck	9	0	27.8	na	na
kopachuck	10	0	21.34	na	na

kopachuck	11	2	31.5	fiber	blue
kopachuck	12	0	47.16	na	na
kopachuck	13	0	38.62	na	na
kopachuck	14	7	22.32	fiber	4 red, 3 dark
kopachuck	17	0	13.76	na	na
kopachuck	18	0	16.68	na	na
kopachuck	19	6	28.51	fiber	4 clear, 2 blue
kopachuck	20	3	47.54	fiber	1 blue, 1 black, 1 gray
kopachuck	21	3	34.18	fiber	2 dark, 1 blue
kopachuck	22	1	33.91	fiber	red
kopachuck	23	0	47.78	na	na
kopachuck	24	0	18.55	na	na
mystery bay	1	1	22.56	fiber	black
mystery bay	2	0	34	na	na
mystery bay	3	1	26.84	fiber	blue
mystery bay	4	1	27.9	fiber	blue
mystery bay	5	0	18.42	na	na
mystery bay	6	0	25.67	na	na
mystery bay	7	0	32.27	na	na
mystery bay	8	0	35.69	na	na
mystery bay	9	0	23.78	na	na
mystery bay	10	0	28.09	na	na
mystery bay	11	0	35.76	na	na
mystery bay	12	0	29.65	na	na
mystery bay	17	4	30.43	fiber	2 black, blue, red
mystery bay	18	1	39.51	fiber	blue
mystery bay	19	0	24.18	na	na

mystery bay	20	1	29.92	fiber	blue
mystery bay	21	6	42.15	fiber	2 green, 2 blue, clear, red
mystery bay	22	1	28.38	fragment	red
mystery bay	23	0	41.04	na	na
mystery bay	24	0	25.66	na	na
mystery bay	25	0	17.27	na	na
north bay	1	6	6.25	fiber	na
north bay	2	0	22.35	na	na
north bay	3	0	8.24	na	na
north bay	4	3	18.67	fiber	na
north bay	5	0	21.01	na	na
north bay	6	0	9.90	na	na
north bay	7	2	16.06	fiber	na
north bay	8	1	8.84	fiber	na
north bay	9	1	11.72	fiber	na
north bay	10	1	5.45	fiber	na
north bay	11	4	28.25	fiber	na
north bay	12	2	27.74	fiber	na
north bay	13	0	31.40	na	na
north bay	14	2	37.77	fiber	na
north bay	15	2	34.87	fiber	na
north bay	19	2	44.26	fiber	na
north bay	20	5	40.2	fiber	na
north bay	21	3	28.91	fiber	na
north bay	22	0	39.77	na	na
north bay	23	0	16.97	na	na
north bay	24	0	34.6	na	na
oakland	1	3	18.05	fiber	2 blue, 1 purple
oakland	2	3	28.07	fiber	1 blue, 2 clear
oakland	3	3	15.31	fiber	2 blue, 1 clear
oakland	4	5	8.30	fiber	na
oakland	5	5	5.79	fiber	na
oakland	6	5	12.16	fiber	na

oakland	7	1	14.64	fiber	na
oakland	8	1	11.20	fiber	na
oakland	9	1	13.71	fiber	na
oakland	10	5	8.42	fiber	na
oakland	11	1	9.86	fiber	na
oakland	12	4	12.40	fiber	2 blue, 2 clear
oakland	13	2	8.47	fiber	na
oakland	14	5	8.04	fiber	1 pink, 4 clear
oakland	15	3	19.25	fiber	1 blue, 4 clear
oakland	17	4	6.13	fiber	na
oakland	18	4	10.93	fiber	2 blue, 1 black, 1 clear
oakland	19	4	12.52	fiber	na
oakland	20	2	11.28	fiber	2 blue
oakland	21	0	9.97	na	na
oakland	22	2	12.50	fiber	na
penrose	1	3	15.35	fiber	2 black, 1 silver
penrose	2	16	19.54	fiber	16 black/blue
penrose	3	2	18.21	fiber	2 black
penrose	4	0	12.79	na	na
penrose	5	0	19.54	na	na
penrose	6	0	13.25	na	na
penrose	7	1	12.16	fiber	clear
penrose	8	0	13.49	na	na
penrose	9	1	28.47	fiber	black
penrose	10	6	18.26	fiber	4 purple, 2 blue
penrose	11	2	32.99	fiber	1 red, 1 purple
penrose	12	1	13.34	fiber	gray
penrose	13	3	21.63	fiber	2 dark, 1 pink
penrose	14	0	27.21	na	na
penrose	15	2	28.14	fiber	2 dark
penrose	16	0	15.29	na	na
penrose	17	2	16.7	fiber	2 amber
penrose	18	0	10.56	na	na
penrose	19	3	25	fiber	blue, red, yellow
penrose	20	2	7.09	fiber	black
penrose	21	1	17	fiber	purple
penrose	22	2	19.98	fiber	black

penrose	23	1	10.97	fiber	blue
penrose	24	0	19.38	na	na
samish	1	7	68.65	fiber	3 amber, 2 blue, 1 black, 1 red
samish	2	0	54.69	na	na
samish	3	3	63.16	fiber	2 blue, 1 red
samish	4	1	86.47	fiber	clear
samish	5	3	57.45	fiber	clear, silver, clear
samish	6	8	63.59	fiber	green, clear, 3 amber, 3 black
samish	7	2	75.55	fiber	clear, gray
samish	8	0	40	na	na
samish	9	1	68.87	fiber	clear
samish	10	2	38.46	fiber	black
samish	12	0	57.5	na	na
samish	14	0	52.91	na	na
samish	15	4	77.36	fiber	2 blue, amber, red
samish	16	3	53.07	fiber	3 amber
samish	17	4	67.88	fiber	3 clear, 1 purple
samish	18	5	53.14	fiber	5 blue
samish	19	6	53.79	fiber	3 purple, 2 amber, 1 blue
samish	20	2	54.65	fiber	black, amber
samish	21	0	50.56	na	na
samish	22	5	59.26	fiber, flake	3 amber, black, red
sequim	7	0	17.1	na	na
sequim	8	5	16.63	fiber	4 black, 1 red
sequim	9	1	23.49	fiber	black
sequim	10	0	20.62	na	na
sequim	11	2	10.98	fiber	2 dark/blue
sequim	12	12	8.15	fiber	9 dark, 1 clear, 2 red
sequim	13	0	15.27	na	na
sequim	15	1	18.86	fiber	black
sequim	16	0	7.36	na	na
sequim	17	0	13.59	na	na
sequim	18	0	9.27	na	na
sequim	19	0	10.88	na	na
sequim	20	0	14.74	na	na
sequim	22	2	16.58	fiber	purple, black
sequim	24	3	13.38	fiber	black

sequim	25	2	18.15	fiber	clear
sequim	26	0	15.81	na	na
sequim	27	3	26.29	fiber and flake (1)	black, purple, black
sequim	28	3	24.79	fiber	black
sequim	29	0	22.64	na	na

Supplementary Table 3.1. 2 Supplementary Table 3.1.2 shows the results from the visual inspection of filters observed during RMS analysis. The columns indicate the site where the oyster came from, the oyster number from that site, the description of the suspected plastics, and its identification (when there was no fluorescence). The numbers of oysters that are for example Oyster 1_1, Oyster 1_2, Oyster 1_3 indicate that multiple particles were observed/measured/analyzed for Oyster 1. Please note that the number of suspected plastics reported in this table may not match the numbers presented in Supplementary Table 3.1.1 as those were observed under a stereomicroscope that has lower resolution.

Site	Oyster	Description	Size (um)	Identification	ID summary
North Bay	Nbay Control 1_5-2	clear fiber	90	fluorescence	fluorescence
North Bay	Nbay Control 1_6	clear fiber	110	cellulose	cellulose
North Bay	Nbay Control 1_7	clear fiber	200	fluorescence	fluorescence
North Bay	Nbay Oyster 1	clear fiber	600	fluorescence	fluorescence
North Bay	Nbay Oyster 1_2	irregular	150	fluorescence	fluorescence
North Bay	Nbay Oyster 1_3	clear spheroid	50	fluorescence	fluorescence
North Bay	Nbay Oyster 1_4	blue fiber	1200	fluorescence	fluorescence
North Bay	Nbay Oyster 1_5	clear fiber	300	fluorescence	fluorescence
North Bay	Nbay Oyster 2	clear fiber	60	fluorescence	fluorescence
North Bay	Nbay Oyster 2_2	clear fiber	900	fluorescence	fluorescence
North Bay	Nbay Oyster 2_4	clear spheroid	75	fluorescence	fluorescence
North Bay	Nbay Control 1	opaque irregular	325	poly(ethylene glycol) monooleate or polyamide resin	PE glycol/PA resin
North Bay	Nbay Control 3	black irregular	35	cellulose	cellulose

North Bay	Nbay Control 4	dark fiber	1000	fluorescence	fluorescence
North Bay	Nbay Oyster 1_1	clear fiber	900	cellulose	cellulose
North Bay	Nbay Oyster 1_2	dark fiber	1100	cellulose	cellulose
North Bay	Nbay Oyster 1_4	opaque fiber	350	other	other
North Bay	Nbay Oyster 1a	clear fiber	250	poly(ethylene glycol) monooleate or polyamide resin	PE glycol/PA resin
North Bay	Nbay Oyster 1c	opaque fiber	250	poly(ethylene glycol) monooleate or polyamide resin	PE glycol/PA resin
North Bay	Nbay Oyster 1d	clear spheroid	60	other	other
North Bay	Nbay Oyster 1f	clear fiber	1500	cellulose	cellulose
North Bay	Nbay Oyster 1h	clear fiber	1800	other	other
North Bay	Nbay Oyster 1j	clear fiber	800	other	other
North Bay	Nbay Oyster 2a	perfect circle	75	poly(ethylene glycol) monooleate or polyamide resin	PE glycol/PA resin
North Bay	Nbay Oyster 2c	clear fiber	250	fluorescence	fluorescence
North Bay	Nbay Oyster 2e	white shard	125	other	other
North Bay	Nbay Oyster 2f	clear fiber	800	poly(ethylene glycol) monooleate or polyamide resin	PE glycol/PA resin
North Bay	Nbay Oyster 2g	dark fiber	1100	other	other
North Bay	Nbay Oyster 2h	clear fiber	550	other	other
North Bay	Nbay Oyster 3a	clear shard	75	polystyrene	polystyrene
North Bay	Nbay Oyster 3c	clear fiber	1200	cellulose	cellulose
North Bay	Nbay Oyster 3e	opaque irregular	100	polypropylene	polypropylene
North Bay	Nbay Control 4a	clear irregular	150	cellulose	cellulose

North Bay	Nbay Control 4b	clear square	15	poly(ethylene glycol) monooleate or polyamide resin	PE glycol/PA resin
North Bay	Nbay Control 4c	clear fiber	225	cellulose	cellulose
North Bay	Nbay Control 4d	dark irregular	100	fluorescence	fluorescence
North Bay	Nbay Control 4e	clear irregular	800	cellulose	cellulose
North Bay	Nbay Control 4f	clear fiber	125	cellulose	cellulose
North Bay	Nbay Control 4g	clear fiber	175	fluorescence	fluorescence
North Bay	Nbay Control 4h	clear irregular	175	other	other
North Bay	Nbay Control 4i	clear irregular	1000	fluorescence	fluorescence
North Bay	Nbay Control 4j	opaque round	75	other	other
North Bay	Nbay Oyster 3g	opaque shard	175	poly(ethylene glycol) monooleate or polyamide resin	PE glycol/PA resin
North Bay	Nbay Oyster 3h	clear shard	50	polystyrene	polystyrene
North Bay	Nbay Oyster 3j	clear spheroid	40	fluorescence	fluorescence
North Bay	Nbay Oyster 4a	clear fiber	350	poly(ethylene glycol) monooleate or polyamide resin	PE glycol/PA resin
North Bay	Nbay Oyster 4b	clear rod	150	poly(ethylene glycol) monooleate or polyamide resin	PE glycol/PA resin
North Bay	Nbay Oyster 4c	blue fiber	800	fluorescence	fluorescence
North Bay	Nbay Oyster 4d	clear fiber	150	fluorescence	fluorescence
North Bay	Nbay Oyster 4e	clear fiber	600	other	other
North Bay	Nbay Oyster 5a	clear fiber	1100	cellulose	cellulose
North Bay	Nbay Oyster 5b	clear round	50	poly(ethylene glycol) monooleate or polyamide resin	PE glycol/PA resin
North Bay	Nbay Oyster 5c	clear fiber	175	poly(ethylene glycol) monooleate or polyamide resin	PE glycol/PA resin

North Bay	Nbay Oyster 5d	clear fiber	250	cellulose	cellulose
North Bay	Nbay Oyster 5e	clear fiber	550	fluorescence	fluorescence
North Bay	Nbay Oyster 6a	clear fiber	150	fluorescence	fluorescence
North Bay	Nbay Oyster 6b	clear fiber	600	cellulose	cellulose
North Bay	Nbay Oyster 6c	macaroni	150	other	other
North Bay	Nbay Oyster 6d	clear rod	100	fluorescence	fluorescence
North Bay	Nbay Control 7c	clear fiber	300	cellulose	cellulose
North Bay	NBay Control 7d	clear fiber	300	fluorescence	fluorescence
North Bay	Nbay Control 7e	pink fiber	175	other	other
North Bay	Nbay Control 7f	clear rod	100	other	other
North Bay	Nbay Oyster 7a	clear spheroid	50	other	other
North Bay	Nbay Oyster 7b	clear irregular	100	poly(ethylene glycol) monooleate or polyamide resin	PE glycol/PA resin
North Bay	Nbay Oyster 7c	round	40	poly(ethylene glycol) monooleate or polyamide resin	PE glycol/PA resin
North Bay	Nbay Oyster 7d	clear fiber	250	poly(ethylene glycol) monooleate or polyamide resin	PE glycol/PA resin
North Bay	Nbay Oyster 7e	clear fiber	450	cellulose	cellulose
North Bay	Nbay Oyster 7f	clear spheroid	75	poly(ethylene glycol) monooleate or polyamide resin	PE glycol/PA resin
North Bay	Nbay Oyster 8a	blue fiber	1000	fluorescence	fluorescence
North Bay	Nbay Oyster 8b	clear fiber	950	fluorescence	fluorescence
North Bay	Nbay Oyster 8c	clear fiber	450	fluorescence	fluorescence
North Bay	Nbay Oyster 8d	clear fiber	500	fluorescence	fluorescence
North Bay	Nbay Oyster 8e	clear rod	75	fluorescence	fluorescence

North Bay	Nbay Oyster 8f	clear fiber	950	fluorescence	fluorescence
North Bay	Nbay Oyster 8g	clear rod	150	poly(ethylene glycol) monooleate or polyamide resin	PE glycol/PA resin
North Bay	Nbay Oyster 8h	clear irregular	300	fluorescence	fluorescence
North Bay	Nbay Oyster 9a	blue fiber	800	other	other
North Bay	Nbay Oyster 9b	clear fiber	750	fluorescence	fluorescence
North Bay	Nbay Oyster 9c	dark fiber	150	other	other
North Bay	Nbay Oyster 9d	clear fiber	600	fluorescence	fluorescence
North Bay	Nbay Oyster 9e	clear fiber	800	poly(ethylene glycol) monooleate or polyamide resin	PE glycol/PA resin
North Bay	Nbay Oyster 9f	clear fiber	600	fluorescence	fluorescence
North Bay	Nbay Oyster 9g	clear fiber	400	cellulose	cellulose
North Bay	Nbay Oyster 9h	straight rod	1200	poly(ethylene glycol) monooleate or polyamide resin	PE glycol/PA resin
North Bay	Nbay Control 10a	clear spheroid	60	poly(ethylene glycol) monooleate or polyamide resin	PE glycol/PA resin
North Bay	Nbay Control 10b	clear spheroid	40	other	other
North Bay	Nbay Control 10c	blue fiber	550	other	other
North Bay	Nbay Control 7-9a	clear square	100	other	other
North Bay	Nbay Control 7-9b	clear fiber	550	fluorescence	fluorescence
North Bay	Nbay Control 7-9c	clear fiber	750	other	other
North Bay	Nbay Control 7-9d	opaque fiber	175	cellulose	cellulose
North Bay	Nbay Control 7-9e	clear fiber	500	cellulose	cellulose
North Bay	Nbay Control 10-12a	clear fiber	225	fluorescence	fluorescence
North Bay	Nbay Control 10-12b	clear irregular	350	fluorescence	fluorescence

North Bay	Nbay Control 10-12c	clear rod	250	fluorescence	fluorescence
North Bay	Nbay Control 10-12d	clear square	100	fluorescence	fluorescence
North Bay	Nbay Control 10-12e	clear fiber	500	fluorescence	fluorescence
North Bay	Nbay Control 10-12f	clear fiber	650	fluorescence	fluorescence
North Bay	Nbay Oyster 10a	clear square	125	poly(ethylene glycol) monooleate or polyamide resin	PE glycol/PA resin
North Bay	Nbay Oyster 10b	clear shard	60	poly(ethylene glycol) monooleate or polyamide resin	PE glycol/PA resin
North Bay	Nbay Oyster 10c	clear shard	150	poly(ethylene glycol) monooleate or polyamide resin	PE glycol/PA resin
North Bay	Nbay Oyster 10d	clear rod	25	poly(ethylene glycol) monooleate or polyamide resin	PE glycol/PA resin
North Bay	Nbay Oyster 10e	dark fiber	925	fluorescence	fluorescence
North Bay	Nbay Oyster 10f	white shard	50	poly(ethylene glycol) monooleate or polyamide resin	PE glycol/PA resin
North Bay	Nbay Oyster 11a	clear fiber	850	cellulose	cellulose
North Bay	Nbay Oyster 11b	clear fiber	800	fluorescence	fluorescence
North Bay	Nbay Oyster 11c	opque round	100	other	other
North Bay	Nbay Oyster 11d	clear fiber	250	fluorescence	fluorescence
North Bay	Nbay Oyster 11e	clear fiber	500	fluorescence	fluorescence
North Bay	Nbay Oyster 11f	clear rod	200	fluorescence	fluorescence
North Bay	Nbay Control 1-3 15a	blue fiber	150	other	other
North Bay	Nbay Control 1-3 16a	pink fiber	250	fluorescence	fluorescence
North Bay	Nbay Oyster 12a	clear fiber, 12	900	fluorescence	fluorescence
North Bay	Nbay Oyster 12b	opaque spheroid	110	other	other

North Bay	Nbay Oyster 12c	clear spheroid	50	other	other
North Bay	Nbay Oyster 12d	clear spheroid	60	fluorescence	fluorescence
North Bay	Nbay Oyster 12e	clear spheroid	75	other	other
North Bay	Nbay Oyster 12f	clear spheroid	60	other	other
North Bay	Nbay Oyster 13a	clear spheroid	40	other	other
North Bay	Nbay Oyster 13b	white shard	100	poly(ethylene glycol) monooleate or polyamide resin	PE glycol/PA resin
North Bay	Nbay Oyster 13c	white spheroid	45	poly(ethylene glycol) monooleate or polyamide resin	PE glycol/PA resin
North Bay	Nbay Oyster 13d	opaque spheroid	150	polypropylene	polypropylene
North Bay	Nbay Oyster 13e	clear shard	60	poly(ethylene glycol) monooleate or polyamide resin	PE glycol/PA resin
North Bay	Nbay Oyster 14a	opaque fiber, 14	500	fluorescence	fluorescence
North Bay	Nbay Oyster 14b	clear fiber	1750	poly(ethylene glycol) monooleate or polyamide resin	PE glycol/PA resin
North Bay	Nbay Oyster 14d	clear fiber	450	cellulose	cellulose
North Bay	Nbay Oyster 14e	opaque irregular	250	fluorescence	fluorescence
North Bay	Nbay Oyster 15a	dark fiber	450	other	other
North Bay	Nbay Oyster 15b	white spheroid	125	fluorescence	fluorescence
North Bay	Nbay Oyster 15c	clear spheroid	75	other	other
North Bay	Nbay Oyster 15d	clear fiber	650	cellulose	cellulose
North Bay	Nbay Oyster 15e	dark irregular	125	fluorescence	fluorescence
North Bay	Nbay Oyster 15f	dark spheroid	150	fluorescence	fluorescence
North Bay	Nbay Control 13-15a	opaque fiber	700	fluorescence	fluorescence
North Bay	Nbay Control 13-15b	clear fiber	250	fluorescence	fluorescence

North Bay	Nbay Oyster 19a	white spheroid	150	other	other
North Bay	Nbay Oyster 19b	clear shard	125	other	other
North Bay	Nbay Oyster 20a	dark fiber	3000	fluorescence	fluorescence
North Bay	Nbay Oyster 20b	clear spheroid	60	other	other
North Bay	Nbay Oyster 20c	opaque fiber	525	fluorescence	fluorescence
North Bay	Nbay Oyster 20d	clear fiber	300	fluorescence	fluorescence
North Bay	Nbay Oyster 20e	clear square	100	other	other
North Bay	Nbay Oyster 21a	clear spheroid	30	other	other
North Bay	Nbay Oyster 21b	clear shard	60	other	other
North Bay	Nbay Oyster 21c	white shard	50	poly(ethylene glycol) monooleate or polyamide resin	PE glycol/PA resin
North Bay	Nbay Oyster 21d	clear circle	150	poly(ethylene glycol) monooleate or polyamide resin	PE glycol/PA resin
North Bay	Nbay Control 19-21a	clear fiber	350	other	other
North Bay	Nbay Control 19-21b	clear fiber	600	fluorescence	fluorescence
North Bay	Nbay Oyster 22a	opaque spheroid	50	other	other
North Bay	Nbay Oyster 22b	clear shard	75	other	other
North Bay	Nbay Oyster 22c	clear shard	100	other	other
North Bay	Nbay Oyster 22d	clear shard	30	poly(ethylene glycol) monooleate or polyamide resin	PE glycol/PA resin
North Bay	Nbay Oyster 23a	clear fiber, 23.1	1050	other	other
North Bay	Nbay Oyster 23b	opaque spheroid	40	poly(ethylene glycol) monooleate or polyamide resin	PE glycol/PA resin
North Bay	Nbay Oyster 23c	clear fiber	200	poly(ethylene glycol) monooleate or polyamide resin	PE glycol/PA resin

North Bay	Nbay Oyster 23d	opaque spheroid	125	other	other
North Bay	Nbay Oyster 23e	opaque fiber	1100	cellulose	cellulose
North Bay	Nbay Oyster 23f	pink fiber	1200	fluorescence	fluorescence
North Bay	Nbay Oyster 24a	clear spheroid	150	other	other
North Bay	Nbay Oyster 24b	opaque spheroid	75	poly(ethylene glycol) monooleate or polyamide resin	PE glycol/PA resin
North Bay	Nbay Oyster 24c	clear spheroid	75	other	other
North Bay	Nbay Oyster 24d	clear fiber	450	fluorescence	fluorescence
North Bay	Nbay Control 22-24a	clear fiber	1100	cellulose	cellulose
North Bay	Nbay Control 22-24b	opaque fiber	750	cellulose	cellulose
North Bay	Nbay Control 22-24c	opaque fiber	400	cellulose	cellulose
Oakland Bay	Oakland Oyster 1a	clear fiber	450	fluorescence	fluorescence
Oakland Bay	Oakland Oyster 1b	White spheroid	50	poly(ethylene glycol) monooleate or polyamide resin	PE glycol/PA resin
Oakland Bay	Oakland Oyster 1c	clear spheroid	25	other	other
Oakland Bay	Oakland Oyster 1d	white irregular	100	poly(ethylene glycol) monooleate or polyamide resin	PE glycol/PA resin
Oakland Bay	Oakland Oyster 1e	clear spheroid	100	poly(ethylene glycol) monooleate or polyamide resin	PE glycol/PA resin
Oakland Bay	Oakland Oyster 2a	pink spheroid	60	other	other
Oakland Bay	Oakland Oyster 2b_2	clear fiber	550	cellulose	cellulose
Oakland Bay	Oakland Oyster 2d_2	white spheroid	75	poly(ethylene glycol) monooleate or polyamide resin	PE glycol/PA resin
Oakland Bay	Oakland Oyster 2e	clear fiber	300	fluorescence	fluorescence
Oakland Bay	Oakland Oyster 2f	blue fiber	250	fluorescence	fluorescence

Oakland Bay	Oakland Oyster 2g	clear spheroid	80	poly(ethylene glycol) monooleate or polyamide resin	PE glycol/PA resin
Oakland Bay	Oakland Oyster 2h	white square	100	poly(ethylene glycol) monooleate or polyamide resin	PE glycol/PA resin
Oakland Bay	Oakland Oyster 3a	blue fiber	550	other	other
Oakland Bay	Oakland Oyster 3b	clear fiber	650	other	other
Oakland Bay	Oakland Oyster 3c	opque fiber	800	other	other
Oakland Bay	Oakland Oyster 3d	clear rod	125	poly(ethylene glycol) monooleate or polyamide resin	PE glycol/PA resin
Oakland Bay	Oakland Oyster 3f	dark fiber	425	fluorescence	fluorescence
Oakland Bay	Oakland Oyster 4a	dark fiber	700	other	other
Oakland Bay	Oakland Oyster 4b	opaque fiber	675	fluorescence	fluorescence
Oakland Bay	Oakland Oyster 4c	dark fiber	1600	other	other
Oakland Bay	Oakland Oyster 4d	clear shard	100	polyethylene	polyethylene
Oakland Bay	Oakland Oyster 4e	white shard	100	gypsum	gypsum
Oakland Bay	Oakland Oyster 4f	clear fiber	250	fluorescence	fluorescence
Oakland Bay	Oakland Oyster 4g	clear fiber	13000	cellulose	cellulose
Oakland Bay	Oakland Oyster 5a	clear fiber	900	fluorescence	fluorescence
Oakland Bay	Oakland Oyster 5b	clear fiber	2000	fluorescence	fluorescence
Oakland Bay	Oakland Oyster 5c	clear fiber	4250	other	other
Oakland Bay	Oakland Oyster 5d	clear fiber	1400	other	other
Oakland Bay	Oakland Oyster 5e	clear fiber	1700	cellulose	cellulose
Oakland Bay	Oakland Oyster 5f	clear fiber	450	fluorescence	fluorescence
Oakland Bay	Oakland Oyster 5g	clear fiber	1800	cellulose	cellulose

Oakland Bay	Oakland Oyster 5h	pink fiber	125	fluorescence	fluorescence
Oakland Bay	Oakland Oyster 5i	dark fiber	650	other	other
Oakland Bay	Oakland Oyster 6a	dark irregular	275	other	other
Oakland Bay	Oakland Oyster 6b	clear fiber	1000	other	other
Oakland Bay	Oakland Oyster 6c	blue spheroid	350	other	other
Oakland Bay	Oakland Oyster 6d	clear fiber	900	other	other
Oakland Bay	Oakland Oyster 6e	clear fiber	600	cellulose	cellulose
Oakland Bay	Oakland Control 1-3a	opaque irregular	600	other	other
Oakland Bay	Oakland Control 1-3b	clear irregular	600	fluorescence	fluorescence
Oakland Bay	Oakland Control 1-3c	clear irregular	425	fluorescence	fluorescence
Oakland Bay	Oakland Control 4-6a	purple fiber	2400	other	other
Kopachuck	Kopachuck Oyster 1a	clear shard	75	poly(ethylene glycol) monooleate or polyamide resin	PE glycol/PA resin
Kopachuck	Kopachuck Oyster 1b	clear spheroid	50	poly(ethylene glycol) monooleate or polyamide resin	PE glycol/PA resin
Kopachuck	Kopachuck Oyster 1c	blue fiber	75	other	other
Kopachuck	Kopachuck Oyster 1d	clear spheroid	150	other	other
Kopachuck	Kopachuck Oyster 2a	opaque fiber	100	fluorescence	fluorescence
Kopachuck	Kopachuck Oyster 2b	clear fiber, 2.1	350	fluorescence	fluorescence
Kopachuck	Kopachuck Oyster 2c	clear spheroid	100	other	other
Kopachuck	Kopachuck Oyster 2d	clear spheroid	75	other	other
Kopachuck	Kopachuck Oyster 2e	clear spheroid	50	other	other
Kopachuck	Kopachuck Oyster 2f	opaque spheroid	100	poly(ethylene glycol) monooleate or polyamide resin	PE glycol/PA resin

Kopachuck	Kopachuck Oyster 2g	opaque spheroid	100	other	other
Kopachuck	Kopachuck Oyster 2h	clear fiber	450	fluorescence	fluorescence
Kopachuck	Kopachuck Oyster 3a	opaque spheroid	350	fluorescence	fluorescence
Kopachuck	Kopachuck Oyster 3b	clear spheroid	50	poly(ethylene glycol) monooleate or polyamide resin	PE glycol/PA resin
Kopachuck	Kopachuck Oyster 3c	clear spheroid	75	poly(ethylene glycol) monooleate or polyamide resin	PE glycol/PA resin
Kopachuck	Kopachuck Control 1-3a	opaque spheroid	300	other	other
Kopachuck	Kopachuck Oyster 4a	opaque spheroid	50	other	other
Kopachuck	Kopachuck Oyster 4b	clear spheroid	50	other	other
Kopachuck	Kopachuck Oyster 4c	opaque spheroid	75	other	other
Kopachuck	Kopachuck Oyster 4d	clear spheroid	75	other	other
Kopachuck	Kopachuck Oyster 4e	pink fiber	425	fluorescence	fluorescence
Kopachuck	Kopachuck Oyster 4f	blue fiber	700	fluorescence	fluorescence
Kopachuck	Kopachuck Oyster 4g	clear spheroid	125	other	other
Kopachuck	Kopachuck Oyster 4h	blue fiber	800	other	other
Kopachuck	Kopachuck Oyster 4i	clear fiber	1100	fluorescence	fluorescence
Kopachuck	Kopachuck Oyster 4j	clear spheroid	75	other	other
Kopachuck	Kopachuck Oyster 5a	opaque spheroid	100	other	other
Kopachuck	Kopachuck Oyster 5b	pink spheroid	75	other	other
Kopachuck	Kopachuck Oyster 5c	clear shard	75	poly(ethylene glycol) monooleate or polyamide resin	PE glycol/PA resin
Kopachuck	Kopachuck Oyster 5d	clear spheroid	100	other	other
Kopachuck	Kopachuck Oyster 6a	circle	125	poly(ethylene glycol) monooleate or polyamide resin	PE glycol/PA resin

Kopachuck	Kopachuck Oyster 6b	clear spheroid	75	other	other
Kopachuck	Kopachuck Oyster 6c	opaque spheroid	50	other	other
Kopachuck	Kopachuck Oyster 6d	clear spheroid	75	other	other
Kopachuck	Kopachuck Control 4-6a	pink fiber	900	fluorescence	fluorescence
Kopachuck	Kopachuck Control 4-6b	pink fiber	800	fluorescence	fluorescence
Kopachuck	Kopachuck Control 4-6c	clear fiber	3125	fluorescence	fluorescence
Kopachuck	Kopachuck Control 4-6d	dark fiber	850	fluorescence	fluorescence
Illahee	Illahee Oyster 1a	pink fiber	900	fluorescence	fluorescence
Illahee	Illahee Oyster 1b	dark fiber, 1.2	850	other	other
Illahee	Illahee Oyster 1c	dark spheroid	275	other	other
Illahee	Illahee Oyster 1d	clear oblong	600	other	other
Illahee	Illahee Oyster 1e	dark fiber	850	fluorescence	fluorescence
Illahee	Illahee Oyster 2a	clear fiber	850	fluorescence	fluorescence
Illahee	Illahee Oyster 2b	clear fiber	500	cellulose	cellulose
Illahee	Illahee Oyster 2c	clear spheroid	50	other	other
Illahee	Illahee Oyster 2d	clear spheroid	40	other	other
Illahee	Illahee Oyster 2e	clear spheroid	75	other	other
Illahee	Illahee Oyster 3a	clear spheroid	25	other	other
Illahee	Illahee Oyster 3b	opaque spheroid	100	other	other
Illahee	Illahee Oyster 3c	clear spheroid	75	other	other
Illahee	Illahee Control 1-3a	clear fiber	825	fluorescence	fluorescence
Illahee	Illahee Control 1-3b	blue fiber	900	other	other
Illahee	Illahee Control 1-3c	dark fiber	300	other	other

Illahee	Illahee Control 1-3d	clear fiber	550	fluorescence	fluorescence
Illahee	Illahee Oyster 22a	dark fiber	3100	fluorescence	fluorescence
Illahee	Illahee Oyster 22b	clear fiber	2250	fluorescence	fluorescence
Illahee	Illahee Oyster 22c	clear fiber, 22.1	900	fluorescence	fluorescence
Illahee	Illahee Oyster 23a	clear fiber	2500	cellulose	cellulose
Illahee	Illahee Oyster 23b	clear fiber	700	fluorescence	fluorescence
Illahee	Illahee Oyster 23c	clear spheroid	350	gypsum	gypsum
Illahee	Illahee Oyster 23d	clear spheroid	100	poly(ethylene glycol) monooleate or polyamide resin	PE glycol/PA resin
Illahee	Illahee Oyster 23e	opaque irregular	125	poly(ethylene glycol) monooleate or polyamide resin	PE glycol/PA resin
Illahee	Illahee Control 22-23a	clear fibers	600	fluorescence	fluorescence
Illahee	Illahee Control 22-23b	dark spheroid	75	other	other
Illahee	Illahee Control 22-23c	clear fiber	700	cellulose	cellulose
Illahee	Illahee Control 22-23d	opaque spheroid	125	fluorescence	fluorescence
Heritage	Heritage Oyster 19a	clear fiber, 19.1	1100	fluorescence	fluorescence
Heritage	Hertiage Oyster 19b	dark fiber, 19.2	650	fluorescence	fluorescence
Heritage	Hertiage Oyster 19c	opaque shard	75	poly(ethylene glycol) monooleate or polyamide resin	PE glycol/PA resin
Heritage	Hertiage Oyster 19d	dark spheroid	100	other	other
Heritage	Heritage Oyster 19e	dark fiber	175	fluorescence	fluorescence
Heritage	Heritage Oyster 19f	clear fiber	900	cellulose	cellulose

Heritage	Heritage Oyster 19g	dark spheroid	250	other	other
Heritage	Heritage Oyster 20a	clear fiber	900	fluorescence	fluorescence
Heritage	Heritage Oyster 20b	clear spheroid	75	other	other
Heritage	Heritage Oyster 20c	clear spheroid	60	other	other
Heritage	Heritage Oyster 20d	dark spheroid	275	fluorescence	fluorescence
Heritage	Heritage Oyster 20e	clear fiber	2200	fluorescence	fluorescence
Heritage	Heritage Oyster 20f	clear spheroid	60	other	other
Heritage	Heritage Oyster 21a	dark spheroid	200	fluorescence	fluorescence
Heritage	Heritage Oyster 21b	white shard	150	other	other
Heritage	Heritage Oyster 21c	opaque fiber	300	fluorescence	fluorescence
Heritage	Heritage Oyster 21d	oblong	1000	other	other
Heritage	Heritage Oyster 21e	dark fiber	350	other	other
Heritage	Heritage Control 19-21a	opaque fiber	525	fluorescence	fluorescence
Heritage	Heritage Control 19-21b	blue rod	150	fluorescence	fluorescence
Heritage	Heritage Control 19-21c	clear fiber	275	other	other
Heritage	Heritage Oyster 22a	pink spheroid	80	poly(ethylene glycol) monooleate or polyamide resin	PE glycol/PA resin
Heritage	Heritage Oyster 22b	pink spheroid	125	fluorescence	fluorescence
Heritage	Heritage Oyster 22c	dark fiber	50	fluorescence	fluorescence
Heritage	Heritage Oyster 22d	clear spheroid	30	other	other
Heritage	Heritage Oyster 23a	opaque spheroid	30	other	other
Heritage	Heritage Oyster 23b	opaque spheroid	50	fluorescence	fluorescence

Heritage	Hertiage Oyster 23c	clear spheroid	60	other	other
Heritage	Hertiage Oyster 23d	dark oblong	60	fluorescence	fluorescence
Heritage	Heritage Oyster 24a	clear spheroid	60	other	other
Heritage	Heritage Oyster 24b	clear spheroid	50	fluorescence	fluorescence
Heritage	Heritage Oyster 24c	dark fiber	30	fluorescence	fluorescence
Heritage	Heritage Oyster 24d	blue fiber	550	fluorescence	fluorescence
Heritage	Heritage Oyster 24e	clear spheroid	35	other	other
Heritage	Heritage Control 22-24a	clear fiber	350	fluorescence	fluorescence
Penrose	Penrose Pt Oyster 10a	pink particle	900	fluorescence	fluorescence
Penrose	Penrose Pt Oyster 10b	clear fiber	1100	fluorescence	fluorescence
Penrose	Penrose Pt Oyster 10c	clear fiber	175	cellulose	cellulose
Penrose	Penrose Pt Oyster 10d	opaque particle	100	poly(ethylene glycol) monooleate or polyamide resin	PE glycol/PA resin
Penrose	Penrose Pt Oyster 10e	opaque shard	75	poly(ethylene glycol) monooleate or polyamide resin	PE glycol/PA resin
Penrose	Penrose Pt Oyster 10f	opaque particle	50	fluorescence	fluorescence
Penrose	Penrose Pt Oyster 10g	clear spheroid	75	poly(ethylene glycol) monooleate or polyamide resin	PE glycol/PA resin
Penrose	Penrose Pt Oyster 10h	dark fiber	1000	fluorescence	fluorescence
Penrose	Penrose Pt Oyster 11a	clear fiber, 11.2	1200	fluorescence	fluorescence
Penrose	Penrose Pt Oyster 11b	clear fiber, 11.1	900	fluorescence	fluorescence
Penrose	Penrose Pt Oyster 11c	clear spheroid	100	poly(ethylene glycol) monooleate or polyamide resin	PE glycol/PA resin
Penrose	Penrose Pt Oyster 12a	opaque irregular	80	fluorescence	fluorescence

Penrose	Penrose Pt Oyster 12b	clear spheroid	100	poly(ethylene glycol) monooleate or polyamide resin	PE glycol/PA resin
Penrose	Penrose Pt Oyster 12c	clear fiber, 12.1	350	fluorescence	fluorescence
Penrose	Penrose Pt Oyster 12d	clear spheroid	75	poly(ethylene glycol) monooleate or polyamide resin	PE glycol/PA resin
Penrose	Penrose Pt Oyster 12e	opaque spheroid	50	poly(ethylene glycol) monooleate or polyamide resin	PE glycol/PA resin
Penrose	Penrose Pt Control 10-12a	clear irregular	450	fluorescence	fluorescence
Penrose	Penrose Pt Control 10-12b	pink fiber	300	other	other
Penrose	Penrose Pt Oyster 19a	dark irregular	300	fluorescence	fluorescence
Penrose	Penrose Pt Oyster 19b	opaque rod	125	other	other
Penrose	Penrose Pt Oyster 19c	clear fiber, 19.1	400	fluorescence	fluorescence
Penrose	Penrose Pt Oyster 19d	clear fiber	1300	fluorescence	fluorescence
Penrose	Penrose Pt Oyster 20a	dark fiber	1800	poly(ethylene glycol) monooleate or polyamide resin	PE glycol/PA resin
Penrose	Penrose Pt Oyster 20b	opaque spheroid	75	poly(ethylene glycol) monooleate or polyamide resin	PE glycol/PA resin
Penrose	Penrose Pt Oyster 20c	white shard	650	gypsum	gypsum
Penrose	Penrose Pt Oyster 20d	clear fiber	500	fluorescence	fluorescence
Penrose	Penrose Pt Oyster 20e	clear fiber	1400	fluorescence	fluorescence
Penrose	Penrose Pt Oyster 20f	blue fiber	700	fluorescence	fluorescence
Penrose	Penrose Pt Oyster 21a	dark spheroid	100	other	other
Penrose	Penrose Pt Oyster 21b	dark fiber	300	fluorescence	fluorescence
Penrose	Penrose Pt Oyster 21c	clear spheroid	75	fluorescence	fluorescence

Penrose	Penrose Pt Oyster 21d	clear spheroid	80	other	other
Penrose	Penrose Pt Oyster 21e	dark spheroid	50	other	other
Penrose	Penrose Pt Oyster 21f	opaque spheroid	40	other	other
Penrose	Penrose Pt Oyster 21g	dark fiber	800	fluorescence	fluorescence
Penrose	Penrose Pt Control 19-21a	clear fiber	3500	fluorescence	fluorescence
Penrose	Penrose Pt Control 19-21b	clear fiber	1900	fluorescence	fluorescence
Penrose	Penrose Pt Control 19-21c	clear fiber	1600	fluorescence	fluorescence
Penrose	Penrose Pt Control 19-21d	opaque irregular	1000	fluorescence	fluorescence
Penrose	Penrose Pt Oyster 21h	dark spheroid	150	other	other
Samish	Samish Oyster 4a	opaque irregular	200	other	other
Samish	Samish Oyster 4b	dark irregular	250	fluorescence	fluorescence
Samish	Samish Oyster 4c	opaque spheroid	20	fluorescence	fluorescence
Samish	Samish Oyster 4d	clear fiber, 4.2	300	fluorescence	fluorescence
Samish	Samish Oyster 4e	opaque spheroid	50	other	other
Samish	Samish Oyster 4f	clear irregular	500	other	other
Samish	Samish Oyster 5a	opaque irregular	300	poly(ethylene glycol) monooleate or polyamide resin	PE glycol/PA resin
Samish	Samish Oyster 5b	blue fiber	300	other	other
Samish	Samish Oyster 5c	clear spheroid	20	fluorescence	fluorescence
Samish	Samish Oyster 5d	opaque irregular	60	other	other
Samish	Samish Oyster 5e	clear fiber	500	cellulose	cellulose

Samish	Samish Oyster 5f	clear shard	80	other	other
Samish	Samish Oyster 6a	opaque fiber	2500	fluorescence	fluorescence
Samish	Samish Oyster 6b	clear fiber	500	cellulose	cellulose
Samish	Samish Oyster 6c	opaque irregular	600	other	other
Samish	Samish Oyster 6d	opaque fiber	500	fluorescence	fluorescence
Samish	Samish Oyster 6e	pink shard	75	other	other
Samish	Samish Control 4-6a	opaque spheroid	100	polystyrene	polystyrene
Samish	Samish Control 4-6b	opaque spheroid	50	poly(ethylene glycol) monooleate or polyamide resin	PE glycol/PA resin
Samish	Samish Control 4-6c	opaque fiber	250	other	other
Samish	Samish Control 4-6d	opaque shard	60	other	other
Samish	Samish Oyster 7a	dark shard	75	poly(ethylene glycol) monooleate or polyamide resin	PE glycol/PA resin
Samish	Samish Oyster 7b	dark shard	75	fluorescence	fluorescence
Samish	Samish Oyster 7c	clear spheroid	50	fluorescence	fluorescence
Samish	Samish Oyster 7d	clear shard	50	poly(ethylene glycol) monooleate or polyamide resin	PE glycol/PA resin
Samish	Samish Oyster 9a	clear fiber	3900	fluorescence	fluorescence
Samish	Samish Oyster 9b	opaque irregular	400	poly(ethylene glycol) monooleate or polyamide resin	PE glycol/PA resin
Samish	Samish Oyster 9c	clear fiber	850	cellulose	cellulose
Samish	Samish Oyster 9d	clear shard	350	gypsum	gypsum
Samish	Samish Oyster 9e	clear fiber	1400	cellulose	cellulose
Samish	Samish Oyster 12a	opaque spheroid	150	fluorescence	fluorescence
Samish	Samish Oyster 12b	dark spheroid	50	fluorescence	fluorescence

Samish	Samish Oyster 12c	clear fiber, 12.1	1300	fluorescence	fluorescence
Samish	Samish Oyster 12d	opaque fiber	800	poly(ethylene glycol) monooleate or polyamide resin	PE glycol/PA resin
Samish	Samish Control 7,9,12a	dark spheroid	100	fluorescence	fluorescence
Samish	Samish Control 7,9,12b	shiney spheroid	175	fluorescence	fluorescence
Sequim	Sequim Oyster 24a	dark fiber	800	fluorescence	fluorescence
Sequim	Sequim Oyster 24b	opaque fiber	450	fluorescence	fluorescence
Sequim	Sequim Oyster 24c	dark fiber	400	fluorescence	fluorescence
Sequim	Sequim Oyster 24d	clear shard	75	other	other
Sequim	Sequim Oyster 24e	opaque irregular	250	fluorescence	fluorescence
Sequim	Sequim Oyster 25a	clear fiber	60	fluorescence	fluorescence
Sequim	Sequim Oyster 25b	clear particle	125	poly(ethylene glycol) monooleate or polyamide resin	PE glycol/PA resin
Sequim	Sequim Oyster 25c	clear fiber	400	cellulose	cellulose
Sequim	Sequim Oyster 25d	opaque shard	150	polypropylene	polypropylene
Sequim	Sequim Oyster 25e	clear fiber	225	fluorescence	fluorescence
Sequim	Sequim Oyster 26a	dark shard	125	fluorescence	fluorescence
Sequim	Sequim Oyster 26b	dark irregular	450	poly(ethylene glycol) monooleate or polyamide resin	PE glycol/PA resin
Sequim	Sequim Control 24-26a	clear fiber	1200	fluorescence	fluorescence
Sequim	Sequim Control 24-26b	clear fiber	700	cellulose	cellulose
Sequim	Sequim Control 24-26c	dark fiber (24.3)	325	other	other

Sequim	Sequim Oyster 27a	dark fiber	1000	fluorescence	fluorescence
Sequim	Sequim Oyster 27b	clear shard	100	other	other
Sequim	Sequim Oyster 27c	clear shard	125	other	other
Sequim	Sequim Oyster 27d	clear shard	140	other	other
Sequim	Sequim Oyster 27e	dark oblong	300	fluorescence	fluorescence
Sequim	Sequim Oyster 29a	blue fiber	400	fluorescence	fluorescence
Sequim	Sequim Oyster 29b	opaque spheroid	100	fluorescence	fluorescence
Mystery Bay	Mystery Oyster 1a	clear rod	500	other	other
Mystery Bay	Mystery Oyster 1b	opaque fiber	400	fluorescence	fluorescence
Mystery Bay	Mystery Oyster 1c	clear rod	75	poly(ethylene glycol) monooleate or polyamide resin	PE glycol/PA resin
Mystery Bay	Mystery Oyster 1d	opaque irregular	150	poly(ethylene glycol) monooleate or polyamide resin	PE glycol/PA resin
Mystery Bay	Mystery Oyster 1e	clear fiber	300	fluorescence	fluorescence
Mystery Bay	Mystery Oyster 3a	opaque spheroid	150	poly(ethylene glycol) monooleate or polyamide resin	PE glycol/PA resin
Mystery Bay	Mystery Oyster 3b	opaque fiber	1100	fluorescence	fluorescence
Mystery Bay	Mystery Oyster 3c	opaque spheroid	100	poly(ethylene glycol) monooleate or polyamide resin	PE glycol/PA resin
Mystery Bay	Mystery Oyster 19a	clear fiber	325	fluorescence	fluorescence
Mystery Bay	Mystery Oyster 19b	clear spheroid	75	poly(ethylene glycol) monooleate or polyamide resin	PE glycol/PA resin
Mystery Bay	Mystery Oyster 19c	opaque shard	75	poly(ethylene glycol) monooleate or polyamide resin	PE glycol/PA resin
Mystery Bay	Mystery Oyster 19d	clear spheroid	60	other	other
Mystery Bay	Mystery Oyster 19e	blue fiber	400	other	other

Mystery Bay	Mystery Control 17-19a	opaque fiber	1250	fluorescence	fluorescence
Mystery Bay	Mystery Control 17-19b	clear fiber	950	fluorescence	fluorescence
Mystery Bay	Mystery Control 17-19c	opaque fiber	1100	fluorescence	fluorescence
Mystery Bay	Mystery Oyster 20a	dark fiber	2000	other	other
Mystery Bay	Mystery Oyster 20b	clear shard	50	poly(ethylene glycol) monooleate or polyamide resin	PE glycol/PA resin
Mystery Bay	Mystery Oyster 21a	dark fiber	2200	fluorescence	fluorescence
Mystery Bay	Mystery Control 20-22a	clear fiber	800	fluorescence	fluorescence
Jacoby	Jacoby Oyster 27a	dark fiber, 27.1	500	other	other
Jacoby	Jacoby Oyster 27b	opaque spheroid	60	other	other
Jacoby	Jacoby Oyster 27c	dark spheroid	75	fluorescence	fluorescence
Jacoby	Jacoby Oyster 29a	dark shard	150	fluorescence	fluorescence
Jacoby	Jacoby Oyster 29b	clear spheroid	25	poly(ethylene glycol) monooleate or polyamide resin	PE glycol/PA resin
Jacoby	Jacoby Oyster 29c	dark fiber	600	other	other
Jacoby	Jacoby Oyster 29d	clear irregular	75	poly(ethylene glycol) monooleate or polyamide resin	PE glycol/PA resin
Jacoby	Jacoby Oyster 30a	dark irregular	300	fluorescence	fluorescence
Jacoby	Jacoby Oyster 30b	white circle	100	poly(ethylene glycol) monooleate or polyamide resin	PE glycol/PA resin
Jacoby	Jacoby Oyster 30c	clear spheroid	90	poly(ethylene glycol) monooleate or polyamide resin	PE glycol/PA resin
Jacoby	Jacoby Oyster 30d	clear shard	75	other	other

Jacoby	Jacoby Oyster 31a	opaque spheroid	125	poly(ethylene glycol) monooleate or polyamide resin	PE glycol/PA resin
Jacoby	Jacoby Oyster 31b	opaque irregular	125	polyethylene	polyethylene
Jacoby	Jacoby Oyster 31c	opaque fiber	175	fluorescence	fluorescence
Jacoby	Jacoby Oyster 31d	clear spheroid	100	gypsum	gypsum
Jacoby	Jacoby Oyster 29-31a	opaque shard	600	other	other
Jacoby	Jacoby Oyster 29-31b	clear fiber	125	fluorescence	fluorescence
Jacoby	Jacoby Oyster 29-31c	blue fiber	125	fluorescence	fluorescence
Jacoby	Jacoby Oyster 29-31d	dark spheroid	1000	fluorescence	fluorescence

Appendix B. Supplementary information for Chapter 4

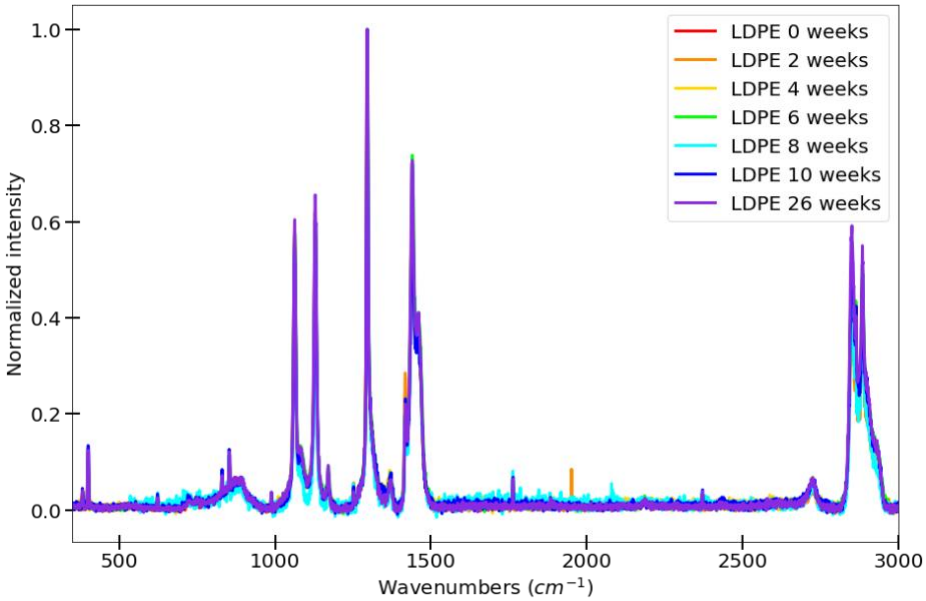

Supplementary Figure 4. 1 Raman spectra of LDPE exposed to sunlight overtime in air

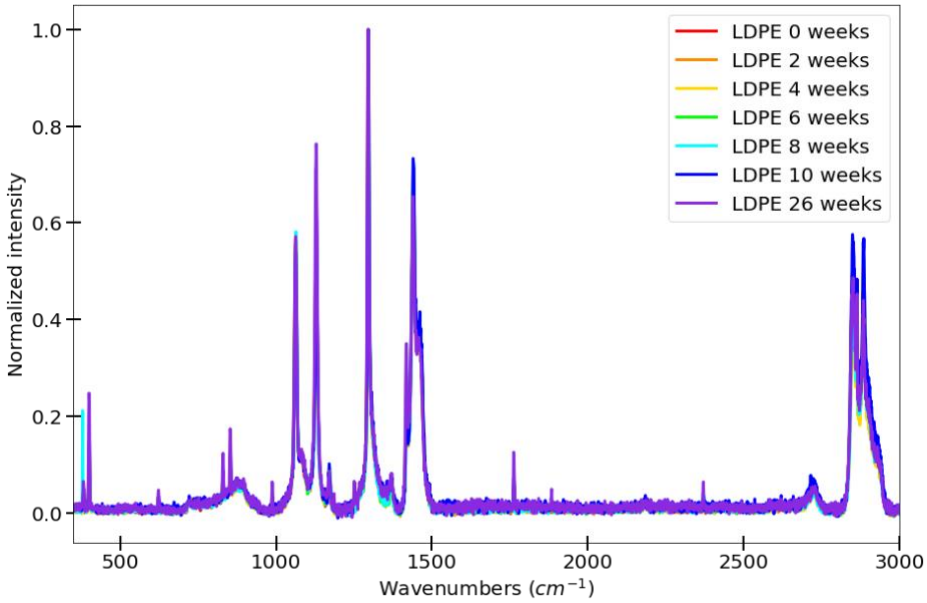

Supplementary Figure 4. 2 Raman spectra of LDPE exposed to sunlight overtime in DI water

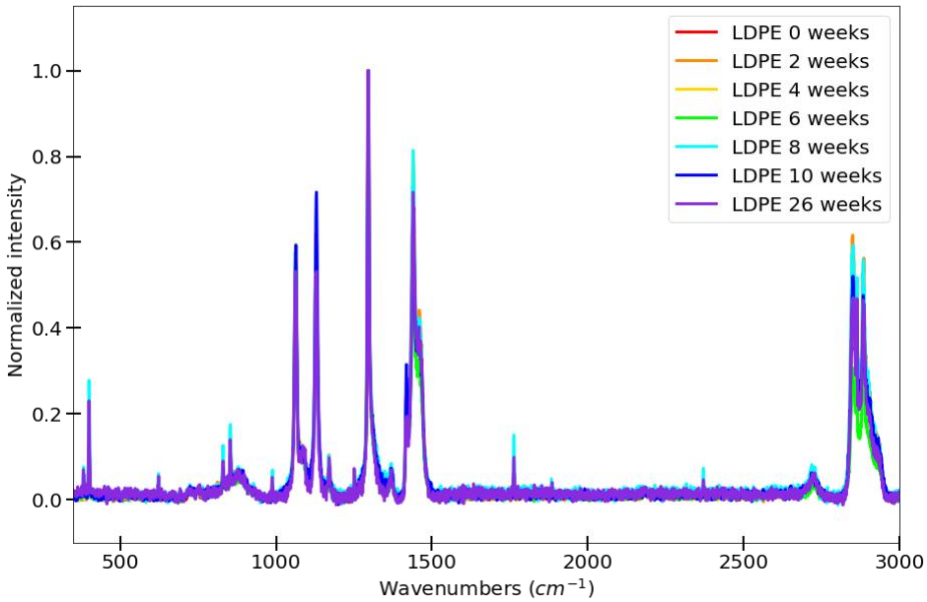

Supplementary Figure 4. 3 Raman spectra of LDPE exposed to sunlight overtime in artificial seawater

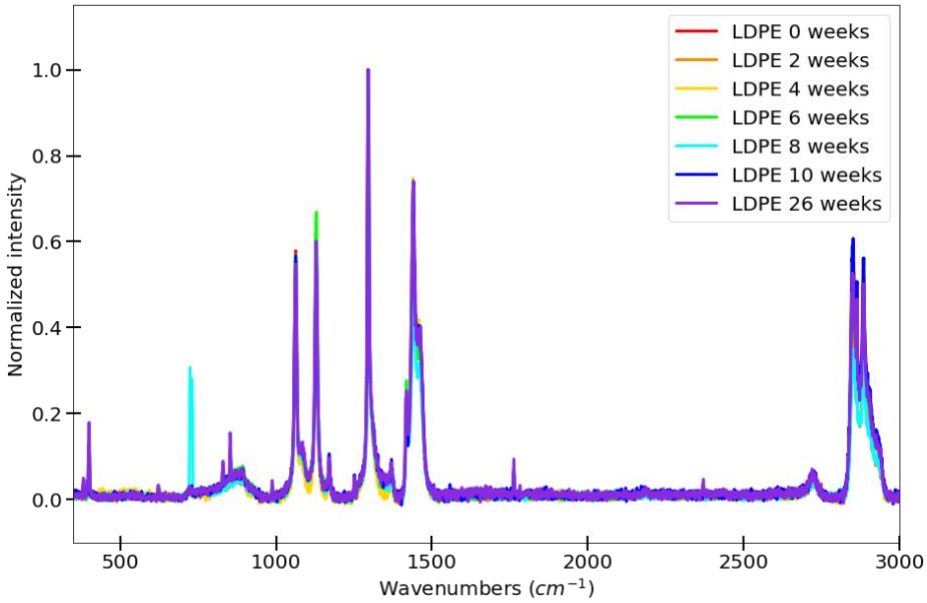

Supplementary Figure 4. 4 Raman spectra of LDPE exposed to sunlight overtime in Puget Sound seawater

Supplementary Table 4. 1 Ratios of I_{2890}/I_{2850} bands of weathered LDPE in different environments with increasing sunlight exposure

Week	Air	DI water	Artificial seawater	Puget Sound seawater
0	0.9101	0.9101	0.9101	0.9101
2	1.0513	1.0120	0.9409	1.1575
4	0.9898	1.0461	0.9882	1.0151
6	0.9732	1.0293	1.2269	0.8953
8	0.9863	1.0684	1.0029	0.9993
10	0.9529	1.0044	0.9613	0.9252
26	0.9299	0.9030	0.9870	0.9619

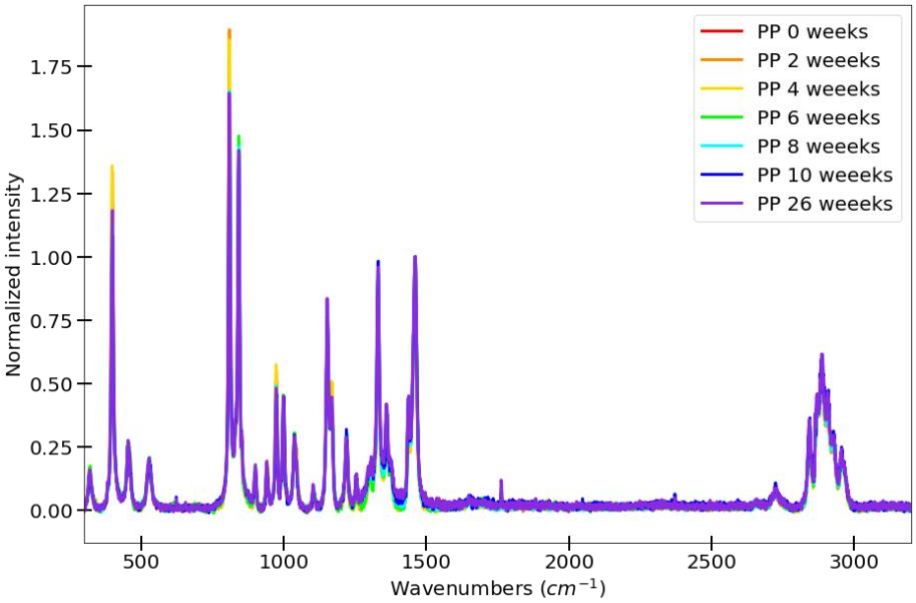

Supplementary Figure 4. 5 Raman spectra of LDPE exposed to sunlight overtime in air

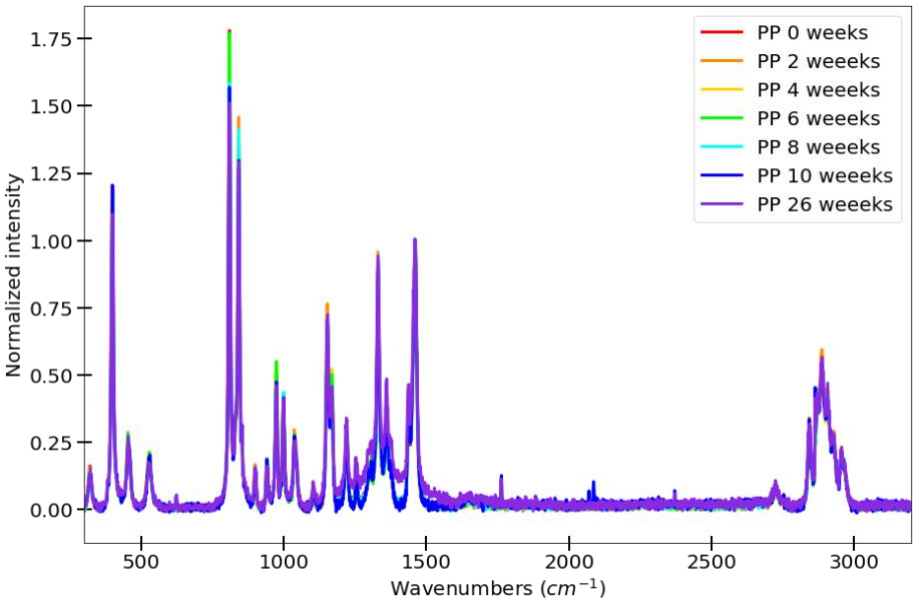

Supplementary Figure 4. 6 Raman spectra of LDPE exposed to sunlight overtime in DI water

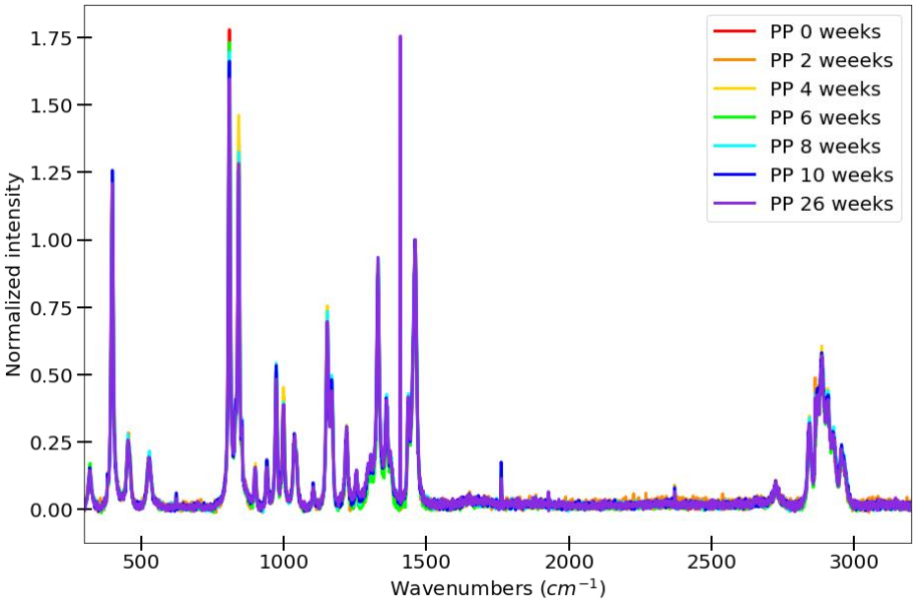

Supplementary Figure 4. 7 Raman spectra of LDPE exposed to sunlight overtime in artificial seawater

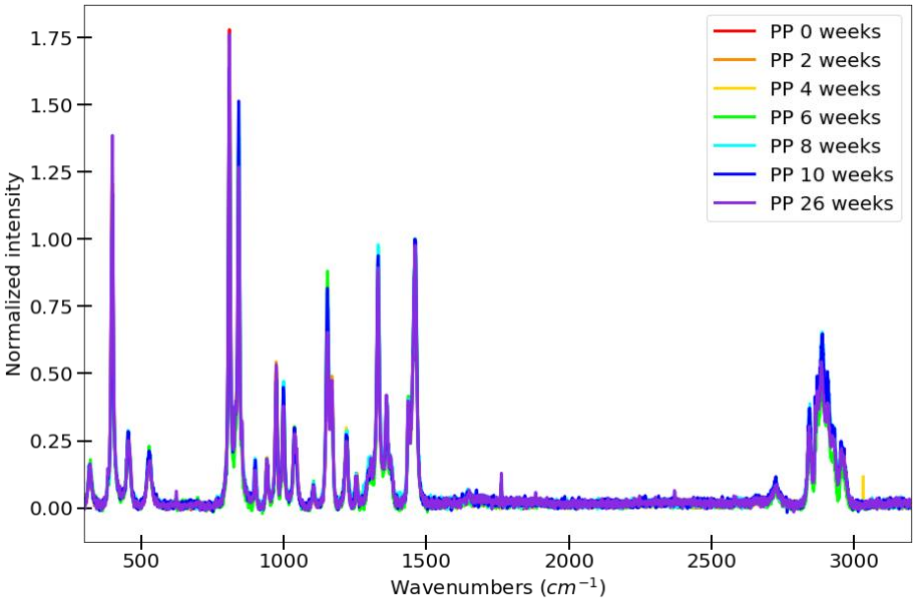

Supplementary Figure 4. 8 Raman spectra of LDPE exposed to sunlight overtime in Puget Sound seawater

Supplementary Table 4. 2 Ratios of I_{809}/I_{841} bands of weathered PP in different environments with increasing sunlight exposure

Week	Air	DI water	Artificial seawater	Puget Sound seawater
0	1.3163	1.3163	1.3163	1.3163
2	1.4827	1.1084	1.1327	1.3978
4	1.3720	1.3098	1.1250	1.2581
6	1.1016	1.3326	1.3334	1.1041
8	1.1543	1.1225	1.2792	1.0737
10	1.0891	1.2094	1.3236	1.0831
26	1.1618	1.1592	1.2452	1.3907

Appendix C. Vita

PROFESSIONAL EXPERIENCE

2017 – Present **PhD Candidate in Chemistry**

University of Washington – Luscombe Lab

- Conjugated polymer synthesis via direct arylation polymerization, microplastic pollution analysis, computer vision, and machine learning

2019 **International Research Assistant**

Institute of Transformative Bio-Molecules, Nagoya University – Itami Lab

- Expanding the scope of living annulative π-extension polymerization for graphene nanoribbons

2015 – 2017 **MS Graduate Student Research Assistant**

University of Washington – Vaughan Lab

- Polymer hydrogels for expansion microscopy

2010 – 2015 **Student Research Assistant**

University of Florida – Schanze Lab

- Conjugated polymer synthesis, thin-film self-assembly, fluorescence spectroscopy, atomic force microscopy, two-photon spectroscopy

AWARDS & FELLOWSHIPS

2021 Outstanding Engineering Woman in the Arts – Awarded by UW Society of Women Engineers

2021 University of Washington Excellence in Teaching Finalist

2020 University of Washington Husky 100

2019 Pacific Science Center Communication Fellowship

2019 Pacific Science Center Targeted Field Scholarship

2019 NSF Center for C-H Functionalization International Research Experience Fellowship

2019 University of Washington Excellence in Teaching Nominee

2019 Clean Energy Institute Graduate Fellowship

2018 University of Washington Excellence in Teaching Finalist

2015 Excellence in Chemistry Graduate Fellowship Award

LEADERSHIP & CIVIC ACTIVITIES

2016 – Present **Research Mentor** *University of Washington*

Luscombe Group

- Jordan Furseth, Applied Master's Program (2020 – 2021)
- Erin Mee, Undergraduate Research (2020 – 2021)
- Min Cho, Applied Master's Program (2019 – 2020)
- Nozomi Suzuki, Applied Master's Program (2019 – 2020)
- Inna Fomina, Undergraduate Research (2018 – 2019)
- Ernesto Borrigo, Summer internship (Summer 2019)

Vaughan Group

- Grant Tremel, Undergraduate Research (2016 – 2017)

2019 – Present **Science Communication Fellow** *Pacific Science Center, Seattle, WA*

2019 – Present **Fellow** *Clean Energy Institute*

2019 – 2021 **Organizer** *2020 Strategies for Cultivating Inclusion in STEM (SCI-STEM) symposium*

2017 – 2021 **CEI Liaison** *Diversity in Clean Energy at UW Clean Energy Institute*

2017 – 2021 **Ensemble Member and Script writer** *Theater for Change at UW and Center for Teaching and Learning*

2015 – 2021 **Webmaster** *Inclusion in Chemical Sciences*

2011 – 2012 **Tutor** *University of Florida Office of Academic Support*

COMMUNICATION

Presentations

2019 11th Annual Frontiers in C-H Functionalization Conference – Atlanta, GA

2019 International C-H Functionalization Workshop – Daejeon, South Korea

2019 Center for C-H Functionalization and Seoul National University Organic Chemistry Symposium – Seoul, South Korea

2018 10th Annual Frontiers in C-H Functionalization Conference – Atlanta, GA

Publications

2020 "Low incidence of microplastic contaminants in Pacific oysters (Crassostrea gigas Thunberg) from the Salish Sea, USA." *Sci Total Environ.* **2020**, 715, 136826.

2019 "Recent advances in green and sustainable synthesis of semiconducting polymers," *Trends in Chemistry*, **2019**, 1, 670−681.

2017 "Two-Photon Absorption of Cationic Conjugated Polyelectrolytes: Effects of Aggregation and Application to 2-Photon Sensitized Fluorescence from Green Fluorescent Protein," *Chem. Mater.* **2017**, 29, 3295−3303.

2015 "Self-Sterilizing, Self-Cleaning Mixed Polymeric Multifunctional Antimicrobial Surfaces," *ACS Appl. Mater. Interfaces* **2015**, 7, 27632−27638.